UNIVERSITY OF CALIFORNIA, SAN DIEGO

Interactions of Mineral Dust with Clouds, Sea Surface Temperature, and Climate Modes of Variability

A dissertation submitted in partial satisfaction of the
requirements for the degree
Doctor of Philosophy

in

Oceanography

by

Michael J. DeFlorio

Committee in charge:

Daniel R. Cayan, Co-Chair
Arthur J. Miller, Co-Chair
Ian Eisenman
Paul S. Goldstein
Ian D. Goodwin
Myrl C. Hendershott
Joel R. Norris

2015

The dissertation of Michael J. DeFlorio is approved, and it is acceptable in quality and form for publication on microfilm and electronically:

_____

_____

_____

_____

_____

_____
Co-Chair

_____
Co-Chair

University of California, San Diego

2015

DEDICATION

To Al Feldstein, who planted the seeds of inquiry and curiosity within me.

EPIGRAPH

It's okay if you don't know everything.

— Benjamin Folds

TABLE OF CONTENTS

LIST OF FIGURES

ACKNOWLEDGEMENTS

I made the decision to pursue a PhD in oceanography largely because I could not imagine a life in which I was not surrounded by others who shared with me an unquenchable thirst for knowledge, truth, and understanding. My teachers are primarily responsible for fostering these traits in my personality. Al Feldstein, Bob Crowley, Al Kunins, Kathy Sapanski, John Schmitt, Carolyn Karl, Benjamin Benbasset, Randy Wayne, Alvaro Lozano-Robledo, Bob Terrell, Mark Wysocki, Stephen Colucci, Arthur DeGaetano: though many of you will never read this dissertation, thank you for instilling a passion for learning within me.

My committee members and co-authors have been integral in helping develop and refine the ideas contained in this dissertation. Ian Eisenman, Steven Ghan, Paul Goldstein, Ian Goodwin, Myrl Hendershott, Joel Norris, Lynn Russell, Balwinder Singh, and Richard Somerville: thank you for your thoughtful and pivotal contributions to my graduate studies.

David Pierce was an important mentor to me during my first few years at Scripps. He was instrumental in teaching me critical scientific concepts, and did so with incredible patience for a new student who was learning the ropes in the field. David has a work ethic and desire to learn that, to this day, I still aspire to achieve. David: thank you for your patience and guidance, both of which helped me gain confidence in myself and enabled me to achieve success at Scripps.

My academic advisors always allowed me the freedom to pursue my interests, and provided me the resources necessary to attain my goals. They have fundamentally shaped my approach to critical thinking and problem solving, and are exemplary professionals in their interactions with peers and colleagues. Dan and Art: thank you for showing me how it's done.

My graduate years have been largely defined by my incredible friends and peers at Scripps and in San Diego. They are the people who made my time at Scripps so formative and so colorful, and were always there to remind me that unwinding from the stress of classes and research is essential. Alain de Verneil, Timmy Myers, Nick Cavanaugh, Nick Pizzo, Sara Sanchez, Brett Lyall, Diego Melgar, Samer Naif, Robert Petersen, Jenan Kharbush, Roland Kersten, Kelley

Gallagher, Riley Gannon, Alan Foreman, and so many others: thank you for enriching my life in so many ways over the past six years.

One unintended consequence of moving to San Diego is the way it brought me closer to many of my friends from New York. I visited home once or twice each year during my graduate studies, and these brief encounters with my core group of friends at home helped accentuate their importance in my life. Nick, Matt, Max, Sophia, Zach, Michelle, Russ, and so many others: thank you for sharing with me the beauty of lifelong friendship.

Finally, my family has made the ultimate sacrifice in allowing me to follow my dreams. They have wholly supported education for education's sake and are committed to helping me achieve a life of happiness and fulfillment. Mom, Dad, Heather and Jimmy: thank you for your unwavering love and support.

Portions of this dissertation have been published in peer reviewed journals.

Chapter 2 is published in its entirety in:

- **DeFlorio, M.J.**, D. W. Pierce, D. R. Cayan, and A. J. Miller, 2013: "Western U.S. Extreme Precipitation Events and Their Relation to ENSO and PDO in CCSM4". *J. Clim.*, **26**, 4231-4243.

Chapter 3 is published in its entirety in:

- **DeFlorio, M.J.**, S. J. Ghan, B. Singh, A. J. Miller, D. R. Cayan, L. M. Russell, and R. C. J. Somerville (2014), "Semi-direct dynamical and radiative effect of North African dust transport on lower tropospheric clouds over the subtropical North Atlantic in CESM 1.0", *J. Geophys. Res. Atmos.*, **119**, 8284-8303, doi:10.1002/2013JD020997.

Chapter 4 is published in its entirety in:

- **DeFlorio, M.J.**, I. D. Goodwin, D. R. Cayan, A. J. Miller, S. J. Ghan, D. W. Pierce, L. M. Russell, and B. Singh (2015), "Interannual modulation of subtropical Atlantic boreal summer dust variability by ENSO", *Clim. Dyn., in press*, doi: 10.1007/s00382-015-2600-7.

Chapter 5 consists of previously unpublished material.

VITA

2009	B.S. (*cum laude*) in Atmospheric Science, Cornell University
2010	M.Sc. in Oceanography, University of California, San Diego
2015	Ph.D. in Oceanography, University of California, San Diego

PUBLICATIONS

DeFlorio, M.J. (2015), "Role of North African Dust Outbreaks in modulating tropical Atlantic SST variability on interannual timescales", *in prep.*

DeFlorio, M.J., I. D. Goodwin, D. R. Cayan, A. J. Miller, S. J. Ghan, D. W. Pierce, L. M. Russell, and B. Singh (2015), "Interannual modulation of subtropical Atlantic boreal summer dust variability by ENSO", *Clim. Dyn., in press*, doi: 10.1007/s00382-015-2600-7.

DeFlorio, M.J., S. J. Ghan, B. Singh, A. J. Miller, D. R. Cayan, L. M. Russell, and R. C. J. Somerville (2014), "Semi-direct dynamical and radiative effect of North African dust transport on lower tropospheric clouds over the subtropical North Atlantic in CESM 1.0", *J. Geophys. Res. Atmos.*, **119**, 8284-8303, doi:10.1002/2013JD020997.

DeFlorio, M.J., D. W. Pierce, D. R. Cayan, and A. J. Miller, 2013: "Western U.S. Extreme Precipitation Events and Their Relation to ENSO and PDO in CCSM4". *J. Clim.*, **26**, 4231-4243.

ABSTRACT OF THE DISSERTATION

Interactions of Mineral Dust with Clouds, Sea Surface Temperature, and Climate Modes of Variability

by

Michael J. DeFlorio

Doctor of Philosophy in Oceanography

University of California, San Diego, 2015

Daniel R. Cayan, Co-Chair
Arthur J. Miller, Co-Chair

Global climate models (GCMs) are a vital tool for ensuring the prosperity and security of modern society. They allow scientists to understand complex interactions between the air, ocean, and land, and are used by policymakers to project future changes in climate on regional and global scales.

The previous generation of GCMs, represented by CMIP3 models, are shown to be deficient in their representation of precipitation over the western United States, a region that depends critically on wintertime orographically enhanced precipitation for drinking water. In addition, aerosol-cloud interactions were prescribed in CMIP3 models, which decreased the value of their represen-

tation of global aerosol, cloud, and precipitation features. This has potentially large impacts on global radiation budgets, since aerosol-cloud interactions affect the spatial extent and magnitude of clouds and precipitation.

The newest suite of GCMs, the Coupled Model Intercomparison Project Phase 5 (CMIP5) models, includes state-of-the-art parameterizations of small-scale features such as aerosols, clouds, and precipitation, and is widely used by the scientific community to learn more about the climate system. The Community Earth System Model (CESM), in conjunction with observations, provides several simulations to investigate the role of aerosols, clouds, and precipitation in the climate system and how they interact with larger modes of climate variability.

We show that CESM produces a realistic spatial distribution of precipitation extremes over the western U.S., and that teleconnected signals of ENSO and the Pacific Decadal Oscillation to large-scale circulation patterns and precipitation over the western U.S. are improved when compared to CCSM3. We also discover a new semi-direct effect between dust and stratocumulus clouds over the subtropical North Atlantic, whereby boundary layer inversion strength increases during the most dusty summers due to shortwave absorption of dust above the planetary boundary layer. We find that ENSO exerts a control on North African dust transport during the summer, and CESM suggests that there is strong multi-decadal variability in the strength of the ENSO-dust relationship. Finally, we compare interactive and prescribed aerosol CESM simulations to demonstrate the importance of dust in increasing tropical Atlantic SST variability, and expose deficiencies in CESM's simulation of the Atlantic Meridional Mode.

Chapter 1

Introduction

1.1 Evolution of Global Climate Models

Numerical computer models have been used since the mid-20th century as a tool for understanding and predicting the general circulation of both the atmosphere and the ocean (*Hartmann*, 1994). The development of computer models was an extension of experimental fluid mechanics during the 19th century, when scientists constructed actual physical models to further their understanding of the Earth's dynamical behavior. Meteorologists, in particular, viewed computer models as a means by which future states of the atmosphere could be rapidly predicted to produce reliable weather forecasts (*Weart*, 2008). The models enabled these predictions by solving a set of primitive, time-dependent dynamical equations of fluid motion.

Since their initial utilization to make weather forecasts, numerical models have evolved in concert with increased computational capacity to include more complex Earth system processes, such that a larger array of questions about the current and future state of the general circulation of the atmosphere can be addressed. It is in this way that weather models, used for short-term prediction of synoptic meteorological phenomena, were extended to climate models, used for long-term prediction of atmospheric and oceanic variables across the entire globe (*Hartmann*, 1994).

In the past, Global Climate Models (GCMs) have been used to study

coupled-ocean atmosphere phenomena such as the El Nino-Southern Oscillation (ENSO), the Pacific Decadal Oscillation (PDO), and hurricanes (*Deser et al.*, 2012, 2006; *Pierce et al.*, 2000; *Emanuel et al.*, 2010). GCMs have also been employed for both observational validation and future prediction of midlatitude storms and precipitation characteristics (*Dai*, 2006; *Ulbrich et al.*, 2008).

The most recent suite of GCMs comprises the Coupled Model Intercomparison Project Phase 5 (CMIP5), a set of experiments aimed at model validation, characterization of climate predictability, and assessment of model dynamics. One widely used CMIP5 model is the National Center for Atmospheric Research Community Earth System Model (NCAR CESM), which will be used throughout this dissertation. CESM is a fully-coupled climate model consisting of five individual, fully-prognostic component models which simultaneously simulate the Earth's atmosphere, ocean, land, land-ice, and sea-ice environments (*Gent et al.*, 2011). The atmospheric component of the model solves the horizontal momentum, vertical momentum (hydrostatic), thermodynamic energy, mass continuity, and water vapor mass continuity equations across the entire globe on a finite volume grid. Similarly, the oceanic component of the model solves the global horizontal momentum, vertical momentum (hydrostatic), mass continuity, tracer transport and state equations on either a tripole or displaced pole grid.

CESM and other CMIP5 GCMs are valuable sources of information for the climate science community because they allow us to make specific quantitative assertions about past, present, and future climates on Earth. These assertions further the current state of knowledge within the scientific community, and have the potential to spawn changes in regional and global economics and domestic and international policy. All of these factors provide ample motivation to assess climate models both in comparison to one another and at a deeper level individually.

1.2 Aerosols in the Climate System

Much like oceanography and meteorology, the field of aerosol science is relatively young. One of the first clues to the scientific community that aerosols

could have a major impact on climate came from volcanoes. Scientists in the 1950's noted that volcanic activity and Northern Hemispheric temperature were anti-correlated during both that decade and the previous century, which prompted investigation into the effect of natural aerosols in the climate system on surface temperature (*Mitchell Jr*, 1971). Contemporaneously, scientists were beginning to understand the role of hygroscopic cloud condensation nuclei (CCN) in cloud formation, and began studying (and at times advocating for) artificial alteration of regional climate through anthropogenic cloud seeding (*Houghton*, 1968). Smog and haze particulates over polluted areas (e.g. Burbank, CA) also attracted attention from atmospheric chemists and physicists (*Haagen-Smit*, 1952). In the 1960's, the effects of dust and wildfire emissions on local meteorology were increasingly studied (*Bryson and Baerreis*, 1967). British meteorologist Hubert Lamb went so far as to coin the metric "Dust Veil Index" to represent anti-correlation between dust concentration and surface temperature (*Weart*, 2008).

For much of the 1970's, debate over the sign of the net radiative forcing of aerosols was rampant, and many aerosol studies focused on the "direct effect" of aerosols on the climate: cooling by scattering of solar radiation or heating by absorption of solar radiation. However, in 1974, the first theory for aerosol "indirect" radiative effects was formalized. Based on observations from Australia, Sean Twomey proposed that higher aerosol concentrations would lead to higher concentrations of CCNs, which would increase cloud droplet number concentration and thus cloud albedo and have a net negative radiative effect on climate (*Twomey*, 1974). This was later dubbed the "Twomey Effect" or "first indirect effect". The "second indirect effect" was formalized by Bruce Albrecht in 1989. Using a one-dimensional model calculation, the "Albrecht Effect" states that an increase in CCNs (from sea salt over the ocean, for example) would cause a decrease in cloud droplet size. This would, in turn, cause a reduction in drizzle production and thus an increase in fractional cloudiness over time. The Albrecht Effect is sometimes called the "cloud lifetime effect" for this reason. Both the first and second indirect effects highlighted the potential for aerosols to affect clouds, and thus radiation, in the climate system.

There were several interesting characteristics of this developmental period of aerosol science: a) the tendency to focus on anthropogenic aerosols and pollution (after the initial focus on volcanoes) and b) the frequent implementation of simple numerical models to try to understand a limited observational database.

1.3 Aerosols in GCMs

These aforementioned models turned more complex over the 1990's and 2000's with the advent of increased computational power and increased spatiotemporal observations of many climate variables. Over the last 15 years in particular, scientists have strived to represent aerosols realistically in fully coupled global climate models. An early example of the importance of representing aerosols in global climate models came in *Mitchell et al.* (1995), who showed that including sulfate aerosols in a global climate model significantly improved model agreement with observational temperature over the late 20th century. However, early attempts at incorporating aerosols into fully coupled global climate models sometimes relied on trial-and-error adjustment of surface albedo, a parameter already contained in GCMs, in each grid cell to approximately account for the existence of aerosols (*Boer et al.*, 2000). The situation improved in the early 2000's, when three-dimensional aerosol distributions were calculated in separate chemical transport models and then added as input to GCMs, mainly with the intent of quantifying the direct effect of aerosols (*Meehl et al.*, 2003; *Collins et al.*, 2006).

Figure 1.1 (modified from *Ghan and Schwartz* (2007)) summarizes differences in treatment of aerosol size distribution and aerosol emissions from fourth generation climate models (those included in the IPCC AR4 report) to some of the fifth generation climate models (those included in the IPCC AR5 report).

One important improvement in representation of aerosol properties in the latest class of GCMs is the representation of aerosol size distribution as variable (modal) rather than prescribed. In addition, emissions of aerosols were prescribed from climatology in IPCC AR4 models, but now interact with modeled meteorology in several IPCC AR5 models. For example, dust emissions, which will be a major

Property/Process	Treatment – AR4	Treatment – AR5
Aerosol size distribution	**Prescribed**	**Variable** for each aerosol type – "modal"
Aerosol emissions	**Prescribed**	Sea salt, dust emissions **depend on modeled meteorology** – e.g. wind speed for both, soil moisture for dust

Figure 1.1: Treatment of aerosol size distribution and aerosol emissions in IPCC AR4 (fourth generation) and several IPCC AR5 (fifth generation) climate models, including CESM (modified from *Ghan and Schwartz* (2007)).

focus of this dissertation, are now dependent on local wind speed/direction and soil moisture. As noted by *Ghan and Schwartz* (2007), continued improvements in GCM aerosol representation rely heavily on advancement of observational studies of aerosols in both laboratory and field settings.

The work in this dissertation makes use of these recent advances in global modeling of aerosol-climate interactions and other related atmospheric processes such as precipitation and clouds in order to: a) evaluate models using available observations and b) use models in the absence of spatiotemporally dense observations to further our understanding of relevant physical processes. In Chapter 2, we evaluate the representation of extreme precipitation statistics over the western U.S. and associated teleconnections to Pacific modes of climate in the NCAR Community Earth System Model (CESM). The results from this study highlight the improved representation of global teleconnections in CESM, which serves as motivation for studying the interaction of North African dust variability with Pacific modes of climate in Chapter 4. In Chapter 3, we evaluate the representation of mineral dust properties and spatial distribution in CESM, and identify a new dust indirect effect linking increased dust concentration over the subtropical North Atlantic with stronger lower tropospheric inversion strength in boreal summer, which promotes the formation of stratocumulus clouds. This is an important finding given the large uncertainty in the sign of the radiative forcing of stratocumulus clouds in future projections of climate (*Bony and Dufresne*, 2005; *Qu et al.*, 2014). In Chapter 4, we show that there is substantial interannual and decadal

variability of the strength of the relationship between ENSO and North African dust transport in a 150-year CESM simulation. This low frequency fluctuation is associated with distinct out-of-phase changes in atmospheric circulation in the North Atlantic, with a spatial pattern distinctly reminiscent of the North Atlantic Oscillation. This finding is important because observations of atmospheric dust are limited to roughly 30 years over the tropical Atlantic and North African regions and therefore may not be extensive enough to fully characterize variability of the signal. In Chapter 5, we compare spatiotemporal variability of tropical Atlantic sea surface temperature anomalies in two 150-year CESM simulations: one with fully interactive aerosols, and one with a prescribed seasonal cycle of aerosol concentration, which eliminates interannual variability of aerosols. The differences between the two simulations demonstrate the importance of mineral dust in increasing month-to-month variability of tropical Atlantic SSTs. We also show that CESM is deficient in simulating the Atlantic Meridional Mode, which is an important mode of coupled ocean-atmosphere interannual variability in the tropical Atlantic.

Chapter 2

Western U.S. Extreme Precipitation Events and Their Relation to ENSO and PDO in CCSM4

Water resources and management over the Western U.S. are heavily impacted by both local climate variability and the teleconnected responses of precipitation to the El Nino Southern Oscillation (ENSO) and Pacific Decadal Oscillation (PDO). In this work, regional precipitation patterns over the western U.S. and linkages to ENSO and PDO are analyzed using output from a CCSM4 preindustrial control run and observations, with emphasis on extreme precipitation events. CCSM4 produces realistic zonal gradients in precipitation intensity and duration over the western U.S., with higher values on the windward side of the Cascade and Sierra Mountains and lower values on the leeward. Compared to its predecessor CCSM3, CCSM4 shows an improved teleconnected signal of both ENSO and the PDO to large scale circulation patterns over the Pacific/North America region and also to the spatial pattern and other aspects of western U.S. precipitation. The so-called "drizzle" problem persists in CCSM4 but is significantly improved compared to CCSM3. In particular, it is found that CCSM4 has

substantially less precipitation duration bias than is present in CCSM3. Both the overall and extreme intensity of wintertime precipitation over the western U.S. show statistically significant linkages with ENSO and PDO in CCSM4. This analysis provides a basis for future studies using GHG-forced CCSM4 runs.

2.1 Overview

Water resources have extensive influence on government policy, quality of life, and regional economics. This is particularly true over the western U.S., which harbors a rapidly growing population, very active climate variability and complex topography that affects regional climate including the spatial and temporal structure of precipitation. The generally arid southwestern U.S., which is the fastest growing region of the United States, is one area where effective water management is of paramount importance (e.g. *Parker* (2010)). The Pacific Northwest lies in the influence of interannual and interdecadal climate variation (*Hamlet and Lettenmaier*, 1999). In addition, flooding has major impacts in the region, and is an important player in regional economic policy, particularly in California (*Pierce*, 2012). For example, in 2010, the Federal Emergency Management Agency forced homeowners in Los Angeles, Orange, Ventura, Riverside, and San Bernardino counties to buy flood insurance because of their proximity to flood-prone rivers and creeks (*Saillant*, 2010).

Synoptic weather patterns over the western U.S. are known to be influenced by the El Nino-Southern Oscillation (ENSO) and the Pacific Decadal Oscillation (PDO). The teleconnected signal of ENSO in climatic variables across the globe has been an important topic of research for many decades (e.g. *Bjerknes* (1969); *Trenberth* (1976); *Ropelewski and Halpert* (1986); *Rasmusson and Wallace* (1983); *Bradley et al.* (1987); *McCabe and Dettinger* (1999); *Meehl et al.* (2007)). Many coupled GCMs have exhibited unrealistic teleconnections between ENSO fluctuations and extratropical circulation patterns, driven in part from having poorly represented physical processes in the core ENSO region (*Solomon*, 2007; *AchutaRao and Sperber*, 2006; *Zhu et al.*, 2004). The warm and cool phases of the PDO are

also associated with distinctly different western U.S. weather patterns (*Hidalgo and Dracup*, 2003), despite the lack of robust evidence for physical causality of decadal North Pacific SST variability (*Pierce*, 2002).

The present climatological study investigates the NCAR Community Climate System Model, version 4 (henceforth CCSM4) skill in simulating several teleconnected signals of ENSO and the PDO over the North Pacific, extreme regional precipitation over the western U.S. and North Pacific, and the relationship of the phase of both ENSO and the PDO to western U.S. extreme precipitation. We also compare CCSM4 to results from CCSM3 (the previous version of the model) and observations.

Extending prior work evaluating GCM simulations of ENSO and PDO teleconnections and regional precipitation events to CCSM4 is timely, since the model was released recently and will be used in the upcoming fifth IPCC assessment, and is important to the applications noted above. The model's simulation of interannual climatic variability, as captured in the frequency of ENSO events, is more realistic than that of its predecessor, CCSM3; however, the magnitude of these events is too large compared to observations (*Gent et al.*, 2011; *Deser et al.*, 2012). The improvement in the frequency of ENSO events is primarily due to improvements in the atmospheric convection parameterization scheme (*Gent et al.*, 2011; *Neale et al.*, 2008). Better parameterizations of cloud physics and atmospheric radiation have also improved simulations of precipitation type and amount (*Neale et al.*, 2013). Given these improvements in simulation of large-scale decadal coupled ocean/atmospheric processes, which have significant impacts on the strength, frequency, and location of midlatitude synoptic storms, and in small-scale moisture microphysics, it is reasonable to consider the model as a viable candidate for realistically simulating global ENSO and PDO teleconnection patterns and extreme regional precipitation events.

Previous work has addressed GCM simulations of Pacific variability and mean and extreme precipitation characteristics in various ways. *Dai* (2006) used monthly and 3-hourly data from 18 coupled GCMs (of which CCSM3 was one) to examine patterns of global precipitation intensity and frequency, with particular

emphasis on tropical Pacific variability and the simulated partitioning of precipitation between large-scale and convective processes. Notably, they found that most models underestimate the contribution to total precipitation and frequency for heavy precipitation and overestimate them for light precipitation. This is often referred to as the "drizzle problem" of GCMs (*Dai*, 2006; *Lee et al.*, 2009). *Wehner et al.* (2010) examined the effect of varying horizontal resolution on the ability of CAM3 (the atmospheric component of CCSM3) to simulate annual precipitation maxima over the continental U.S. They found that model fidelity was a strong function of horizontal resolution; specifically, a resolution of 0.5° x 0.625° allowed for adequate simulation of extreme precipitation events. However, such a resolution is computationally expensive for long climate simulations, especially on a global scale.

This study aims to build on these prior works by investigating CCSM4's representation of mean and extreme precipitation events and ENSO and PDO teleconnections, with a focus on the western U.S. and North Pacific. Besides comparing to observations, many of the CCSM4 results are compared to simulations by its predecessor CCSM3. Several concluding analyses specifically compare various measures of or relating to precipitation in CCSM4 with observations, since CCSM4 proves to be superior in many ways to CCSM3 in comparison to observations. Particular emphasis will be placed on precipitation duration and intensity over the western United States.

2.2 Models and Data

Below, we describe the models and data used in our study. A summary of all models and data is included in Figure 2.1.

2.2.1 CCSM4 Model Runs

We use a 1300 year pre-industrial control CCSM4 simulation with monthly data and a horizontal resolution of 1.25° (lon) x 0.9° (lat). This run is used to examine ENSO/PDO teleconnection patterns over the western U.S and North

Pacific. We also use a 150 year subset of this run with daily data to examine mean and extreme precipitation statistics and their relationship to ENSO and the PDO. Data were obtained from the Earth System Grid website (earthsystemgrid.org).

2.2.2 CCSM3 Model Runs

In order to evaluate improvements in CCSM4's simulation of ENSO/PDO teleconnection patterns and extreme precipitation events, we also use 500 years of monthly data and 50 years of daily data from a pre-industrial control CCSM3 simulation at T85 resolution (1.4° (lon) x 1.4° (lat)). This run is similarly used to examine ENSO/PDO teleconnection patterns over the western U.S. and North Pacific and western U.S. precipitation.

2.2.3 Observational data

When comparing model precipitation fields to observations, one must distinguish between results obtained at a point (station data) and results averaged over an area. The distinction arises because model grid cells, even at T85 resolution, are considerably larger than the length scales associated with patches of heavy precipitation. The most appropriate way to think about model precipitation may be to view it as an area-averaged quantity, rather than as a model representation of precipitation at a point (*Chen and Knutson*, 2008). This suggests that observed gridded precipitation fields, not station data, are preferable for validating model results. We compare the model results to the gridded observed precipitation data set of *Hamlet and Lettenmaier* (2005). This is a daily gridded data set based on National Weather Service co-operative stations, augmented by higher quality Global Historical Climatology Network and other stations. Techniques from the Parameter-elevation Regressions on Independent Slopes Model (PRISM) project are used to interpolate the observations over the entire domain while accounting for elevation and slope aspect effects (*Daly et al.*, 1994, 2002). This data set is produced on a 1/8° x 1/8° grid and spans the period 1915-2002. However, since meteorological station coverage increased substantially after WWII, the period an-

alyzed here in 1950-2002. *Cayan et al.* (2010) found that when the Hamlet and Lettenmaier data set is used to drive the Variable Infiltration Capacity (VIC) hydrological model, the simulated streamflows are realistic when compared to the available observations, which suggests that the data are capturing the features of observed precipitation relevant to hydrology.

For observations of sea surface temperature (SST), a combined data set is used: the da Silva data over the period 1948-1982 (*Da Silva et al.*, 1994), and the National Meteorological Center data from 1983 through the end of 2009 (*Reynolds et al.*, 2002). We choose to analyze only post-World War II SST data because the density of available observations over the North Pacific is much higher during this time period. In addition, it is desirable to have precipitation and sea surface temperature data sets that are of comparable length.

Dataset	Type	Horizontal resolution	Temporal resolution	Length	Used for
CCSM4 preindustrial control	Model	1.25° (lon) × 0.9° (lat)	Monthly and daily	1300 yr (monthly); 150 years (daily)	ENSO–PDO teleconnection patterns and precipitation statistics
CCSM3 preindustrial control	Model	T85	Monthly	500 yr	ENSO–PDO teleconnection patterns
CCSM3 preindustrial control	Model	T85	Daily	50 yr	Precipitation statistics
Hamlet and Lettenmaier (2005)	Obs	0.125° (lat) × 0.125° (lon)	Daily	53 yr	Precipitation statistics
da Silva/National Meteorological Center	Obs	1° (lat) × 1° (lon)	Monthly	52 yr	ENSO–PDO teleconnection patterns

Figure 2.1: List of modeled and observational datasets, and associated characteristics, used in this study

2.2.4 Regridding

To compare with the GCM output, the observational data were regridded to match the grid of the GCM (*Chen and Knutson*, 2008). Aggregating the finer observed data (i.e. regridding from high resolution to low resolution) smooths the high density observed data over the region of interest, but is necessary for the matching the coarser topography representation in the GCM. The finer observed data sets are regridded to match the coarser CCSM4 daily model data grid, using a bilinear interpolation scheme. Equating the grid sizes of the modeled and ob-

served data sets enables easier comparison of differences in modeled and observed precipitation.

2.2.5 Precipitation terminology

We define several terms related to mean and extreme precipitation statistics that will be used throughout the rest of this study: a precipitating day, precipitation intensity, and precipitation duration. Given the model issues with drizzle noted previously, we define a "precipitating day" as a day on which precipitation totaling >0.1 mm/day falls. "Precipitation intensity" is defined as the daily value of precipitation rate (mm/day) over a grid cell on a precipitating day. "Precipitation duration" is defined as the number of consecutive precipitating days.

2.3 Western U.S. Precipitation Climatology

2.3.1 Base seasonal climatology

Figure 2.2 shows the seasonal climatology of mean precipitation for the Hamlet and Lettenmaier data set compared to both CCSM3 monthly data at T85 (1.4°) resolution and CCSM4 daily data at 1.25° lat x 0.9° lon resolution. It is clear that climatological precipitation is more realistic in CCSM4, both in spatial structure and seasonal agreement with observations. Some of this improvement may be due to the slightly finer grid used by CCSM4 compared to CCSM3. In particular, CCSM4 does a better job simulating the magnitude and spatial structure of several important features during the wet (September thru February) season, including the large Pacific Northwest/northern California zonal gradient in precipitation and the circular "bullseye" pattern of enhanced precipitation over north-central Idaho. The former feature can be attributed to the presence of the Cascade Mountains and northern Sierra Nevada; the latter feature is likely due to large height gradients caused by the meeting of the Snake River Plain and the Salmon River Mountains. Thus, CCSM4 demonstrates regional dexterity in simulating orographically enhanced precipitation across the domain. In comparison, CCSM4's predecessor,

CCSM3, smeared the Pacific Northwest precipitation gradient over a wide region and was unable to capture the complex precipitation response over central Idaho. One deficiency in CCSM4's simulation is that it is drier than observations over the Pacific Northwest by several mm/day during the winter.

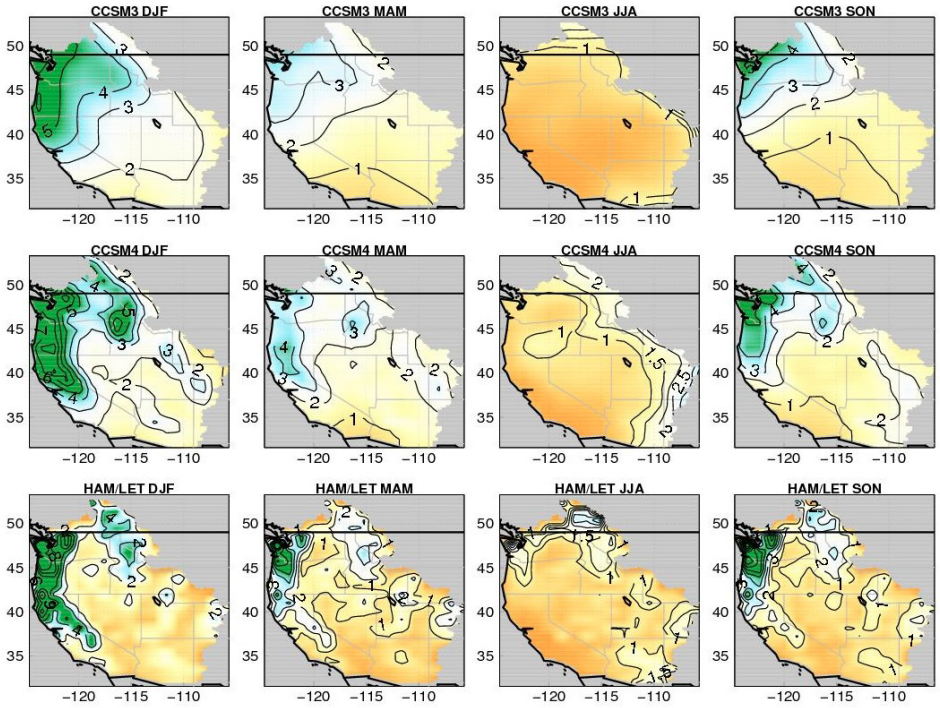

Figure 2.2: Seasonal climatology of precipitation (mm/day) for CCSM3, CCSM4, and observations; contour intervals are every 1 mm/day. CCSM4 shows improvement in capturing the strong observed zonal gradient in precipitation over the western U.S.

2.3.2 Fraction of precipitating days

As mentioned earlier, the "drizzle problem" of GCMs is a major barrier to realistic simulations of regional precipitation patterns. This problem manifests itself in the consistent over-prediction of the number of light precipitation days in GCM simulations (*Dai*, 2006). Here, we test for precipitation biases in CCSM4.

Figure 2.3 shows the fraction of precipitating days by season in CCSM3, CCSM4, and observations; again, a "precipitating day" is defined as a day on

which <0.1mm precipitation falls. Overall, the spatial distribution of precipitating day fraction in CCSM3 and CCSM4 is similar; both models have more frequent precipitation than is seen in observations. The discrepancy between the models and the observations is particularly large during the winter and spring, when the models have 20-30% more precipitating days than in observations over the majority of the domain. Notably, the sense of the model error is to over-predict precipitating days over both climatologically dry (southwest U.S.) and wet (Pacific northwest) regions. Figure 2.3 shows that precipitation biases, as determined from fraction of precipitating days, are similar in CCSM4 and CCSM3.

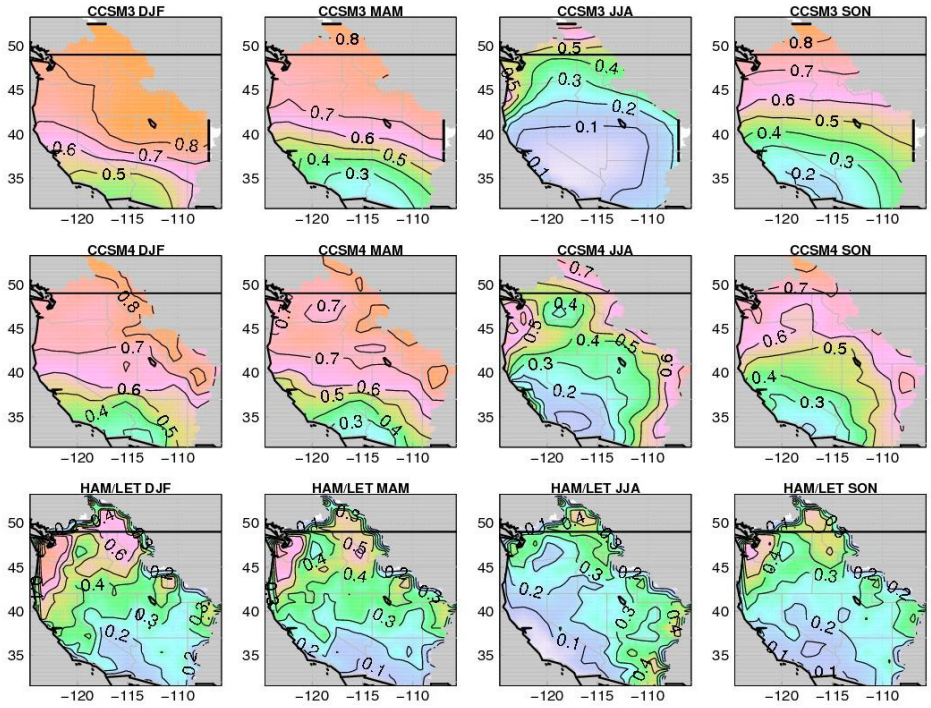

Figure 2.3: Fraction of precipitating days (>0.1 mm/day) for CCSM3, CCSM4, and observations. Both CCSM3 and CCSM4 exhibit wet biases across much of the domain during all seasons.

2.3.3 Precipitation intensity at the 90th percentile

Figure 2.4 shows the 90th percentile value of precipitation intensity in mm/day, by season, for CCSM3, CCSM4, and observations. The calculation is

made by averaging 90th percentile values for individual seasons, rather than choosing the 90th percentile value of the entire precipitation distribution. Choosing the former result is more robust, as the latter result could be skewed by a few extreme outlying years.

CCSM4 adeptly simulates the wet tail (i.e. 90th percentile) of the precipitation distribution across the entire domain, except in summer. Notably, during wet seasons, precipitation is most intense in north-central California, but has the greatest accumulation in the Pacific Northwest. The spatial displacement between precipitation intensity and accumulation manifests itself in the observations, and CCSM4 captures this feature quite well.

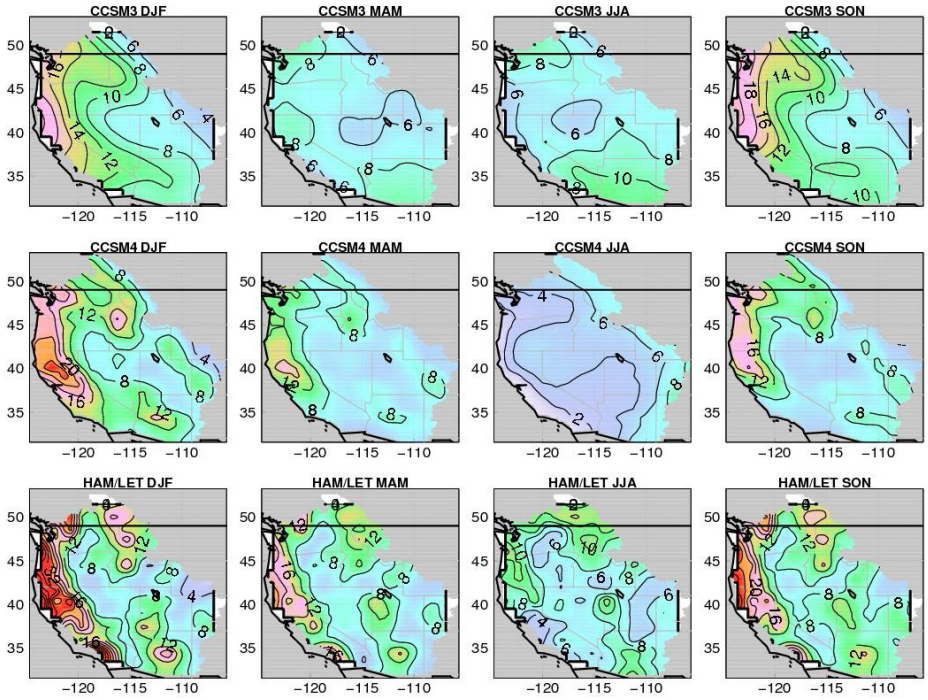

Figure 2.4: 90th percentile plot of precipitation intensity (mm/day) for CCSM3, CCSM4, and observations; contour labels are every 4 mm/day. CCSM4 captures observed extreme intensity events over the Sierra Nevadas, western Idaho, and central Arizona which were less resolved in CCSM3.

2.3.4 Precipitation duration at the 90th percentile

Figure 2.5 shows the 90th percentile value of precipitation duration in days, by season, for CCSM3, CCSM4, and observations. Again, precipitation duration is defined as consecutive strings of precipitating days. The 90th percentile calculation is made as in section 2.3.3, except that the 90th percentile value of interest is in units of "days" rather than "mm/day".

CCSM4's representation of extreme precipitation duration is markedly improved from that of CCSM3. Precipitation in CCSM3 persisted for several weeks too long during fall and winter, while precipitation duration in CCSM4 is consistent with observations to within several days during those times. When the "precipitating day" threshold is increased from 0.1 mm/day to 1 mm/day, 90th percentile precipitation duration values in CCSM3 decrease by about a week, suggesting that much of the persistence bias is occurring on low accumulation precipitation days (not shown). This is an apparent manifestation of the GCM drizzle problem. Though CCSM4 shows an improved simulation of 90th percentile precipitation duration, one notable error is that precipitation persists for too long in regions east of the Cascade Mountains, particularly during the summer and fall. In addition, CCSM4 does not reproduce the observed persistency in precipitation over the Pacific Northwest during winter, underestimating the duration of precipitation by several days.

2.4 El Nino Southern Oscillation (ENSO) and Pacific Decadal Oscillation (PDO)

Aside from its immediate association with climate in the tropics, ENSO also affects the global climate due to coupled ocean/atmosphere feedbacks and a redistribution of heat, moisture and momentum. ENSO shifts the location of the subtropical jet stream, which is the primary determinant of storm tracks over the midlatitudes (*Rasmusson and Wallace*, 1983; *Holton*, 2013). Additionally, it has been shown that the phase of ENSO directly affects the strength and direction of

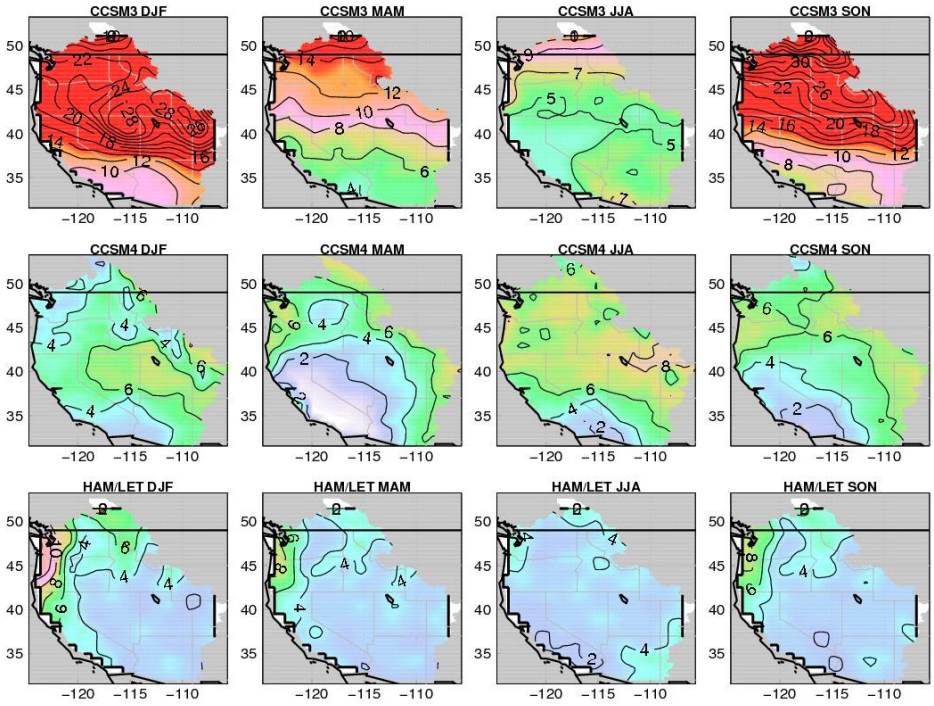

Figure 2.5: 90th percentile plot of precipitation duration (days) for CCSM3, CCSM4, and observations; contour labels are every 2 days. CCSM4 drastically reduces the persistent precipitation bias in CCSM3, especially during the winter and spring.

moisture transport from the tropics to the midlatitudes (*Dettinger et al.*, 2004).

Figure 2.6 shows a Pearson correlation map between the cold-seasonally averaged (NDJFM) PCs of the leading EOF of tropical SST anomalies and the cold-seasonally averaged precipitation anomaly field over the western U.S. for CCSM3 (a), CCSM4 (b), and observations (c). The seasonal mean fields are calculated with 1300 years of CCSM4 data, 500 years of CCSM3 data, and 50 years of observed data. CCSM4 captures both the dipole-like structure of the ENSO-precipitation teleconnection and, compared to CCSM3, a stronger magnitude commensurate with the observed pattern over much of the western United States (*Gershunov and Barnett*, 1998). However, the model underestimates the observed eastward extension of moderate positive correlation into Arizona and western New Mexico.

The Pacific Decadal Oscillation (PDO) is often defined as the leading EOF of North Pacific SST anomalies, and substantially impacts oceanic and atmospheric

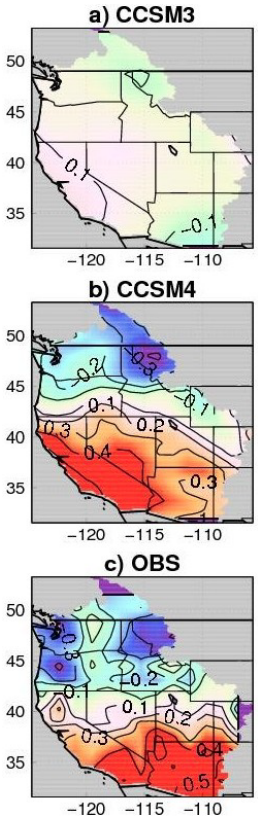

Figure 2.6: Pearson correlation map between NDJFM leading ENSO PCs and NDJFM precipitation anomalies for CCSM3 (a), CCSM4 (b), and observations (c)

climate variables (e.g. temperature, precipitation) in both hemispheres (*Trenberth and Hurrell*, 1994; *Mantua and Hare*, 2002). In addition, the PDO has been shown to modulate teleconnected patterns of oceanic and atmospheric circulation associated with ENSO (*Gershunov and Barnett*, 1998; *McCabe and Dettinger*, 1999). Significant peaks in the observed 20th century energy spectrum of the PDO have been shown at 50-70 year and 15-25 year timescales (*Mantua and Hare*, 2002). Notably, the PDO has not been robustly proven to be a dynamical mode, but rather the superposition of SST variability from multiple dynamical origins (*Pierce*, 2001; *Schneider and Cornuelle*, 2005).

Figure 2.7 shows a Pearson correlation map between the cold-seasonally averaged (NDJFM) PCs of the leading EOF of North Pacific SST anomalies and the cold-seasonally averaged precipitation anomaly field over the western U.S. for

CCSM3 (a), CCSM4 (b), and observations (c). The observed correlation map shows that the southern part of the domain experiences enhanced precipitation during positive PDO events, and vice versa, though the values are weak. (Note: positive PDO events are warm along the west coast of North America, and cold in the center of the Pacific Ocean). It is important to note the similarity between teleconnected responses of western U.S. precipitation to ENSO (Figure 2.6) and the PDO (Figure 2.7); that is, the tropical equatorial and North Pacific modes of SST variability in the Pacific are not independent, particularly in CCSM4 (*Newman et al.*, 2003; *Deser et al.*, 2012).

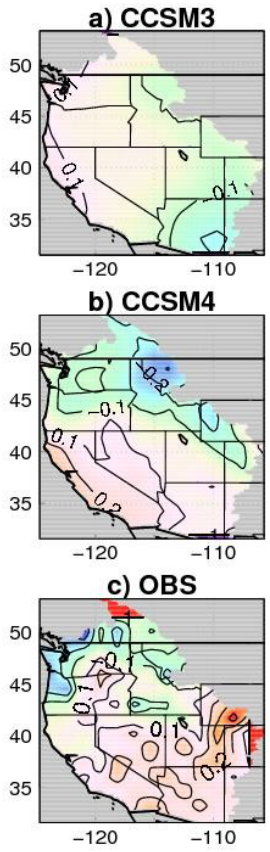

Figure 2.7: Pearson correlation map between NDJFM leading PDO PCs and NDJFM precipitation anomalies for CCSM3 (a), CCSM4 (b), and observations (c)

Using the observed teleconnection pattern (Figure 2.7c) as a metric, it would be appear that CCSM4's simulation of the teleconnected response of precipitation to PDO SST anomalies is improved compared to CCSM3. However, caution must

be taken when comparing results from multi-century model runs to decadal observational records. This is especially true when the signal of interest has a periodicity on the same order of the observed record, as in the case of the PDO. For example, Figure 2.8 shows two correlation maps as in Figure 2.7, but calculated in independent 50-year periods of the 1300-year run. To illustrate the range of variability, we chose the two 50-year periods that were most similar and dissimilar to the observed teleconnection pattern (Figure 2.7c). Although the sign of the relationship is consistent, with negative values over the Pacific Northwest and positive values in the Southwest, substantial spatial variability and differences in the magnitude of the correlations exist between the 1300 year average and the two 50-year segments. This temporal variation underscores the uncertainty of any particular estimate of the PDO teleconnection derived from a 50 year observed sample. Ideally, a sufficiently resolved, multi-centurial North Pacific observational dataset would be needed in order to make meaningful comparisons to multi-centurial model runs when considering the relationship of the PDO to western U.S. precipitation. In addition, a 50-year period is not sufficient to define the PDO itself.

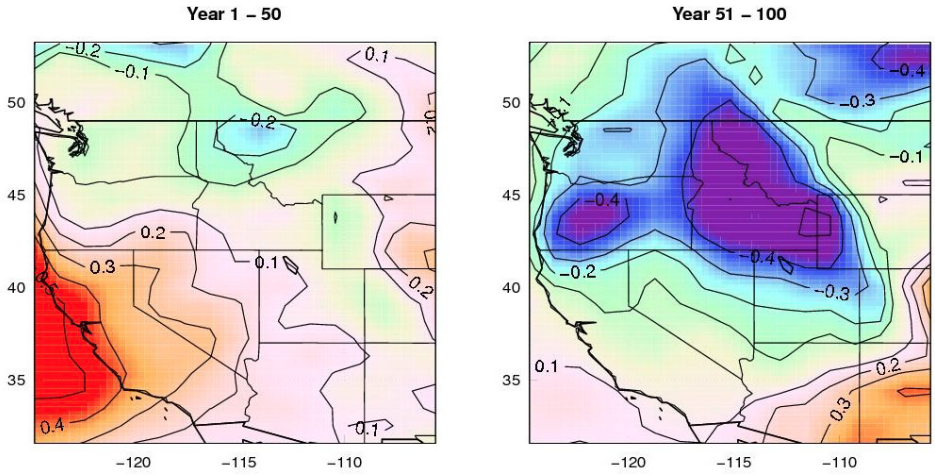

Figure 2.8: Pearson correlation map between CCSM4 NDJFM leading PDO PCs and NDJFM precipitation anomalies for two 50 year partitions. There is substantial variability in the spatial pattern.

2.5 Relating Extreme Precipitation Statistics to ENSO and PDO

We have shown that CCSM4 does an improved job of simulating western U.S. mean and extreme precipitation patterns and the teleconnected signal of ENSO and the PDO to western U.S. precipitation. However, the correlation analyses shown in section 2.4 assume a linear relationship between precipitation and ENSO/PDO. In this section, we employ composite techniques which do not require the assumption of linearity, and answer the questions: what are the characteristics of CCSM4 extreme precipitation statistics on warm and cool ENSO and PDO periods, are they asymmetric with respect to SST anomalies, and how do they compare to observations? We focus on CCSM4 since we have shown that CCSM3 is deficient compared to CCSM4 in the measures of western U.S. precipitation of interest here.

2.5.1 Extreme precipitation event composites

Figure 2.9 shows tropical and North Pacific surface temperature anomalies composited on wet (top 20th percentile) and dry (bottom 20th percentile) years for CCSM4 (top) and observations (bottom). The wet and dry periods were determined by calculating annual averages of monthly precipitation anomalies, averaged over a subset of the southwestern U.S. (240E to 250E, 32N to 35N for CCSM4; 245E to 249E, 34N to 37N for observations). Separate regions are chosen for the model and observations based on the positive correlation with ENSO seen in each region in Figure 2.6. Based on the results shown in Figure 2.6, one would expect tropical Pacific surface temperatures to be anomalously warm during wet periods (or anomalously cold during dry periods) over this subsetted region. It is evident that this occurs in both the model and observations; that is, the most anomalously warm values of surface temperature occur in the eastern equatorial Pacific on wet years, and vice versa on dry years. However, the model shows an almost completely symmetric response (the composite pattern for wet years is nearly the negative of the pattern for dry years), unlike the observations, which show a more tropical

connection for wet years and North Pacific connection for dry years. The model matches the observations in wet years, but in dry years, the differences between the model and observations are more pronounced.

This difference between the composite patterns for wet and dry years is shown in the rightmost column in Figure 2.9. The magnitude of CCSM4 equatorial Pacific SST anomalies on wet and dry years is greater than observations, reflecting the greater symmetry between wet and dry years found in the model.

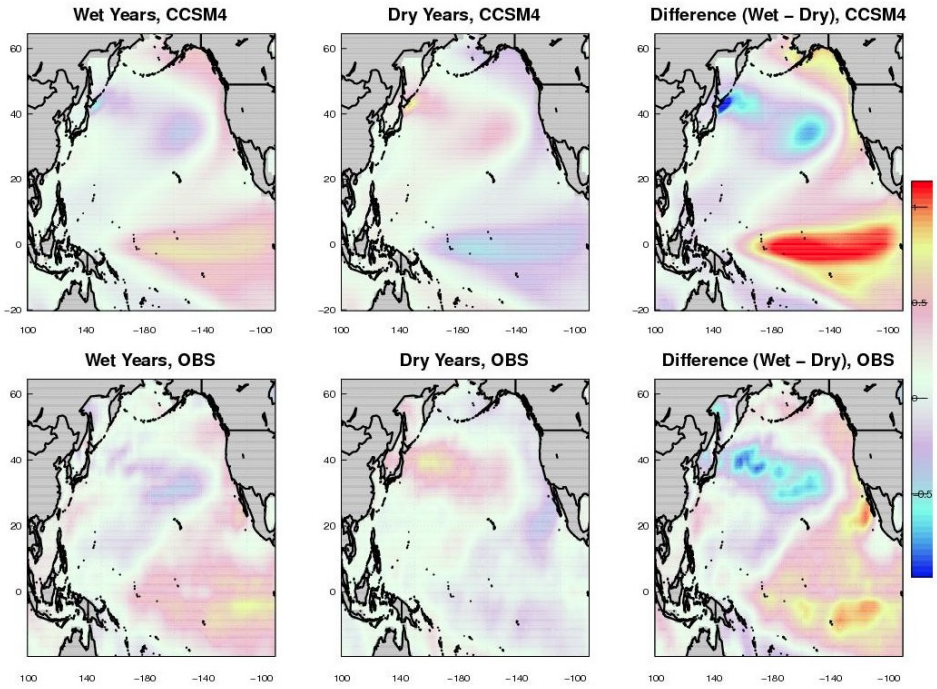

Figure 2.9: CCSM4 (top) and observed (bottom) annually averaged (January-December) monthly surface temperature anomalies (K) composite on wet (>80th percentile, left) and dry (<20th percentile, middle) southwestern U.S. years and their difference (right). There is a strong tropical Pacific SST anomaly signal associated with southwestern U.S. extreme precipitation regimes, particularly on the annual time scale; the signal is stronger and more symmetric in CCSM4 than in observations.

2.5.2 Precipitation intensity composites

To investigate the effect of ENSO and the PDO on extreme weather statistics, we composite extreme (90th percentile) wintertime (NDJFM) precipitation

intensity on wintertime seasons when the NDJFM ENSO index (top panel) or NDJFM PDO index (bottom panel) is warm (leading PC >0.75) or cool (leading PC <-0.75). Here, the PC is standardized and is thus unitless. Note that this analysis differs slightly from those used in section 2.3.3 in that 90th percentile precipitation intensity is calculated for each season (as before); those seasonal values then are composited on warm (leading PC >0.75) and cool (leading PC <-0.75) ENSO/PDO seasons and averaged. Thus, the calculation methodology is the same, but the compositing step is exclusive to this figure. Precipitation duration composites are not shown here due to the lack of a broad statistically significant relationship.

Figure 2.10 shows the difference between mean 90th percentile values of NDJFM precipitation intensity (mm/day) composited on warm and cool NDJFM ENSO (top panel) and NDJFM PDO (bottom panel) seasons. Differences significant at the 1σ and 2σ ($p < 0.32$ and $p < 0.05$) levels are shown as dark and light grey shading, respectively. CCSM4 is shown in the left column, while observations are shown in the right column.

The response seen in NDJFM ENSO seasons strengthens three important conclusions drawn from Figure 2.9. Firstly, Figure 2.10 shows that 90th percentile precipitation events in the cool season are stronger over the southwest during warm ENSO seasons than during cool ENSO seasons; the opposite is true over the Pacific Northwest. This is roughly consistent with Figure 2.9, which shows that warm ENSO conditions are prevalent during extreme wet periods over the southwest, and vice versa during extreme dry periods. Secondly, as in Figure 2.9, Figure 2.10 shows that CCSM4 overestimates the magnitude of extreme precipitation events during warm and cool NDJFM ENSO seasons. However, CCSM4 underestimates the observed PDO signal, especially during cool NDJFM seasons. Finally, there is a greater symmetry of the response of extreme precipitation on positive and negative ENSO and PDO phases in CCSM4 than in observations.

The results from figures 2.9 and 2.10 demonstrate the relationship in CCSM4 between the phase of ENSO (and to a lesser degree, the PDO) and extreme precipitation statistics over the western U.S., and underscore the model's exaggeration

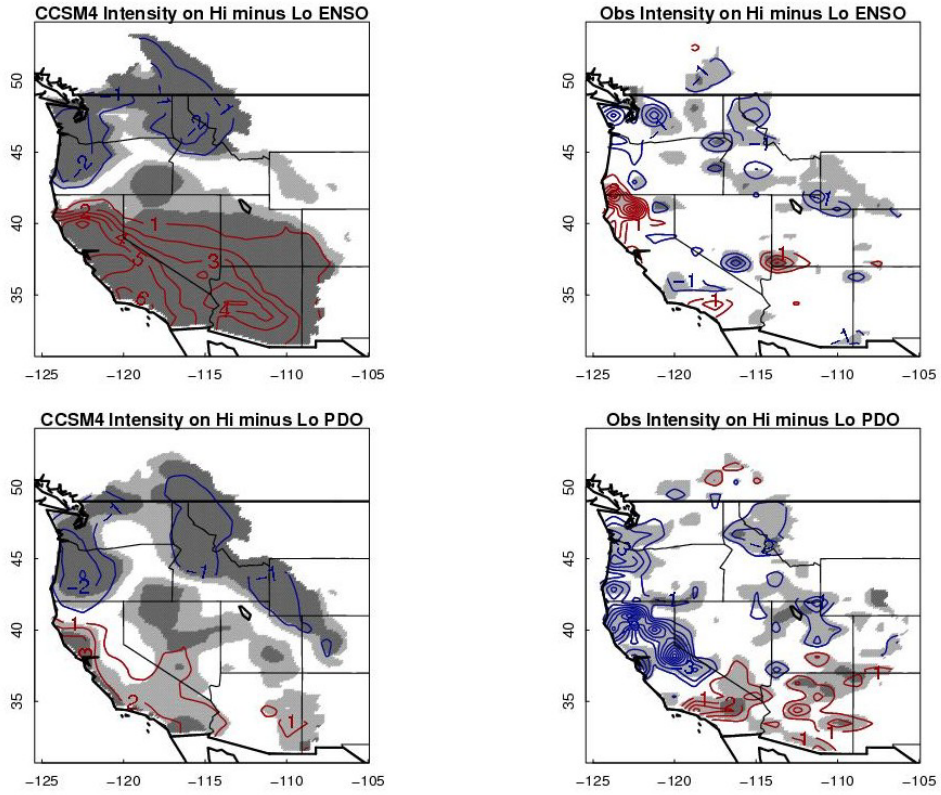

Figure 2.10: Difference (warm - cool) of mean 90th percentile value of NDJFM precipitation intensity (mm/day) on warm (leading PC >0.75) and cool (leading PC <-0.75) NDJFM (top) ENSO and (bottom) PDO years, with 95% (dark gray) and 68% (light gray) confidence intervals shaded, for (left) CCSM4 and (right) observations. Positive values are indicated by red contours, indicating that 90th percentile precipitation intensity values are higher in warm NDJFM seasons than in cool seasons; the opposite is true for negative values, indicated by blue contours. For ENSO, heavy wintertime (NDJFM) precipitation intensity in CCSM4 is significantly stronger over the southwest during warm ENSO years than in cool ENSO years, and the response is stronger than in observations. This is consistent with expectations from Fig. 2.9. For the PDO, a similar qualitative pattern to ENSO years exists in CCSM4, but it is weaker. The observations are consistent and show a much stronger cool season signal that extends farther south.

of this relationship compared to observations.

2.6 Discussion and Conclusions

Results shown here demonstrate that, in comparison to CCSM3, the newer CCSM4 version of the United States Community Climate Model produces improved simulations of both regional, synoptic precipitation events over the western U.S. and tropical pacific (ENSO) and North Pacific (PDO) teleconnections to western U.S precipitation. We concentrate on the differences between model generations rather than the effects of varying horizontal resolution on model results, although future studies of the latter are required to paint a complete picture of model behavior.

Notably, observed teleconnected signals of equatorial SST anomalies to western U.S. precipitation anomalies are well captured by CCSM4 and represent a substantial improvement from CCSM3. The correlation between PDO SST anomalies and western U.S. precipitation is also well-simulated in CCSM4, although the relatively short observational record means that the patterns can differ appreciably due to natural internal climate variability (see Figure 2.8).

Over the western U.S., CCSM4 captures several important local and regional precipitation features. The climatological pattern of CCSM4 western U.S. precipitation agrees with that from observations, and the amounts are similar to within several mm/day. In comparison to CCSM3, the zonal gradient of precipitation in CCSM4, which is influenced heavily by the Cascade and Sierra Mountains, is correctly larger over Northern California and the Pacific Northwest. CCSM3's simulation of this gradient was too small, causing precipitation estimates to be smeared eastward across the region. This could be partially due to the fact that CCSM3's horizontal resolution (1.4°) is slightly coarser than CCSM4's (1.25° lon x 0.9° lat) in the runs analyzed here, but since the resolutions are close, it is likely that CCSM4 is handling the impact of orography on precipitation more realistically. In addition, the wintertime secondary maximum in precipitation over north-central Idaho seen in observations is found in CCSM4, but absent in CCSM3. The displacement between the wettest climatological region (over central Oregon and southwestern Washington) and the most intense storm region (which spreads further southward) that is seen in observations is captured by CCSM4 during the

wet season. Extreme precipitation duration, which was too persistent by several weeks in CCSM3, is now correct in CCSM4 to within several days of observations.

Compositing extreme cold-season precipitation metrics on warm and cool ENSO and PDO seasons in CCSM4 revealed that precipitation intensity is particularly sensitive to the phase of ENSO, and that there is a relationship in CCSM4 between the phase of ENSO (and to a lesser degree, the PDO) and extreme precipitation statistics over the western U.S.

This study demonstrates that CCSM4 shows many improvements in simulating the teleconnected response of western U.S. precipitation to ENSO and the PDO, and that the model's relationship between ENSO and extreme western U.S. weather statistics is consistent with observations, though too strong. Similar studies investigating CCSM4's regional climate in other locations could prove useful, so that the consistency of the model dynamics in CCSM4 can be tested across different regions. Studies investigating effects of varying model horizontal resolution may wish to consider how model spatial resolution affects precipitation duration and intensity. On balance, though, the similarity of a range of characteristics of CCSM precipitation to those in observations indicate that the results shown here could provide a basis to understand possible future changes using CCSM4 under greenhouse gas emissions scenarios.

2.7 Acknowledgements

This study forms a portion of the Ph.D. dissertation of MJD. Funding was provided by NSF (OCE-0960770 and AGS-1048995), DOE (DE-SC0002000) and NOAA (ECPC: NA17RJ1231). Thanks to Andrew Gettelman (NCAR) for providing information about CCSM4 runs, Alexander Gershunov (SIO) for enlightening discussions regarding North Pacific variability, and Stephen Colucci (Cornell University) for theoretical background on midlatitude synoptic storms. We also thank Aneesh Subramanian (SIO) for assistance in accessing the CCSM4 monthly run. Suggestions by three reviewers were very useful in improving the paper.

Chapter 2 is published in its entirety in:

- **DeFlorio, M.J.**, D. W. Pierce, D. R. Cayan, and A. J. Miller, 2013: "Western U.S. Extreme Precipitation Events and Their Relation to ENSO and PDO in CCSM4". *J. Clim.*, **26**, 4231-4243.

2.8 Appendix

The following analyses supplement Section 2.4 and provide further evaluation of the representation of CCSM4 ENSO teleconnection patterns across the North Pacific. These figures were omitted from the published version of our paper for brevity, but are included here for completeness.

2.8.1 Teleconnected signal of upper-level zonal wind anomalies

In accordance with its influence on extratropical precipitation patterns, the phase of El Nino substantially alters the strength and position of both the subtropical and polar jet stream. These jets act both independently and together to impact weather patterns across the United States (*Holton*, 2013). We therefore choose to investigate CCSM4 simulation of upper-level zonal wind anomalies, a relevant jet stream metric. Examining results over the tropical Pacific is also insightful, since Hadley Cell dynamics are heavily influenced by anomalies in the upper-level zonal wind field.

Figure 2.11 shows a Pearson correlation map between the Nino 3.4 index (190E to 240E; 5S to 5N) and upper-level (225 hPa) zonal wind anomalies for CCSM4 (a) and NCEP Climate Forecast System Reanalysis (*Saha et al.*, 2010) (b). Positive values show where warm SST anomalies are associated with upper level westerly wind anomalies, and negative values, with easterly wind anomalies. To digest the ramifications of Figure 2.11, first consider the near-equatorial domain spanning from 175E to 225E; 5S to 5N, where the strongest negative reanalyzed correlations are located. During an El Nino event, the area-averaged SST anomalies used in the correlation calculation will be positive due to the eastward extension of the west Pacific warm pool. Thus, negative correlations in this region imply that

the upper-level westerlies formed as a result of large-scale Hadley cell circulation will weaken. It follows that the opposite scenario will occur during a La Nina event, where area-averaged equatorial SST anomalies will be negative. Both the spatial structure (zonal and meridional) and magnitude of this alteration in the upper-level anomalous zonal circulation is captured in CCSM4 throughout the North Pacific. Notably, however, the weakly negative correlation that appears in the reanalyzed data over eastern China and southern Japan is weakly positive in the modeled correlation.

2.8.2 Teleconnected signal of sea level pressure anomalies

Mean sea level pressure is a common metric used to diagnose synoptic storm intensity (*Holton*, 2013). Fluctuations of sea level pressure will occur as a result of various dynamical mechanisms in the atmosphere.

To better understand the response of sea level pressure to dynamical forcings, consider a dry atmosphere in hydrostatic balance,

$$\frac{\partial z}{\partial p} = \frac{-RT}{pg} \tag{2.1}$$

where z is geopotential height, p is pressure, R is the dry gas constant, T is temperature, and g is the gravitational constant. In addition, consider the Eulerian thermodynamic energy equation for a dry atmosphere, which can be written as

$$\frac{\partial T}{\partial t} = \frac{1}{c_p}\frac{dh}{dt} - V_h \cdot \bigtriangledown_p T + \frac{\omega \sigma p}{R} \tag{2.2}$$

where c_p is the specific heat capacity of air at a constant pressure, h is the heat content of an air parcel, V_h is the horizontal wind, ω is vertical velocity in pressure coordinates ($= \frac{dp}{dt}$), and σ is the static stability parameter ($= \frac{-\alpha}{\theta}\frac{\partial \theta}{\partial p}$, where α is the specific volume of an air parcel and θ is the potential temperature of an air parcel). The first term on the right hand side of 2.2 represents the rate of diabatic heating of an air parcel; the second term represents the advection of temperature on a constant pressure surface by the horizontal wind; the third term represents the rate of adiabatic heating of an air parcel.

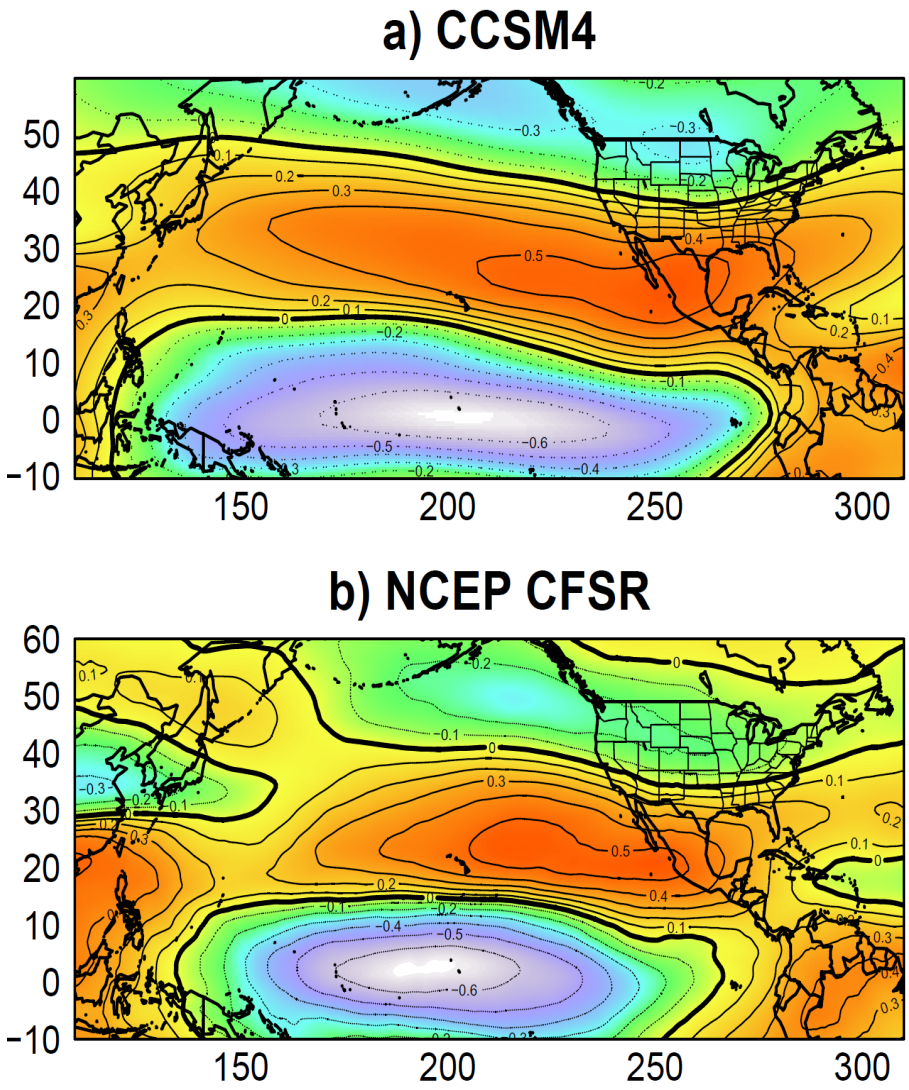

Figure 2.11: Pearson correlation map between area-averaged Nino 3.4 SST anomalies and 225hPa zonal wind anomalies for CCSM4 and NCEP CFSR.

Differentiating 2.1 with respect to time, integrating 2.1 with respect to pressure from the surface (1000hPa) to the top of the atmosphere (approximately 10hPa), and substituting 2.2 for $\frac{\partial T}{\partial t}$ yields

$$(\frac{\partial z}{\partial t})_{1000hPa} = (\frac{\partial z}{\partial t})_{10hPa} - \frac{R}{g}\int_{10hPa}^{1000hPa}(-V_h \cdot \bigtriangledown_p T + \frac{\omega\sigma p}{R} + \frac{1}{c_p}\frac{dh}{dt})\frac{dp}{p} \qquad (2.3)$$

Furthermore, $(\frac{\partial z}{\partial t})_{1000hPa} = \frac{\partial SLP}{\partial t}$. Thus, sea level pressure will fall where

there is vertically integrated warm air advection, adiabatic warming, and diabatic warming, and rise where there is vertically integrated cold air advection, adiabatic cooling, and diabatic cooling. Though a dynamical budget for cyclone intensification and weakening in CCSM4 is outside of the scope of our paper, the above analysis demonstrates the necessity for the model to appropriately capture the teleconnection between equatorial SST anomalies and sea level pressure, since the latter is an insightful metric by which storm intensification can be measured.

Figure 2.12 shows a Pearson correlation map between the Nino 3.4 index and sea level pressure anomalies for CCSM4 (a) and NCEP CSFR (b). Positive values show where warm SST anomalies are associated with positive SLP anomalies, and negative values, with negative SLP anomalies. The model does well in the tropics, capturing the features of the Walker Cell: both the decrease of SLP during El Nino events in the eastern Pacific (or increase of SLP during La Nina events), and the increase of SLP during El Nino events in the western Pacific (or decrease of SLP during La Nina events). Elsewhere, some disparities exist. For example, along the California coast, $corr_{ccsm4} < corr_{cfsr}$, which implies that CCSM4 simulates anomalously low SLP during El Nino events (or anomalously high SLP during La Nina events) compared to CFSR. However, the off-equatorial teleconnected signal of sea level pressure anomalies is generally very well represented in CCSM4.

2.8.3 Teleconnected signal of 500hPa geopotential height anomalies

500hPa geopotential height is a synoptic storm metric that can be used to identify synoptic storm type and intensity in the absence of boundary layer friction (*Holton*, 2013). In addition, 500hPa is a mid-tropospheric level that is well suited to represent large scale atmospheric circulation and key processes involved in mid-latitude storms and teleconnections. Figure 2.13 shows a Pearson correlation map between the Nino 3.4 index and 500hPa geopotential height for CCSM4 (a) and NCEP CSFR (b). Positive values show where warm SST anomalies are associated with positive 500hPa height anomalies, and negative values, with negative 500hPa anomalies. The correlation between these two variables is unrealistic in both mag-

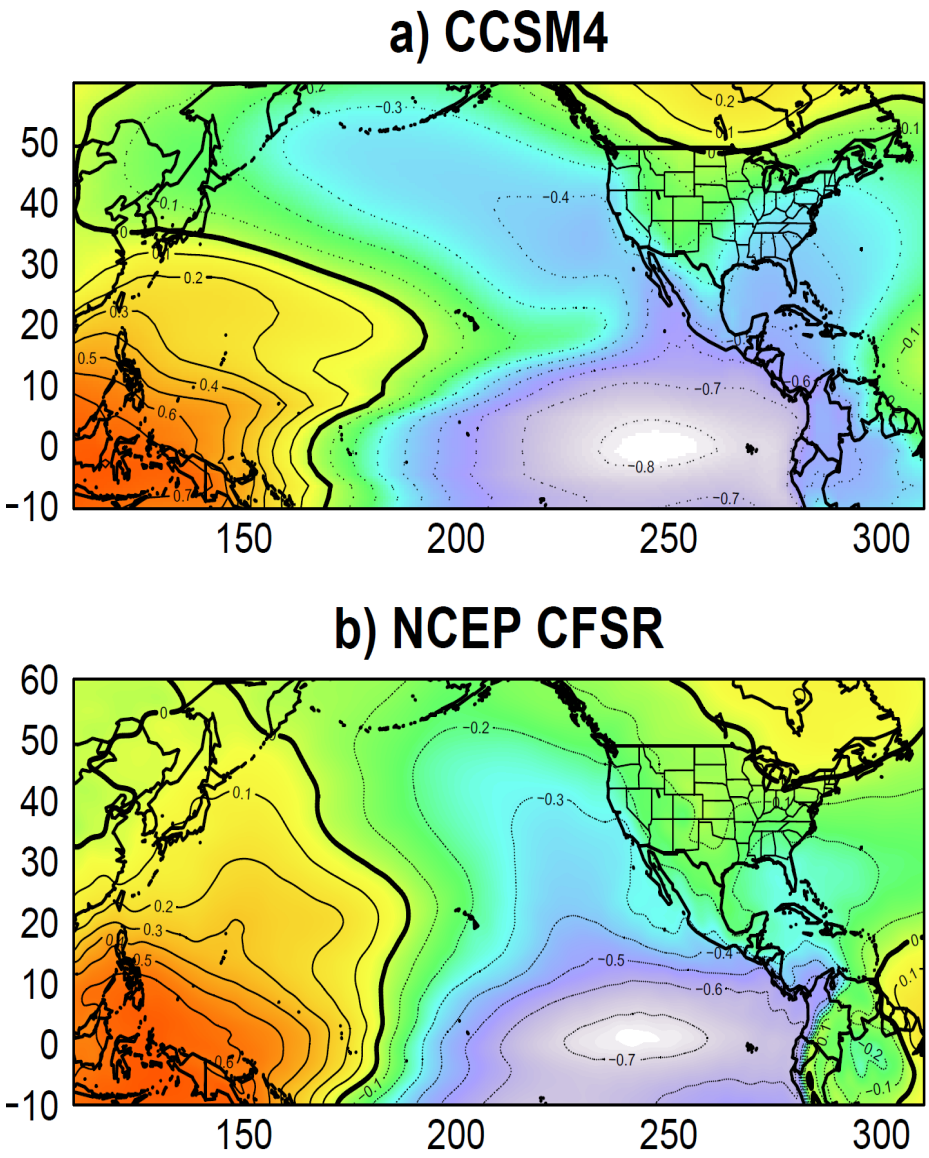

Figure 2.12: Pearson correlation map between area-averaged Nino 3.4 SST anomalies and sea level pressure anomalies for CCSM4 and NCEP CFSR.

nitude and spatial distribution. Although broad reanalyzed patterns of positive and negative correlation in the tropics and over North America, respectively, are present in CCSM4, the modeled correlation magnitude is almost double the observed magnitude over the tropical Pacific, and the sign of the modeled correlation is incorrect over the subtropical North Pacific region.

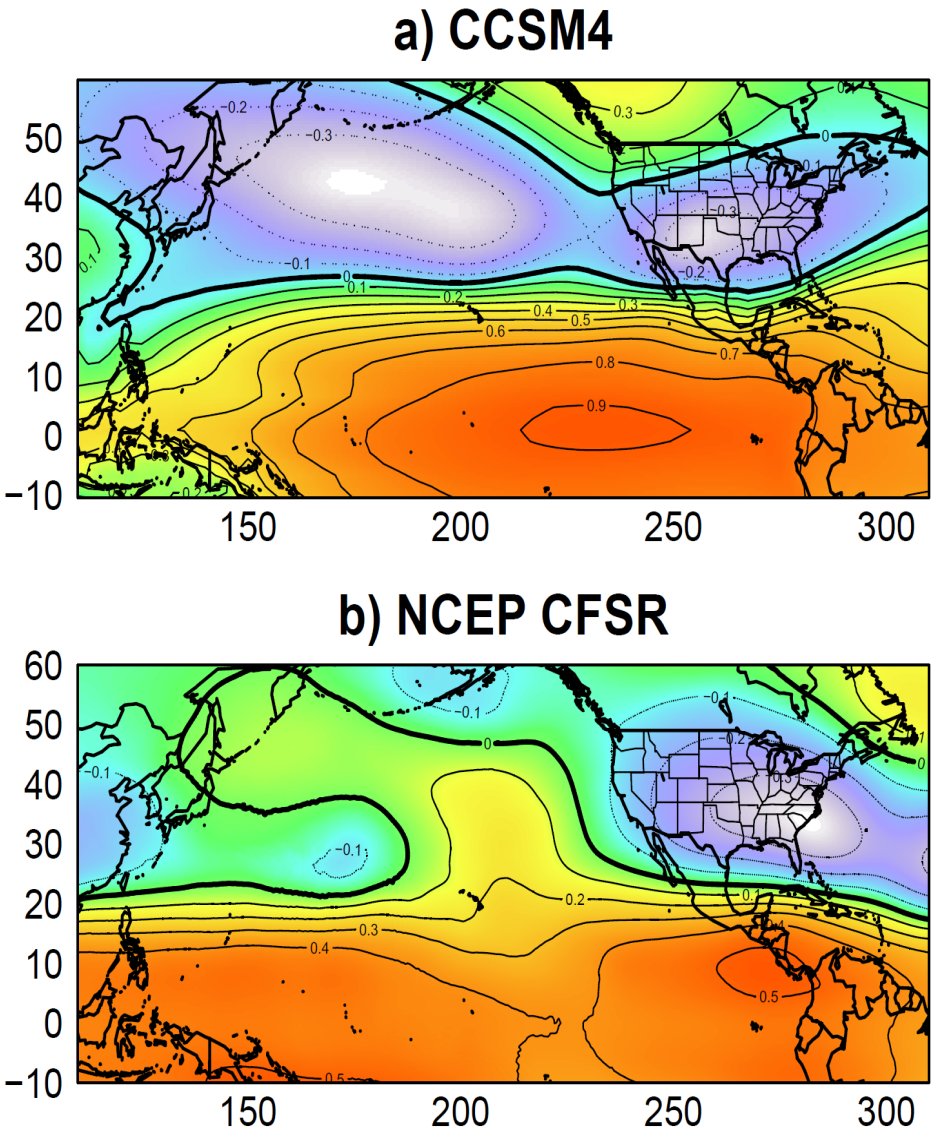

Figure 2.13: Pearson correlation map between area-averaged Nino 3.4 SST anomalies and 500hPa geopotential height anomalies for CCSM4 and NCEP CFSR.

Chapter 3

Semi-direct dynamical and radiative effect of North African dust transport on lower tropospheric clouds over the subtropical North Atlantic in CESM 1.0

This study uses a century length preindustrial climate simulation by the Community Earth System Model (CESM 1.0) to explore statistical relationships between dust, clouds, and atmospheric circulation and to suggest a semi-direct dynamical mechanism linking subtropical North Atlantic lower tropospheric cloud cover with North African dust transport. The length of the run allows us to account for interannual variability of North African dust emissions and transport in the model. CESM's monthly climatology of both aerosol optical depth and surface dust concentration at Cape Verde and Barbados, respectively, agree well with available observations, as does the aerosol size distribution at Cape Verde. In addition, CESM shows strong seasonal cycles of dust burden and lower tropospheric cloud

fraction, with maximum values occurring during boreal summer, when a strong correlation between these two variables exists over the subtropical North Atlantic. Calculations of Estimated Inversion Strength (EIS) and composites of EIS on high and low downstream North African dust months during boreal summer reveal that dust is likely increasing inversion strength over this region due to both solar absorption and reflection. We find no evidence for a microphysical link between dust and lower tropospheric clouds in this region. These results yield new insight over an extensive period of time into the complex relationship between North African dust and North Atlantic lower tropospheric clouds, which has previously been hindered by spatiotemporal constraints of observations. Our findings lay a framework for future analyses using different climate models and sub-monthly data over regions with different underlying dynamics.

3.1 Introduction

The role of aerosols in the climate system is complex, and their forcing on the climate system remains a large uncertainty in model projections of climate change (*Stevens and Feingold*, 2009). Aerosols originate from a variety of natural and anthropogenic sources and induce both direct (via scattering, reflection, and absorption) and indirect (via cloud seeding) effects on Earth's radiative budget (*Twomey*, 1974; *Albrecht*, 1989; *Leaitch et al.*, 1992; *Kiehl and Briegleb*, 1993; *Jones et al.*, 1994; *Lohmann and Feichter*, 2005; *Carslaw et al.*, 2010).

Mineral dust in particular interacts with local and remote climate in a variety of ways. It is an effective absorber and scatterer of incoming shortwave radiation and an effective absorber and emitter of outgoing terrestrial longwave radiation (*Tegen et al.*, 1996; *Penner et al.*, 2001; *Sokolik et al.*, 2001; *Tegen*, 2003), and has been linked to modification of cloud properties and precipitation (e.g. *Kaufman et al.* (2005)). Dust has been shown to suppress precipitation by acting as cloud condensation nuclei (CCN) that decrease droplet size (*Rosenfeld et al.*, 2001), and to alter radiative and meteorological characteristics of upper tropospheric clouds by serving as ice condensation nuclei (*DeMott et al.*, 2003;

Sassen et al., 2003; *Smoydzin et al.*, 2012). The impact of dust on cold-phase clouds and subsequent precipitation has received considerable attention recently, as several studies have examined the remote influence of transported Asian dust on heavy orographically enhanced precipitation over the Sierra mountain range (*Rosenfeld et al.*, 2008; *Ault et al.*, 2011).

The largest global source of dust is the North African Sahel-Sahara desert region, which emits approximately 800 Tg of dust each year (*Huneeus et al.*, 2011). Consequently, the impact of North African dust on global climate has received considerable attention over the past several decades, and has spawned a number of biogeochemical, meteorological, and climatic studies that focus on the effect of mineral dust on clouds, circulation, and radiation both locally and in remote regions downwind of dust sources (*Prospero and Nees*, 1986; *Martin*, 1990; *Okin et al.*, 2004; *Chiapello et al.*, 2005; *Evan and Mukhopadhyay*, 2010; *Mahowald et al.*, 2010).

This transport of mineral dust in Earth's atmosphere downwind of arid high source regions has been observed for centuries. 19th and early-to-mid 20th century observations were made by ships (*Darwin and Bettany*, 1890; *Prospero and Bonatti*, 1969) or by land stations that measured advected dust (*Prospero et al.*, 1970). Many subsequent studies of observed mineral dust were greatly aided by the onset of the satellite era and the development of remote sensing techniques for mineral aerosols (*Ackerman and Chung*, 1992; *Moulin et al.*, 1997; *Evan et al.*, 2006c). These improvements allowed for the detection of dust over the ocean at improved spatial resolutions, spanning longer continuous periods of time. Specific to the North African region, *Evan and Mukhopadhyay* (2010) implemented a simple statistical model to extend satellite-retrieved dust measurements over the northern tropical Atlantic from 1955-2008.

Despite these improvements, it remains challenging to obtain a coherent spatiotemporal record of dust, circulation, and clouds over North Africa and the tropical-subtropical north Atlantic that is extensive enough to calculate robust statistics that are of sufficient length to address climate-related questions. To provide such a record, this study uses oceanic and atmospheric output from a

state-of-the-art century length global coupled climate model simulation with an interactive aerosol treatment to address several important questions: a) What are the characteristics of seasonal variability in dust emissions, dust transport, and other relevant meteorological variables over North Africa and the North Atlantic basin? b) Is there a multi-year mode of variability in the emissions and transport of dust over North Africa, and is the interannual variability stronger during particular seasons? c) How are North African dust emissions and transport related to lower tropospheric stratiform clouds over the tropical and subtropical North Atlantic, downstream of high dust source regions? d) Does dust residing in the lower troposphere in boreal summer promote boundary layer stratiform cloud growth by strengthening the inversion in the lower troposphere downstream of North Africa?

These questions are important because the response of radiative forcing of optically thick stratiform clouds in the lower troposphere to climate change is still one of the largest sources of uncertainty in climate models (*Yokohata et al.*, 2010; *Klocke et al.*, 2011). In addition, enhanced lower tropospheric cloud growth due to increased dust transport could further decrease the likelihood of hurricane formation in the Atlantic due to reduced sea surface temperature (*Evan et al.*, 2009), which has the potential to strongly impact the economy of Caribbean island nations, Mexico, and the eastern United States.

This is the first study to use a century length coupled model simulation with an interactive modal aerosol treatment to explore statistical relationships between North African dust, clouds and circulation. The Community Earth System Model (CESM 1.0) (*Hurrell et al.*, 2013) is chosen for this study because of its inclusion of the aerosol indirect effect and its ability to capture observed spatiotemporal variability of aerosol mass and number concentrations, size distributions, and aerosol optical properties (*Liu et al.*, 2012). Our results suggest a dynamical and radiative, rather than microphysical, mechanism linking subtropical North Atlantic lower tropospheric cloud cover with dust transported from North Africa. This semi-direct mechanism is similar to the one identified by *Koch and Del Genio* (2010) for black carbon aerosols.

3.2 Data Used

3.2.1 CESM 1.0 150 Year Simulation

We ran a 150-year pre-industrial global simulation using CESM 1.0.3 with interactive dust emission and transport, which allows dust as well as other components of the aerosol to affect radiative budgets and cloud properties at each time step (*Hurrell et al.*, 2013). The simulation was run at a horizontal resolution of 2.5° (lon) x 1.9° (lat). The component set for this simulation is 1.9x2.5gx1v6 B1850CAM5CN, and the code base is CESM 1.0.3. Monthly simulation output was saved for several species of aerosols, including mineral dust (e.g. surface emissions, optical depth, atmospheric burdens, absorption, vertical concentrations) and associated variables relevant to understanding aerosol and cloud processes. This CESM simulation features a realistic seasonal cycle of dust and African easterly jet formation and improved parameterizations of boundary layer clouds and cloud microphysics (*Bretherton and Park*, 2009; *Park and Bretherton*, 2009; *Gent et al.*, 2011; *Neale et al.*, 2013; *Hurrell et al.*, 2013).

A century-length simulation is necessary due to interannual variability of boreal summer dust emissions and transport over the North African and eastern subtropical North Atlantic associated with the El Nino-Southern Oscillation (ENSO) in CESM (not shown).

3.2.2 CAM5 Trimodal Treatment of Aerosols in Long CESM Runs

For extensive climate runs (decades to millennia), CAM5 treats aerosols using a tri-modal aerosol module (MAM3) that includes an Aitken (small), accumulation (medium), and coarse (large) mode representation of aerosol species. Figure 3.1 lists the species in each mode, whose properties are predicted forward in time over the course of the simulation (see *Liu et al.* (2012) for more details). Mineral dust is emitted in both the coarse and accumulation modes using the *Zender et al.* (2003) Dust Entrainment and Deposition Model, as described by

Liu et al. (2012). The cut-off size range for dust emissions is 0.1-1.0μm for the accumulation mode, and 1.0-10μm for coarse. Dust is assumed to be internally mixed with the other components in each mode, with the bulk hygroscopicity and refractive index of each mode calculated assuming volume mixing of the hygroscopicity and refractive index values of each component (including water in the case of refractive index) in the mode. Water uptake is calculated using κ-Kohler theory (*Petters and Kreidenweis*, 2007). Volume mixing enhances absorption by dust when coated with sulfate, organic, and water. The hygroscopicity (κ) for mineral dust is specified as 0.068, while the dust refractive indices are from OPAC (*Hess et al.*, 1998). The imaginary part of the refractive index for the OPAC dust is known to be greater than that retrieved for Saharan dust (*Sinyuk et al.*, 2003), so excessive absorption by dust in the simulation should be kept in mind. Dust optical properties (extinction efficiency, absorption efficiency, asymmetry factor) are parameterized from Mie calculations (*Ghan and Zaveri*, 2007). Dust is transported by the resolved winds, vertical diffusion, and cumulus mass flux in CAM5. And removed by dry deposition, nucleation scavenging, and impact scavenging as described by *Liu et al.* (2012).

Aitken	**Accumulation**	**Coarse**
Sulfate	Sulfate	Soil dust
Secondary OM	Secondary OM	Sea salt
Sea salt	Primary OM	Sulfate
	Black carbon	
	Soil dust	
	Sea salt	

Figure 3.1: Trimodal treatment of aerosols in century length interactive CESM 1.0 runs similar to the one used in this study.

3.2.3 NASA AERONET Observational Data Set

We evaluate aerosol optical depth and volume size distribution in CAM5 using approximately 20 years of NASA AERONET (Aerosol Robotic Network) Version 2 Direct Sun Algorithm and Inversions data (Level 2.0) collected at Cape Verde (16N, -22W). Station data at this site are available from January 1996 to

April 2013, and were quality controlled to distinguish between aerosol and cloud (*Smirnov et al.*, 2000). Pre- and post-field calibration were applied to the AOD data, which were also automatically cloud cleared and manually inspected for quality control. The dataset at Cape Verde is limited by an instrument malfunction, which caused missing data for several months in the 17-year record. We also evaluate AOD at Ragged Point near Barbados (13N, -60W), where data is available from August 2007 to April 2014. Retrieval development and implementation techniques for AERONET inversion products were introduced in (*Dubovik and King*, 2000).

3.2.4 Barbados Dust Observational Data Set

We evaluate surface dust concentration in CAM5 by using 44 years of monthly mean data recorded at Barbados from 1965-2008 (*Prospero and Lamb*, 2003). Recorded concentrations are based on the ash weight of the filter after extracting solubles. The monthly means are comprised of samples where the run time was greater than 10%; samples whose run times were under 10% were not included because of limited data and unreliable surface wind measurements.

3.2.5 ISCCP Cloud Data

For evaluation of lower tropospheric cloud fraction, we use the ISCCP D1 series global dataset, which spans from January 1984 to December 2009 and has a horizontal resolution of 2.5° (lon) x 2.5° (lat) (*Rossow and Schiffer*, 1991). The dataset has been corrected for artifacts with normalization and meteorological indices, and the cloud fraction is averaged to monthly values. Although the CALIPSO dataset has superior vertical resolution, it is only available from 2006-2012, which is a major drawback given the length of our CESM simulation.

3.2.6 Dust Variables Used in This Study

In this study, we will focus on analyzing three dust variables: A) total atmospheric dust burden (g/m^2), which vertically integrates all dust modes to obtain

a column dust mass at each grid cell; B) accumulation mode dust concentration (kg dust/kg air); and C) coarse mode dust concentration (kg dust/kg air). B) and C) are saved at 30 vertical levels in the atmosphere and allow us to examine the vertical structure of dust over our regions of interest. We calculate seasonal averages of all variables used in this study to discern the strong seasonal cycle of dust observed in the North African region (*Prospero and Nees*, 1986).

3.3 Evaluation of CAM5 Aerosol Optical Depth, Volume Size Distribution, and Surface Dust Concentration

Before analyzing CAM5 output, it is important to determine whether or not its representation of aerosol optical depth (AOD), volume size distribution, and surface dust concentration are in reasonable agreement with limited available observations. For AOD and volume size distribution, we use AERONET observations near Cape Verde; for surface dust concentration, we evaluate CAM5 using the observations from Barbados. This approach gives a sense of the realism of CAM5 dust both near and downstream of the high source region over North Africa.

Most of the AOD near Cape Verde is produced by dust, so AOD is a good indicator of the dust column burden. Figure 3.2 shows monthly climatologies of 530nm AOD near Cape Verde (16N, -22W) for AERONET (red) and CAM5 (black). Recall that the AERONET dataset spans 17 years, while the CAM5 simulation is 150 years long. We obtained AERONET AOD at 530nm by calculating the Angstrom exponent using measurements at 440nm and 675nm, since AERONET does not retrieve AOD at 530nm at Cape Verde. The annual cycle of AOD is similar for all three datasets, though boreal autumn values are approximately 30% higher in AERONET. The error bars are larger for AERONET due in part to the shorter record length relative to CAM5, and the error bars generally increase during the spring and summer. The width of the error bars is larger in summer relative to late fall and winter, which suggests that interannual variability

of AOD is larger during summer.

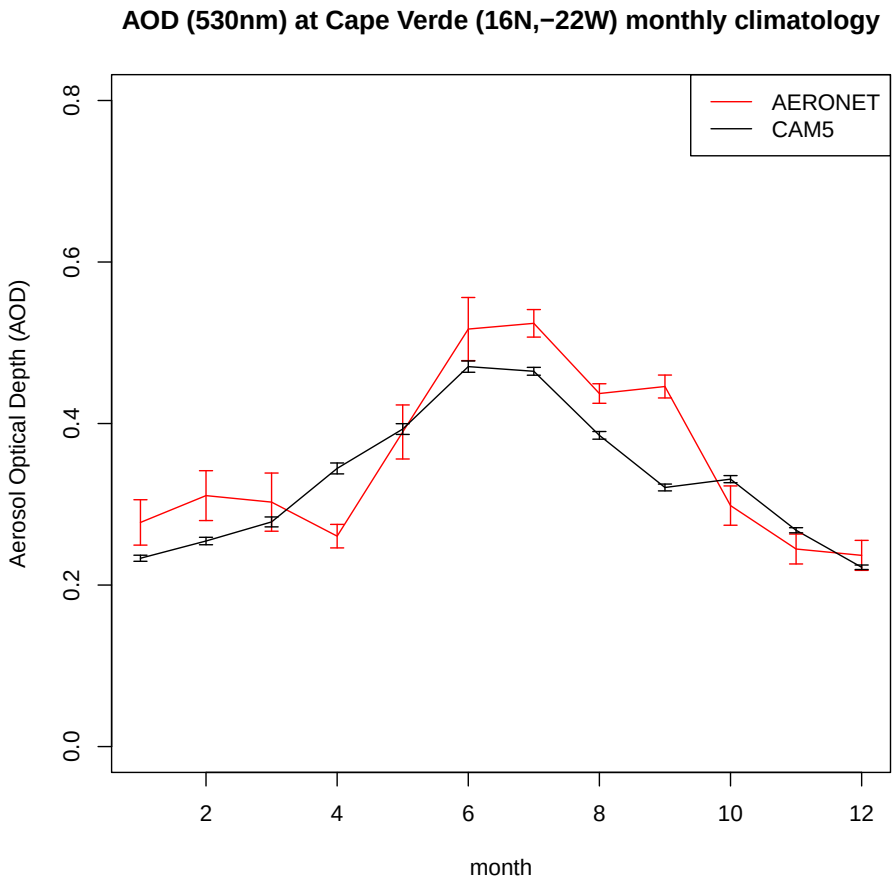

Figure 3.2: Mean monthly climatology of 530 nm aerosol optical depth (AOD) near Cape Verde (16°N, −22°W)

Aerosol particle size affects both atmospheric residence time and physical and chemical properties of aerosols in the atmosphere (*Seinfeld and Pandis*, 2012). Therefore, it is important to evaluate CESM aerosol size distribution using available observations. Figure 3.3 shows the time-averaged column-integrated volume size distribution of aerosols near Cape Verde from AERONET (red) and CESM (black). Both distributions were calculated using 22 bins of logarithmically spaced radii from 0.5μm to 15μm, and assuming a lognormal distribution of number mode radius. For CESM data, average volume mixing ratios were calculated for each mode using the aerosol species listed in Figure 3.1. CESM's distribution

is biased towards slightly coarser radii, and its standard deviation in the coarse mode is larger. The magnitudes of the distributions are comparable.

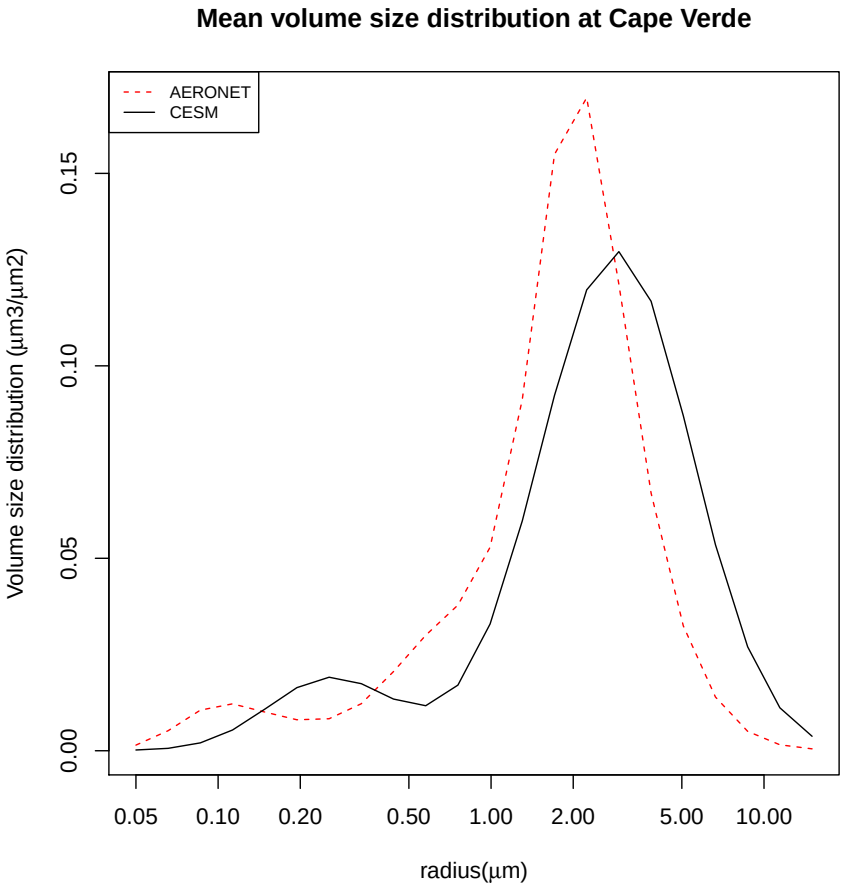

Figure 3.3: Column-integrated volume size distribution ($\mu m^3/\mu m^2$) of aerosols at Cape Verde from AERONET (red) and CESM (black).

It is also useful to evaluate dust in the atmosphere downstream of the high source regions over North Africa. Similar to Figure 3.2, Figure 3.4 shows monthly climatologies of 530nm AOD near Barbados (13N, -60W) for AERONET (red) and CAM5 (black). The timing of the seasonal cycle of AOD is similar, with peak values occurring in June and July, but CAM5 overestimates the magnitude of AOD by a factor of 2 across all seasons.

Figure 3.5 shows monthly climatologies of surface dust concentration ($\mu g/m^3$) near Barbados (13N, -60W) for observations (red) and CAM5 (black). In this case,

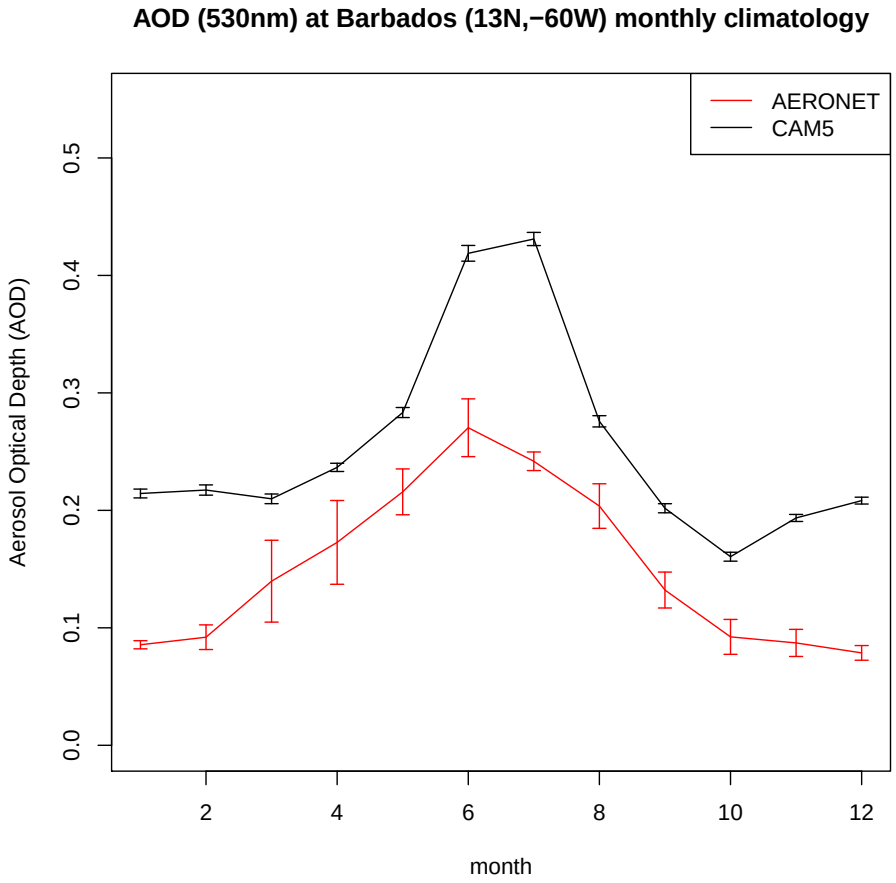

Figure 3.4: Mean monthly climatology of 530nm aerosol optical depth (AOD) near Barbados (13N, -60W) from AERONET (red) and CAM5 (black). The AERONET data are available from 2007 to the present, and the CAM5 simulation is 150 years. Vertical bars represent +/- 1 standard error for each month.

the observations only span 44 years, while the CAM5 simulation is 150 years long. Similar to the Cape Verde AOD comparison, CAM5?s monthly climatology of surface concentration is realistic. The peak in observed surface dust concentration precedes that of the model by approximately one month and has larger error bars in all months. The error bars for both observations and CAM5 are largest during boreal summer, when the mean surface dust concentration is highest.

Overall, the model's representation of the seasonal cycle of AOD both near the continental source regions and downstream of the continent near Barbados are quite realistic, with some discrepancies in magnitude. There are several possi-

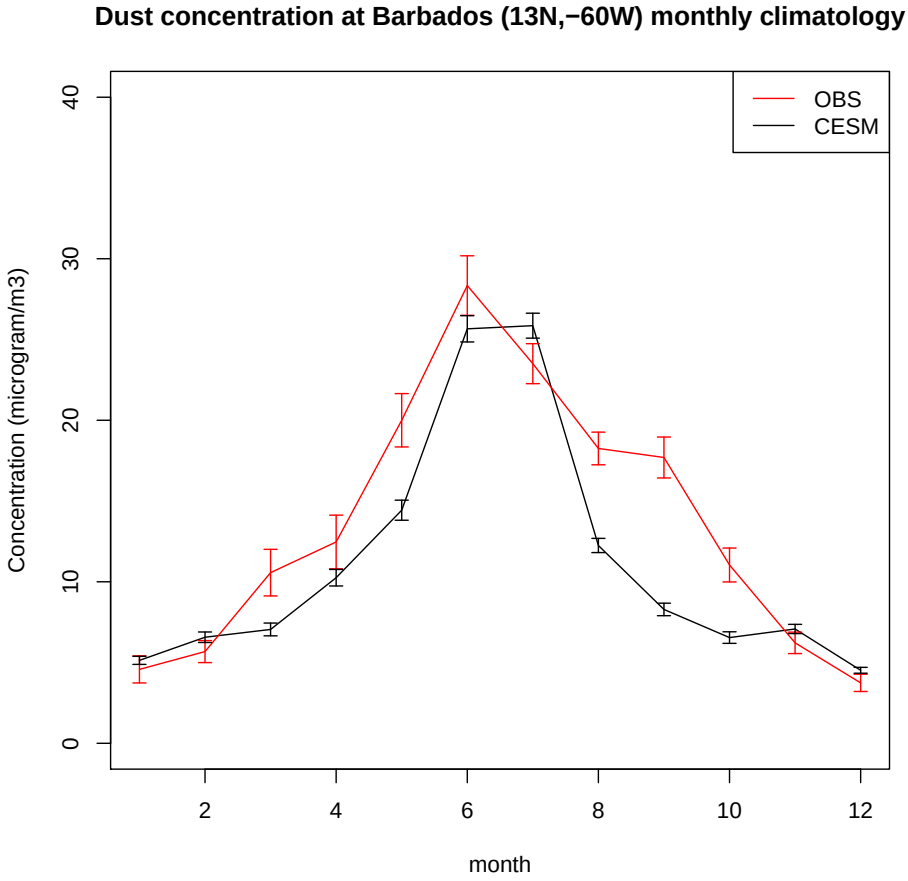

Figure 3.5: Mean monthly climatology of surface dust concentration($\mu g/m^3$) near Barbados (13N, -60W) from AERONET (red) and CAM5 (black). Data at Barbados are available from 1965 to 2008, while the CAM5 simulation is 150 years. Vertical bars represent +/- 1 standard error for each month.

ble explanations for differences between the two distributions. Perhaps the most likely cause is attributable to unreliable emissions in CAM5. In particular, the sources of dust described in *Zender et al.* (2003) do not include sources in the Sahel, a region where local emission contributes substantially to high daily dust concentration at the end of spring and early summer (*Marticorena et al.*, 2010). In addition, our model does not resolve cold pool downdrafts over the North African region that produce haboobs, which could account for a significant amount of dust emission during the spring to summer transition period (*Marticorena et al.*, 2010; *Ashpole and Washington*, 2013). Dust emission is also a complex function of other

variables including soil moisture and particle size distribution (*Kok*, 2011). Other possible explanations include relatively low dry and wet deposition rates of dust in CAM5 over the North Atlantic, or differences between the observed and modeled horizontal wind field over the open ocean.

Figure 3.6 shows histograms of monthly averaged surface dust concentration near Barbados from CAM5 (top panel) and observations (bottom panel). The means and variances of the CAM5 and observed surface dust concentration distributions are very similar, much like the AOD comparison at Cape Verde. Both distributions are positively skewed, though extreme values are larger in CAM5 than in observations. In summary, figures 3.2-3.6 show that the seasonal climatologies and distribution shapes of AOD and surface dust concentration in CAM5 are generally realistic when compared to limited available observations, as is the volume size distribution of aerosols near Cape Verde.

3.4 Mean Seasonal Climatologies and Vertical Structure of Dust

3.4.1 Dust Burden

150-year averages of dust burden over North Africa in our simulation account for 61% of global dust burden in boreal winter, and 68% in boreal summer (not shown). Despite uncertainties and constraints of observations, these percentages are qualitatively similar to observational estimates (*Engelstaedter et al.*, 2006). We note that our model simulation ignores anthropogenic sources of dust, which have been estimated to represent 8% of North African dust and 25% of global dust burden (*Ginoux et al.*, 2012). Additionally, there is a strong seasonal cycle of dust burden and emissions in CESM.

Figure 3.7 shows 150-year seasonal averages of total dust burden (g/m^2) over North Africa and the tropical-subtropical North Atlantic. Increased atmospheric dust loading during boreal spring and summer and subsequent downstream transport over the open ocean in CESM are consistent with observations from pre-

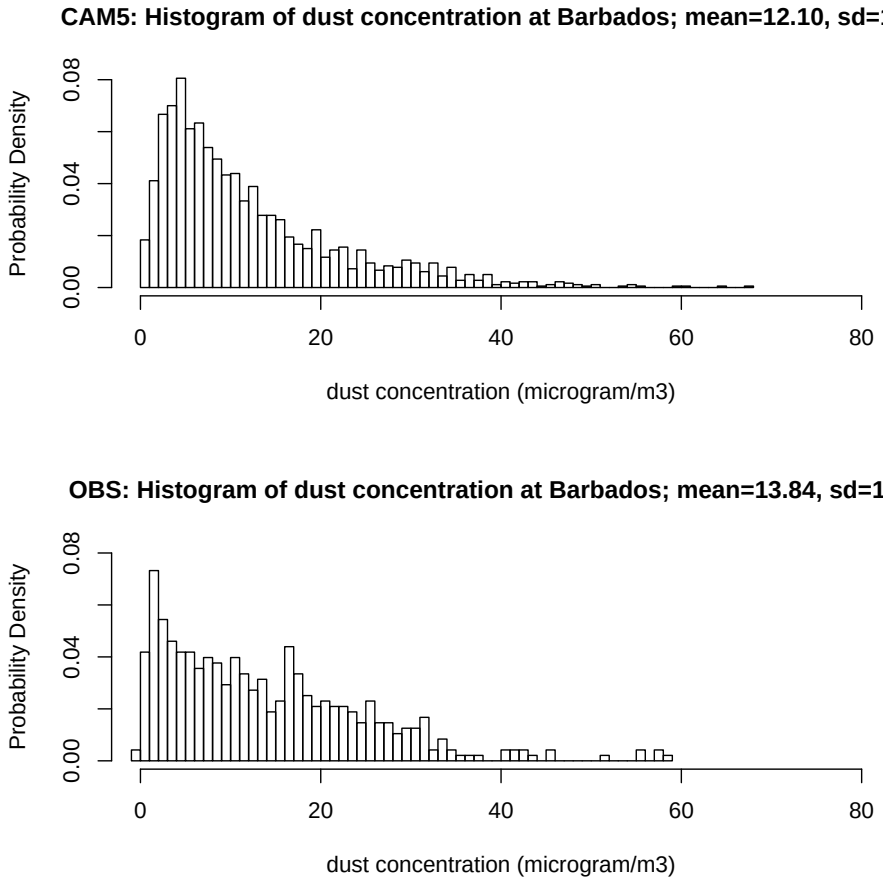

Figure 3.6: Histograms of dust concentration near Barbados (13N, -60W) from CAM5 (top) and from observations (bottom).

vious satellite and in situ based studies (*Engelstaedter et al.* (2006) and *Prospero and Lamb* (2003), respectively, e.g.), though comparisons between limited spatiotemporal observational data and a century coupled climate model run must be made with caution. Notably, there are three major Saharan dust source regions in the model that are most pronounced during boreal summer: A) West Africa, near southern Morocco (-20W to 0W, 15N to 30N); B) North Africa, near Northern Algeria (0W to 10W, 30N); C) East Africa, near northern Sudan and southern Egypt (20W to 40W, 10N to 25N). The dust burdens in regions A and C are generally an order of magnitude greater in boreal summer; the burden in region B is near zero during boreal winter, but of comparable magnitude to regions A and C

during boreal summer.

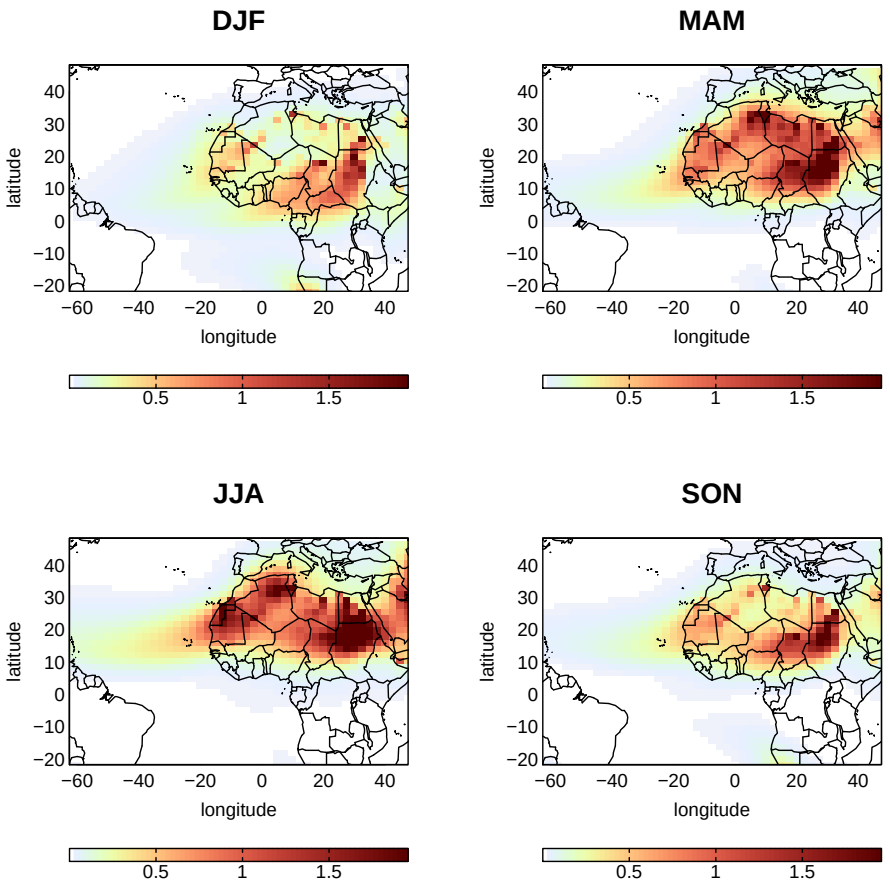

Figure 3.7: One hundred fifty year seasonal averages of CAM5 total dust burden (g/m^2) for December-January-February (DJF), March-April-May (MAM), June-July-August (JJA), and September-October-November (SON).

3.4.2 Vertical Structure of Dust over North Africa and Subtropical North Atlantic

To better understand the zonal and vertical structure of dust transport, Figures 3.8 and 3.9 show vertical profiles of 150-year seasonal averages of accumulation mode (a1) and coarse mode (a3) dust concentration, respectively, over the subtropical Atlantic downstream N. Africa region (-35W to -20W, 15N to 25N; blue), West Africa (-15W to -5W, 15N to 25N; red), and East Africa (20W to 40W,

15N to 25N; black). Dust concentrations are highest over the East African surface across all seasons compared to the other two locations. This indicates that dust transport over the open ocean during these seasons is primarily occurring in the lower troposphere, near 700hPa.

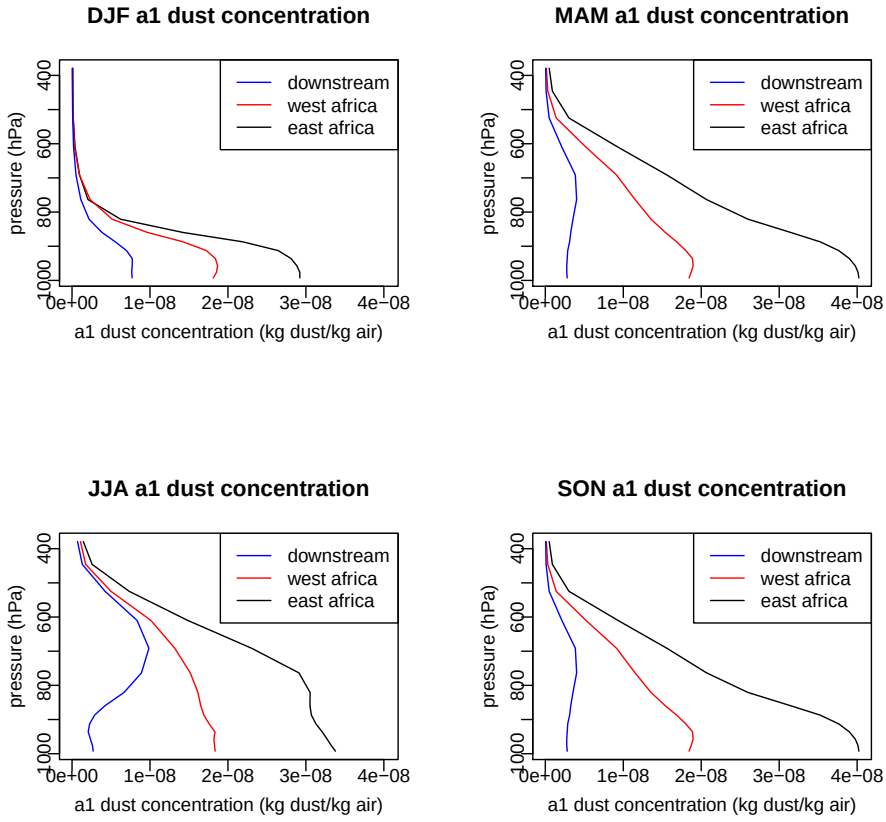

Figure 3.8: Vertical profiles of 150 year seasonal averages of CAM5 accumulation mode (a1) dust concentration.

Assessing the realism of Figures 3.8 and 3.9 is important, but observational records of the vertical structure of aerosols are very limited. *Koffi et al.* (2012) evaluated CALIOP aerosol extinction coefficient profiles at over North Africa and the subtropical North Atlantic from 2007-2009 using twelve AEROCOM 2000 simulations. Figures 3.10 and 3.11 show CESM aerosol extinction coefficient profiles over the North African and subtropical North Atlantic regions defined in *Koffi*

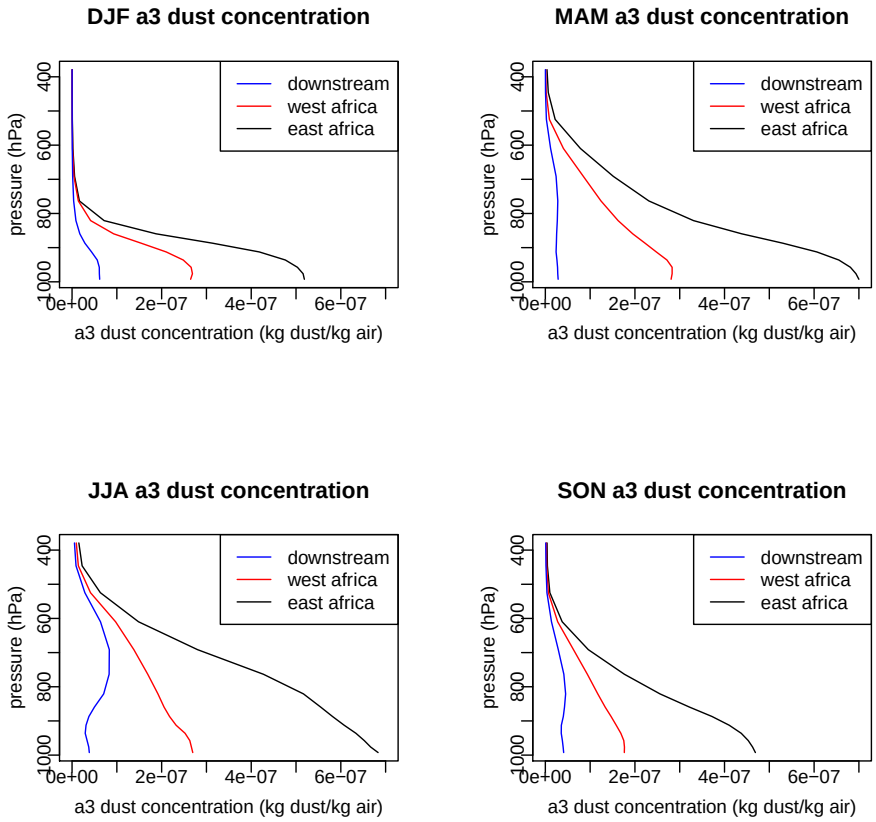

Figure 3.9: As in Figure 3.8 but for coarse mode (a3) dust concentration.

et al. (2012). The values were normalized according to the method described in *Koffi et al.* (2012) such that the total AOD is normalized over the first 10 kilometers of the atmosphere. The vertical structure of CESM aerosol extinction is generally realistic in these regions, especially during boreal summer over the subtropical North Atlantic. Observations used by *Koffi et al.* (2012) show advection of Saharan dust to the Atlantic between 2 and 5 km, which is confirmed by Figures 3.8, 3.9 and 3.10.

Figure 3.12 shows a comparison of mean extinction height Z_α for CAM5 and the CALIPSO data used in *Koffi et al.* (2012) over the North African and subtropical North Atlantic regions. Mean extinction height is defined as

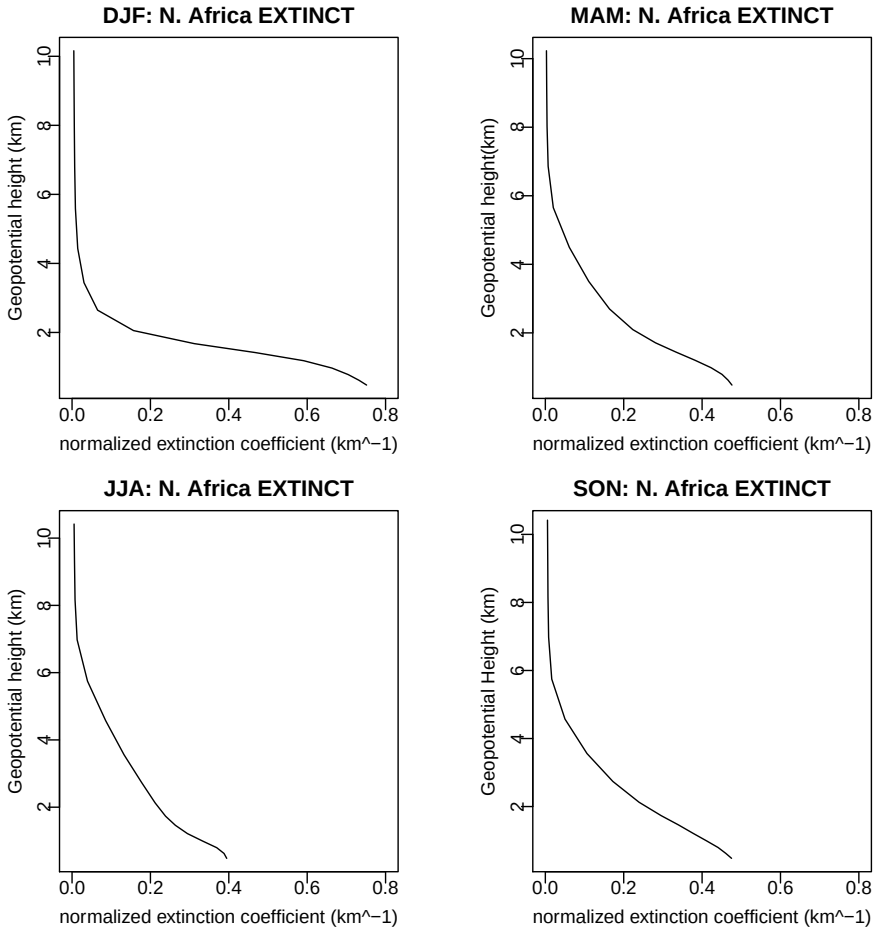

Figure 3.10: Vertical profiles of 150 year seasonal averages of CAM5 normalized aerosol extinction coefficient (km^{-1}) over North Africa.

$$Z_\alpha = \frac{\sum_{i=1}^{n} b_{ext,i} * Z_i}{\sum_{i=1}^{n} b_{ext,i}} \,, \tag{3.1}$$

where $b_{ext,i}$ is the aerosol extinction coefficient (km^{-1}) at level i, and Z_i is the altitude (km) at level i. In both CAM5 and CALIPSO, the lowest values of Z_α occur during boreal winter, while the highest values occur during boreal summer. However, CAM5 systematically underestimates Z_α, particularly during boreal summer in both regions. It is important to note that CALIPSO data used here to calculate mean extinction height are only available for three years, while the CAM5 simulation is 150 years.

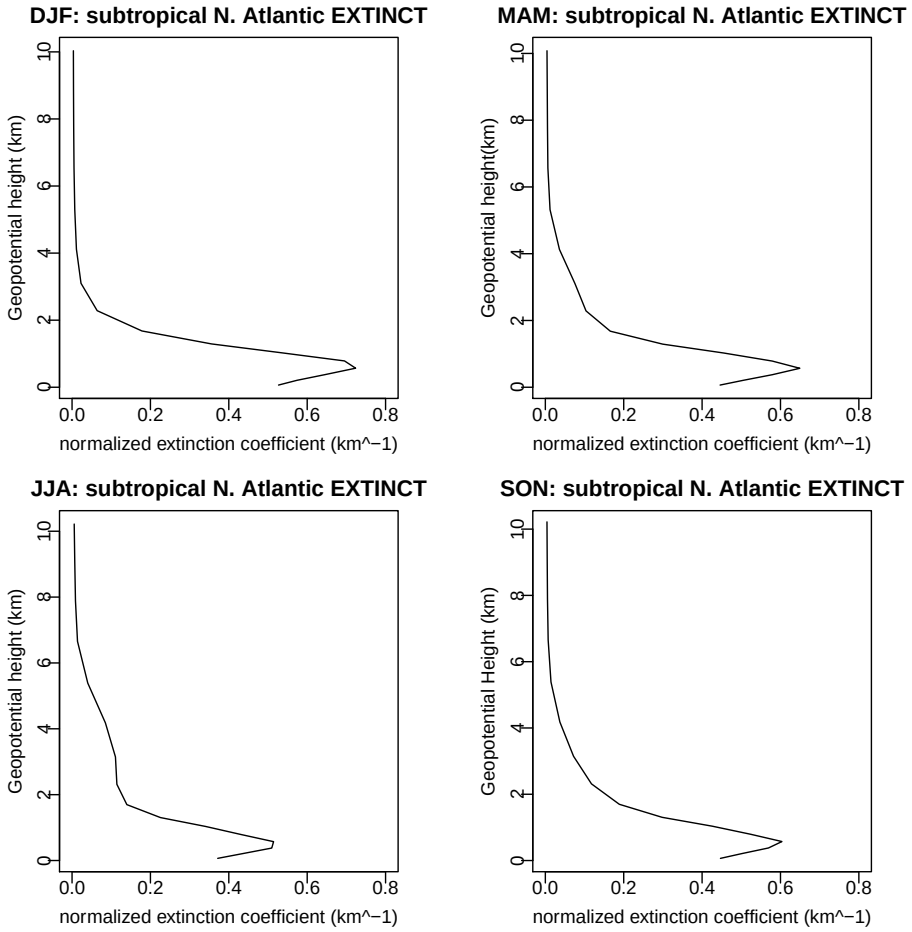

Figure 3.11: Vertical profiles of 150 year seasonal averages of CAM5 normalized aerosol extinction coefficient (km^{-1}) over the subtropical North Atlantic.

	CAM5	**CALIPSO (*Koffi et al.* [2012])**
NAF DJF	1.10 +/- 0.002	1.23
NAF MAM	1.36 +/- 0.001	2.10
NAF JJA	1.58 +/- 0.001	2.44
NAF SON	1.41 +/- 0.003	1.85
CAT DJF	0.75 +/- 0.002	1.10
CAT MAM	0.85 +/- 0.002	1.33
CAT JJA	1.04 +/- 0.003	1.96
CAT SON	0.88 +/- 0.002	1.31

Figure 3.12: Comparison of mean aerosol extinction height (km) for CAM5 and the CALIPSO data used in *Koffi et al.* (2012) for the North Africa (NAF) and subtropical North Atlantic (CAT) regions. Indicated for CAM5 are +/- 1 standard errors.

3.4.3 Relationship of Lower Tropospheric Zonal Wind to Downstream North Africa Dust

Figure 3.13 shows a Pearson correlation of boreal summer 820hPa zonal wind and downstream North African dust burden. Dust values were area-averaged over the subtropical North Atlantic (10N to 25N; -35W to -20W) and correlated with 820hPa zonal wind at each grid cell across the region shown. Hatched regions indicate areas where the true correlation is not equal to zero at the 95% confidence level, computed using a two-sample t-test. Large negative correlation values ($\sim$ 0.8) over northwest Africa and the eastern subtropical North Atlantic indicate that increased mass of atmospheric dust downstream of North Africa is associated with stronger lower tropospheric easterly flow. In addition, there is a strong meridional gradient in the correlation pattern, with an inflection point near Cape Verde. This is evidence of a strong meridional gradient in the mean zonal wind at 820hPa (not shown).

3.4.4 Evaluation of CESM North Atlantic Lower Tropospheric Cloud Fraction

Figure 3.14 shows 150-year seasonal averages of vertically integrated lower tropospheric cloud fraction over North Africa and the tropical-subtropical North Atlantic. Lower tropospheric cloud fraction is defined as the seasonal average of percentage of cloud cover over a given grid cell, averaged over the 1000hPa to 700hPa layer. Subtropical North Atlantic cloud fraction downstream of high Saharan source regions of dust increases by up to 80% from boreal winter to boreal spring and summer. In addition, the location of maximum lower tropospheric cloud fraction shifts northward during the summer, coincident with the northward shift in downstream dust transport during that season. Mid-to-upper (i.e. above 700hPa) tropospheric cloud fraction does not increase during the spring and summer over this region (not shown).

Figure 3.15 shows seasonal averages of ISCCP low level cloud fraction, spanning from January 1984 to December 2009. Low level cloud fraction is estimated

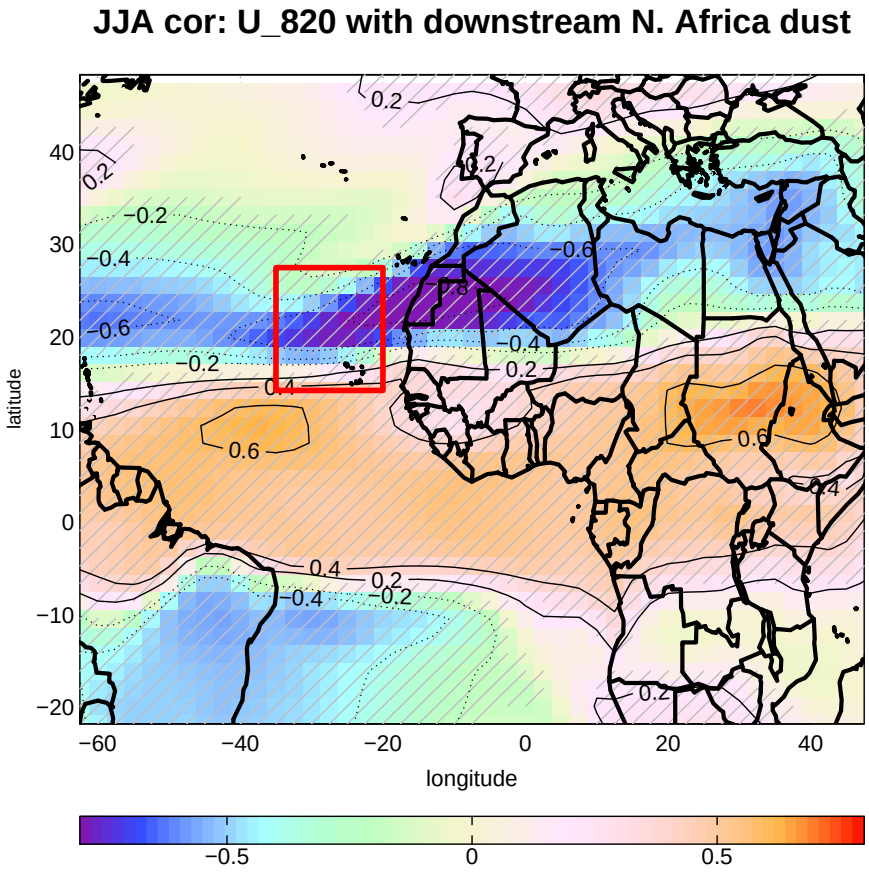

Figure 3.13: Pearson correlation of boreal summer CAM5 820hPa zonal wind and area-averaged downstream North African dust burden. Gray hatches indicate regions where there is 95% confidence that the true correlation is not equal to zero, using a two-sample t test.

using a random overlap correction, such that

$$LLCF = \frac{LOW}{1 - HIGH - MID} \tag{3.2}$$

where LOW = ISCCP low level cloud fraction, $HIGH$ = ISCCP high level cloud fraction, and MID = ISCCP mid level cloud fraction. The random overlap correction is applied because ISCCP often misplaces low clouds into the mid level category over strong inversions (*Garay et al.*, 2008) and if there are overlying cirrus (*Mace et al.*, 2006), and because ISCCP can only see low clouds unobscured by higher clouds (*Rozendaal et al.*, 1995). Observed low level cloud

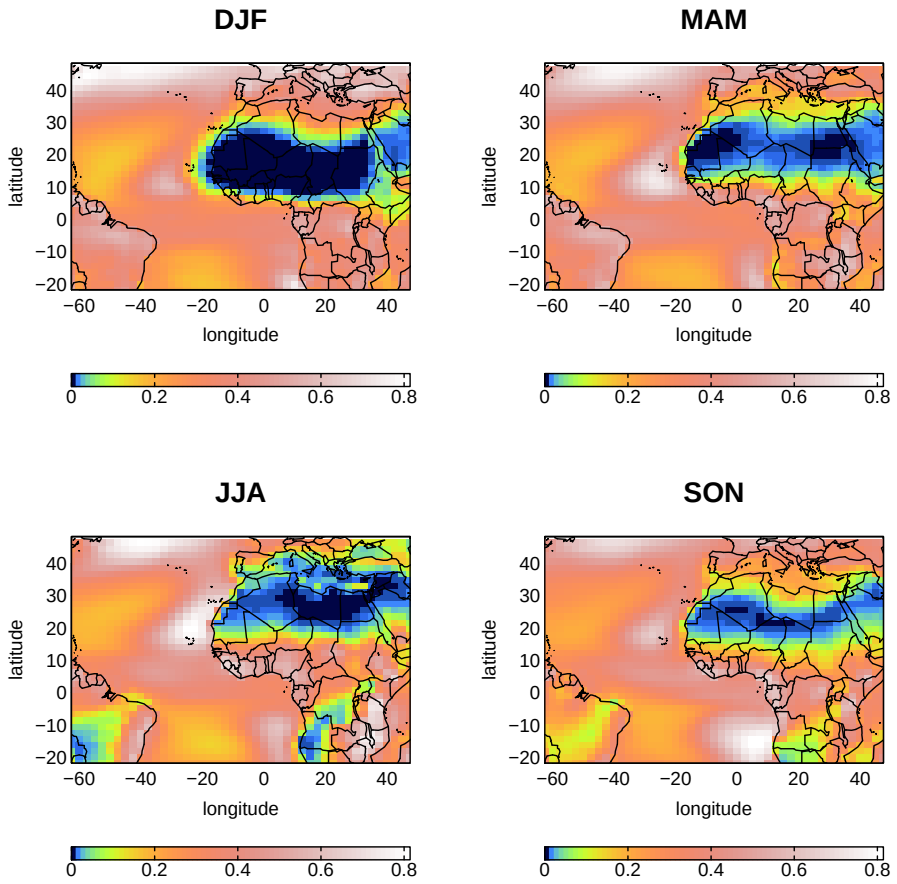

Figure 3.14: One hundred fifty year seasonal averages of CAM5 vertically integrated lower tropospheric cloud fraction.

fraction downstream of high dust source regions increases substantially during boreal summer, but the increase is not as large as is seen in CESM. Like CESM, the highest values of ISCCP low level cloud fraction shift northward downstream of North Africa during boreal summer. Large differences ISCCP and CESM can be found over the Sahara desert. ISCCP values are much higher in this region because ISCCP cannot distinguish between aerosol and cloud in regions where AOD is high, and because ISCCP may mistake the bright desert surface for cloud droplets (e.g. *Engelstaedter et al.* (2006)).

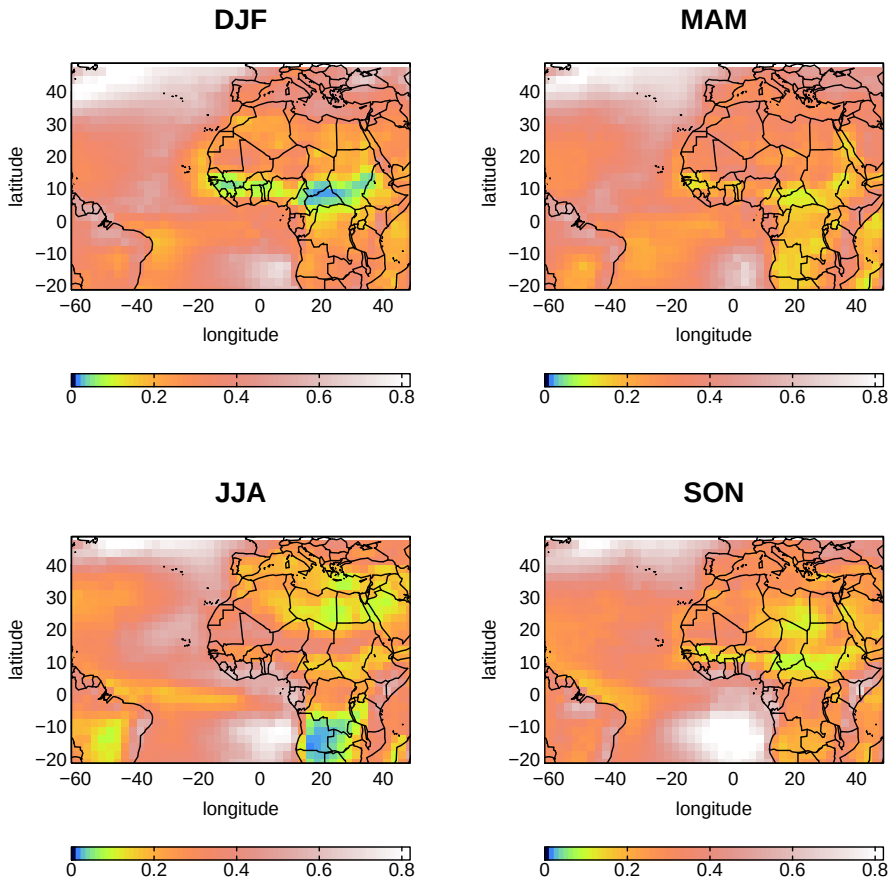

Figure 3.15: Seasonal averages of ISCCP low cloud fraction, from January 1984 to 2009.

3.5 Relating North African Dust Transport to Subtropical Atlantic Lower Tropospheric Cloud Fraction Increase During Boreal Summer

The results from section 3.4 suggest a possible link between boreal summer North African dust transport and increased subtropical Atlantic lower tropospheric cloud fraction in CESM 1.0. *Mahowald and Kiehl* (2003) were the first to correlate subtropical and tropical North Atlantic cloud cover with North African dust, using

a 16-year subset of the ISCCP dataset. They found that surface dust concentrations at the Barbados in situ observing site in the western subtropical Atlantic (*Prospero and Nees*, 1986) were moderately correlated with only low thin clouds over the subtropical North Atlantic, downstream of the Sahara desert source region. However, due to observational data constraints, the authors could not distinguish between a microphysical (Saharan dust acting as CCN for low thin clouds) or dynamical link between the two variables. Here, we explore this relationship in CESM 1.0.

3.5.1 Dust Burden and Lower Tropospheric Cloud Fraction Correlation

Figure 3.16 shows Pearson correlations of seasonally averaged dust burden and lower tropospheric cloud fraction over North Africa and the tropical-subtropical North Atlantic. Hatched regions indicate areas where the true correlation is not equal to zero at the 95% confidence level, computed using a two sample t-test. During boreal spring, and particularly during boreal summer, a modest-to-strong correlation pattern emerges over the eastern subtropical North Atlantic, downstream of North Africa. This area is coincident with increases in both transported Saharan dust over the open ocean and increased lower tropospheric cloud fraction during these seasons. In contrast to positive correlations observed at lower levels, the correlation of mid and upper tropospheric cloud fraction to dust burden during these seasons is close to zero (not shown).

Figure 3.17 shows a scatterplot of boreal summer average dust burden anomalies (abscissa) and lower tropospheric cloud fraction anomalies (ordinate), area-averaged over the modest-to-strong correlation region shown in Figure 3.16; each point represents a seasonal average anomaly value. Clearly, a strong linear relationship between the two variables exists over this region during boreal summer ($R \sim 0.75$). The seasonal anomalies of lower tropospheric cloud fraction over the subtropical North Atlantic during boreal summer are approximately 10-20% of the raw values over the 150 year simulation, while the seasonal anomalies of dust burden in this region are a similar fraction of raw values, but with several highly

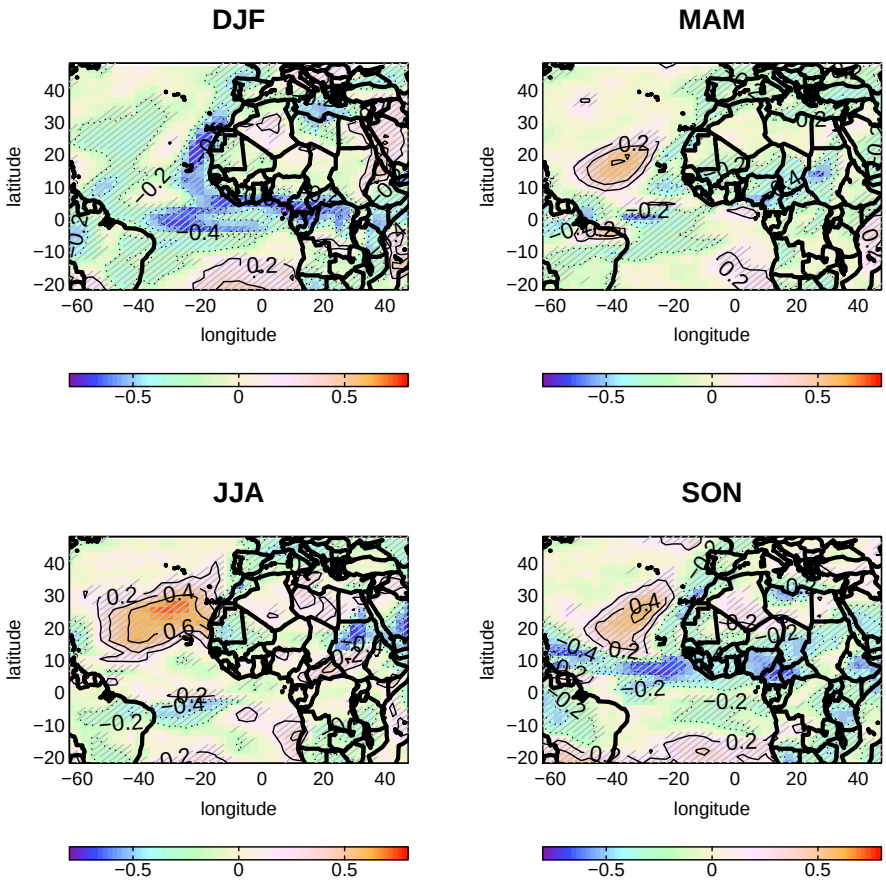

Figure 3.16: Pearson correlation of seasonally averaged CAM5 dust burden and lower tropospheric cloud fraction anomalies over North Africa and the tropical-subtropical North Atlantic. Gray hatches indicate regions where there is 95% confidence that the true correlation is not equal to zero, using a two-sample t test.

anomalous seasons where the fraction increases to near 60% (not shown). Subsequent analyses are aimed at determining whether a microphysical or dynamical mechanism is primarily involved in linking the cloud variation to the fluctuating dust concentration over the eastern North Atlantic.

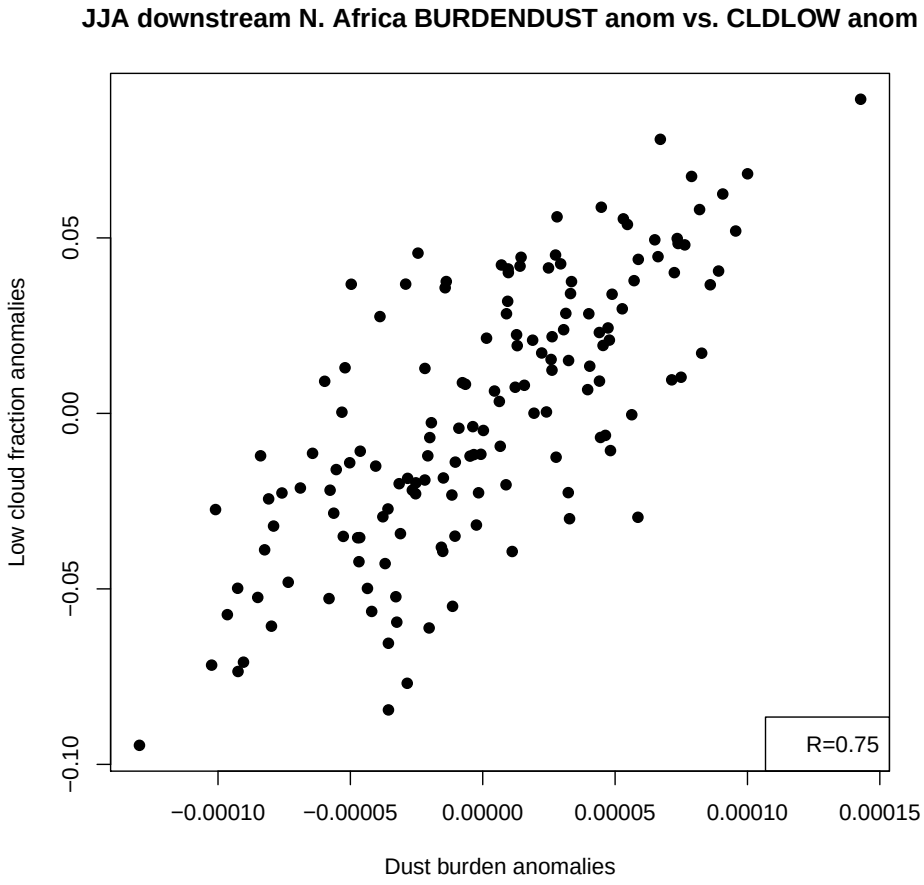

Figure 3.17: Scatterplot of boreal summer CAM5 average dust burden anomalies (abscissa; kg/m^2) and lower tropospheric cloud fraction anomalies (ordinate; unitless), area averaged over the modest-to-strong correlation region shown in Figure 3.16.

3.5.2 Vertical Structure of Downstream North African Dust, Cloud Fraction, and Solar Heating Rate

Figure 3.18 builds upon the results of Figures 3.16 and 3.17 to gain more insight into the strong boreal summer correlation between dust burden and lower tropospheric cloud fraction over the subtropical Atlantic. It plots vertical profiles of 150-year averages of coarse and accumulation mode dust concentration (black), cloud fraction (red), and solar heating rate (green) area-averaged over the subtropical North Atlantic region downstream of North Africa during boreal winter

(top row) and summer (bottom row). During boreal winter, the maximum dust concentration is close to the surface, and cloud fraction is generally low over the subtropical North Atlantic region. However, a very different vertical structure is present during the summer, when the maximum dust concentration is located several hundred hectopascals above the maximum cloud fraction, which is located in the boundary layer (see also Figures 3.8 and 3.9). Additionally, the vertical structure of cloud fraction is very similar in both seasons, but the $\sim$ 900hPa maximum is nearly twice as large in the summer. This suggests that dust may be affecting clouds radiatively or dynamically in this region, but not microphysically, since the vertical structure of cloud fraction is distinct from that of dust concentration, but the magnitude of maximum boundary layer cloud fraction doubles when dust transport in the layer above increases.

In both boreal winter and summer, solar heating rate is maximum near the top of the maximum cloud layer. This is due to weak solar absorption by cloud droplets and water vapor at the cloud top (*Wood*, 2012). However, in boreal summer, a secondary maximum of solar heating rate emerges within the layer of maximum dust concentration. This additional heating due to solar absorption by dust will heat the air locally and decrease the amount of solar radiation reaching the lower troposphere. Both heating near the cloud top and cooling at the surface will promote lower tropospheric cloud growth by increasing inversion strength (i.e. $\frac{dT}{dz}$ becomes more positive). Vertical profiles of air temperature during boreal summer over this region show a maximum near the bottom of the maximum dust layer around 750hPa, but not near the maximum cloud layer around 900hPa. This 750hPa temperature maximum is absent during boreal winter, when dust concentrations are lower aloft than in the summer. This is further evidence supporting the hypothesis that dust is strengthening the boreal summer subtropical North Atlantic temperature inversion, at least in part by increased temperatures aloft due to solar absorption by advected North African dust. However, we must note that the likely overestimate of absorption from using the OPAC dust refractive indices means this inversion strengthening mechanism is likely overestimated by CESM (*Albani et al.*, 2014).

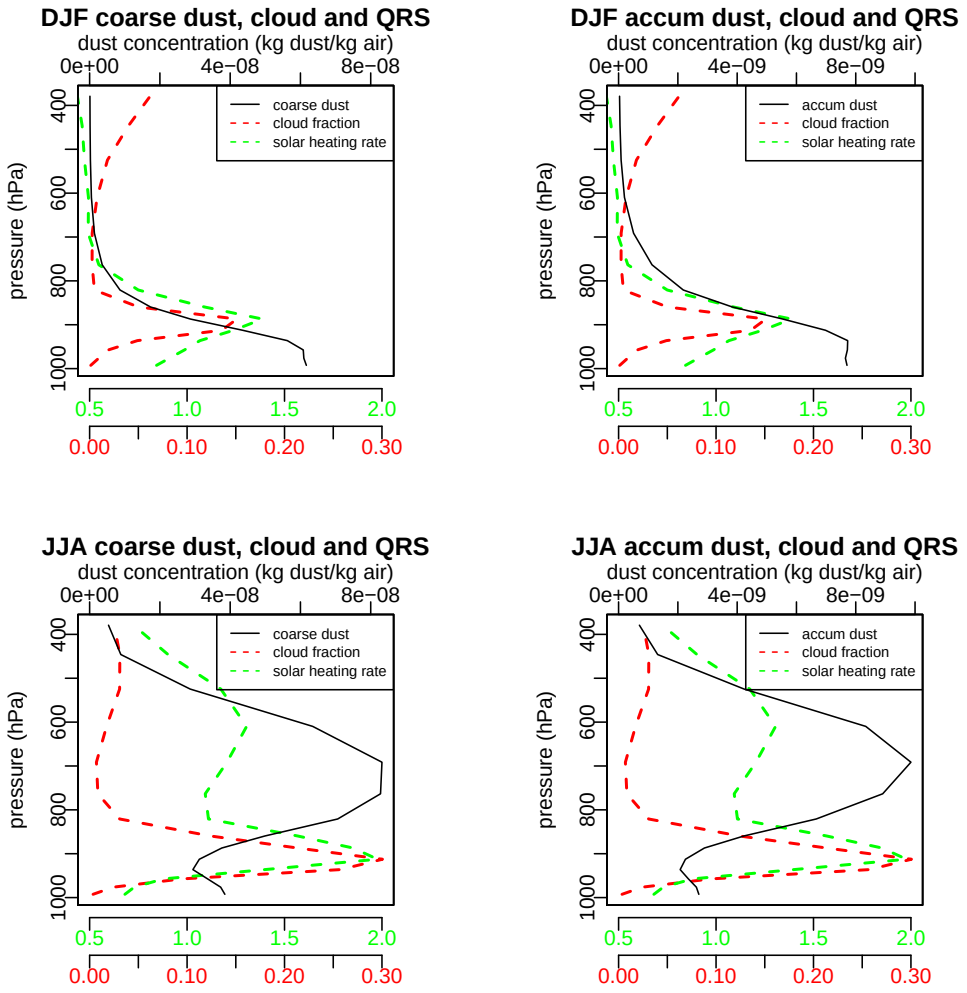

Figure 3.18: Vertical profiles of 150 year boreal winter (DJF) and summer (JJA) averages of CAM5 downstream North African coarse and accumulation dust mode concentration (black), cloud fraction (red), and solar heating rate (green).

The high summertime correlation between dust burden and lower tropospheric cloud fraction in Figure 3.18 may be explained in several possible ways: A) the correlation is spurious and has no physical significance; B) dust particles advected off the North African continent are acting as cloud condensation nuclei in the lower troposphere (*Rosenfeld et al.*, 2001); C) dust particles advected off the North African continent reflect shortwave radiation back to space, heat the air locally due to solar absorption by the dust, cool the boundary layer, and promote

lower tropospheric cloud growth by strengthening the lower tropospheric inversion and bringing the air closer to saturation (*Koch and Del Genio*, 2010); D) the correlation is driven by the response of both dust and cloud to another factor, such as vertical velocity. Although vertical velocity is related to inversion strength because of its influence on air temperature due to adiabatic heating and cooling, it can also be dynamically important in transporting quantities of dust away from or closer to the boundary layer. Hypothesis A appears unlikely, given the strong statistical significance of the results from the long CESM simulation and also the well-known radiative, dynamical, and microphysical impact of dust particles in the atmosphere. These impacts have been elucidated by a body of (aforementioned) previous studies that have explored hypotheses B and C in a variety of experimental situations. Hypothesis B can be eliminated because the maximum dust concentration (around 700hPa) is located above the maximum cloud fraction (around 900hPa). In addition, as mentioned previously, dust particles are usually associated with cold cloud ice nucleation rather than warm cloud droplet nucleation which must be at work in the low cloud structure under consideration here. However, coarse mode dust particles in CAM5 are large enough that droplets can form on them, in spite of relatively low hygroscopicity (0.068). In addition, the results from Figure 3.18 suggest that elevated summertime dust concentrations over the subtropical North Atlantic could potentially promote cloud growth due to their location above the boundary layer and above the maximum cloud layer. Results presented in the following sections further suggest that hypothesis C is a likely explanation for the link between boreal summer North African dust transport and lower tropospheric cloud growth in CESM 1.0. Hypothesis D will also be explored by looking at correlations of dust and cloud with a measure of vertical velocity.

3.5.3 Estimated Inversion Strength (EIS) Calculation

To further test hypothesis C, we use model output to calculate Estimated Inversion Strength (EIS) over the subtropical North Atlantic region for boreal winter (when downstream North Africa dust concentration is low, and when the relationship between North African dust and lower tropospheric cloud fraction is

weak) and boreal summer (when downstream North Africa dust concentration is high, and when the relationship between North African dust and lower tropospheric cloud fraction is strong). EIS is a formulation introduced by *Wood and Bretherton* (2006) that estimates boundary layer inversion strength, which promotes stratiform low cloud cover along western continental boundaries around the globe (*Myers and Norris*, 2013). Recall that an inversion is defined as a layer in the atmosphere where $\frac{dT}{dZ} > 0$. *Wood and Bretherton* (2006) note that EIS is a superior metric to Lower Tropospheric Stability (LTS), since it is independent from a region's background climatology. The calculation of EIS is summarized below, and derived in *Wood and Bretherton* (2006).

EIS is defined as:

$$EIS = LTS - \Gamma_m^{850} * (Z_{700} - Z_{LCL}), \tag{3.3}$$

where $LTS = \Theta_{700} - \Theta_{sfc}$, Γ_m^{850} = moist adiabatic lapse rate centered at 850hPa $= \Gamma_m(T_{avg}, 850hPa)$, $T_{avg} = \frac{(T_{sfc}+T_{700})}{2}$, and $Z_{LCL} = \frac{R_d(T_{sfc}+T_{LCL})}{(2*g_o)}, * \ln(\frac{SLP}{p_{LCL}})$.

Therefore, $EIS = EIS(T_{sfc}, T_{dew}, T_{700}, Z_{700}, SLP)$, where T_{dew} is the dew point temperature. All variables but T_{dew} can be acquired from CAM5 output; T_{dew} can be calculated using the Clausius-Clapeyron Equation.

3.5.4 EIS Over the Subtropical North Atlantic During Boreal Summer

Figure 3.19 shows 150-year boreal winter and summer averages of estimated inversion strength (degrees K). Larger values of EIS indicate a stronger inversion near the boundary layer. Indeed, the largest values of EIS are found downstream of North Africa during boreal summer, and are co-located with regions of maximum dust transport near 700hPa and maximum cloud fraction near 900hPa.

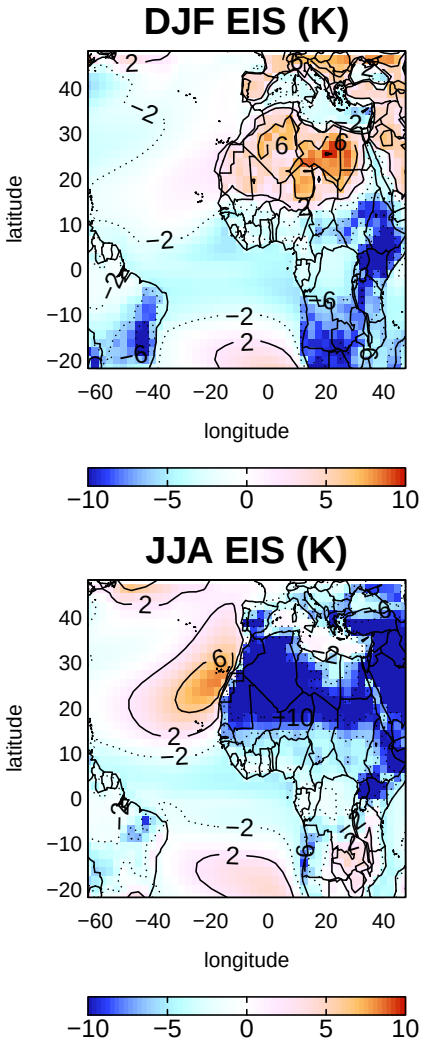

Figure 3.19: One hundred fifty year boreal winter and summer averages of CAM5 estimated inversion strength (K).

3.5.5 Composites of EIS on Most Dusty and Least Dusty Summers Downstream of North Africa

Figures 3.17, 3.18, and 3.19 suggest that dust may be acting to increase EIS downstream of North Africa by cooling the boundary layer and/or heating the atmosphere near 700hPa. However, it is still possible that the relationship between dust burden and lower tropospheric cloud fraction is coincidentally caused by the same underlying dynamics in the atmosphere. In addition, increased EIS during

boreal summer could be a result of increased lower tropospheric cloud fraction alone, independent of North African dust. Figure 3.20 further investigates this relationship by showing composites of EIS, averaged on the five most dusty (left) and five least dusty (middle) boreal summers over the downstream North Africa region. The right panel shows the difference between the left and middle plots, and indicates that EIS increases by up to 20% in some regions on extremely dusty summers downstream of North Africa. This result suggests that the dust-low cloud relationship in this region is driven primarily by a semi-direct dynamical effect rather than cloud microphysics, since both solar absorption and reflection by dust near 700hPa promote increased inversion strength. But again, it is likely the semi-direct effect is overestimated by CESM.

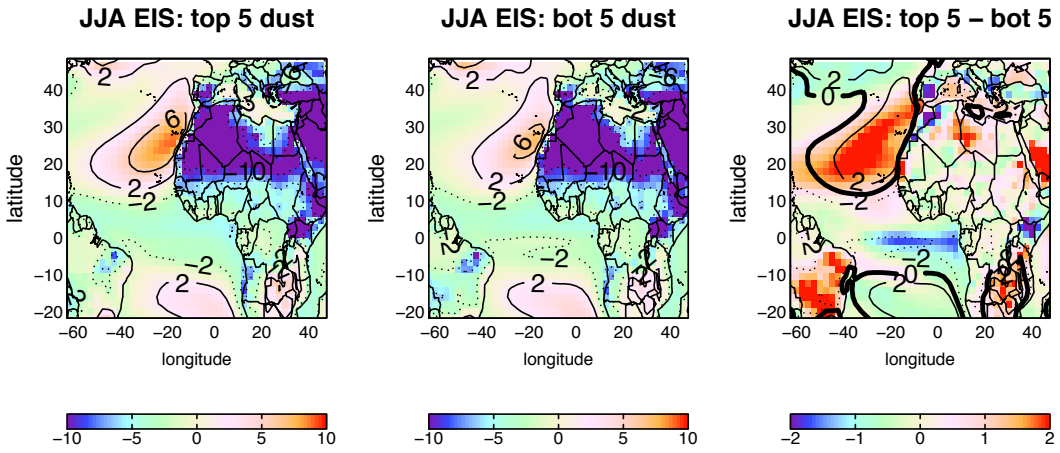

Figure 3.20: One hundred fifty year boreal summer averages of CAM5 estimated inversion strength (K) on the five most dusty downstream North African seasons (left), five least dusty seasons (middle), and the difference between the top and bottom five seasons (right).

3.5.6 Relationship of Downstream North Africa Dust Burden and Lower Tropospheric Cloud Fraction to Vertical Velocity

Hypothesis D states that the correlation shown in Figure 3.16 is driven by the response of both dust and cloud to an external meteorological factor, such

as vertical velocity. Figure 3.21 explores these relationships by showing Pearson correlations of boreal summer downstream North Africa dust burden anomalies with 700hPa $\omega = \frac{dp}{dt}$ anomalies (top panel) and boreal summer downstream North Africa lower tropospheric cloud fraction anomalies with 700hPa ω anomalies (bottom panel). Hatched regions indicate areas where the true correlation is not equal to zero at the 95% confidence level, computed using a two sample t-test. As shown in Figure 3.16, the area from around 20N to 30N, -40W to -20W is where boreal summer dust and low cloud anomalies were most strongly correlated.

In the top panel of Figure 3.21, values in this region are weakly to moderately negative, indicating that increased values of downstream North Africa low cloud anomalies are associated with decreased values of 700hPa ω anomalies, which means weaker subsidence. Note that the mean 700hPa ω field in this region is strongly positive due to large-scale subsidence associated with the descending branch of the Hadley Cell circulation. *Myers and Norris* (2013) showed observational evidence suggesting that enhanced subsidence reduces subtropical marine boundary layer cloudiness, which is consistent with the sign of the correlation in the top panel of Figure 3.21. In the bottom panel, values in this region are strongly negative, indicating that increased values of downstream North Africa dust burden anomalies are associated with decreased values of 700hPa ω anomalies, which also means weakened subsidence. Figures 3.8 and 3.9 showed that in this region, boreal summer dust concentration is maximum around 700hPa.

While we have shown evidence that dust increases inversion strength and therefore enhances lower tropospheric cloud fraction (hypothesis C), it is difficult to evaluate hypothesis D without a complementary CAM5 simulation that does not include the interactive dynamical and radiative effects of dust in the atmosphere. In addition, calculation of heat and moisture budgets using monthly data is insufficient to demonstrate that the presence of dust is weakening subsidence and therefore promoting lower tropospheric cloud growth. This hypothesis will be explored in future studies using daily or sub-daily data, with a comparison to a prescribed aerosol CAM5 simulation to further examine the relationship between weakened subsidence, increased dust burden, and increased cloud fraction

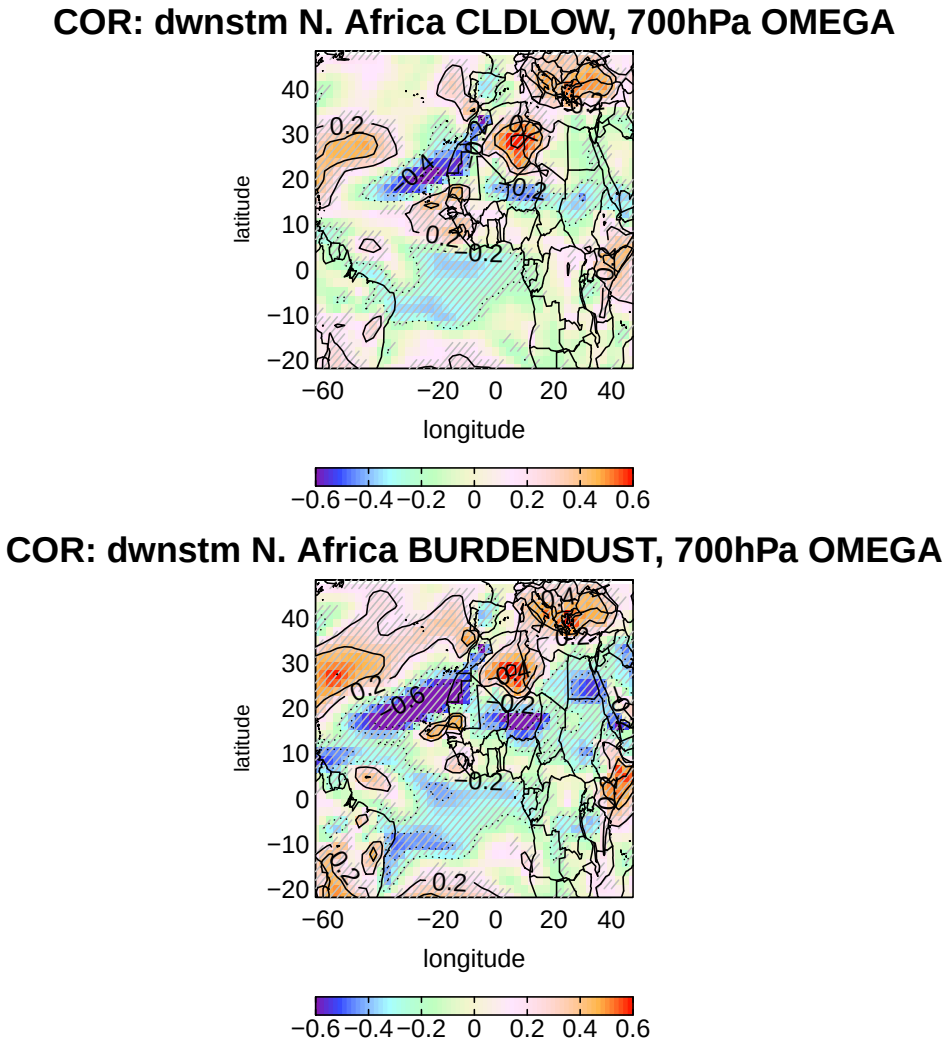

Figure 3.21: Pearson correlations of average boreal summer CAM5 downstream North African lower tropospheric cloud fraction and 700hPa omega anomalies (top) and downstream North African dust burden and 700hPa omega anomalies (bottom). Gray hatches indicate regions where there is 95% confidence that the true correlation is not equal to zero, using a two-sample t test.

anomalies.

3.6 Summary

In this study, we used a 150-year pre-industrial CESM 1.0 simulation to investigate the seasonal cycle of dust burden and transport, circulation, and lower

tropospheric cloud fraction over North Africa and the subtropical North Atlantic, and employed simple statistical techniques and dynamical calculations to explain the semi-direct mechanism relating boreal summer lower tropospheric transport of dust downstream of North Africa and lower tropospheric cloud cover over the eastern subtropical North Atlantic.

The model's seasonal cycle of aerosol optical depth near Cape Verde is strong, and is consistent with AERONET observations in this region. The surface concentration of dust downstream of North Africa at Barbados is also in reasonable agreement with observations. Aerosol volume size distribution in CAM5 at Cape Verde peaks at a radius of approximately 2-3μm, which is consistent with AERONET observations, though the magnitude is too small. Transport of dust downstream of North Africa is strongest during boreal summer, in association with the formation of the downward flank of the African easterly jet forms and persists into the fall. Vertical profiles of dust concentration and cloud fraction over the subtropical North Atlantic show that in the summer, the maximum dust concentration is near 700hPa, while the maximum cloud fraction is near 900hPa. *Koch and Del Genio* (2010) note that this is a favorable vertical setup for absorbing aerosols to stabilize the atmosphere below and enhance lower tropospheric stratiform clouds. In addition, during boreal spring and especially during boreal summer, lower tropospheric cloud fraction and dust burden are moderately to strongly correlated downstream of North Africa. Solar heating rate increases during boreal summer near the location of maximum dust around 700hPa, which increases inversion strength and promotes lower tropospheric cloud growth. Modeled EIS values increase by up to 60% during boreal summer over this region, indicating that lower tropospheric cloud growth there is caused by increased inversion strength in the boundary layer that appear to be related to increased dust transport off the North African coast. We also show that EIS increases by up to 20% during summers where dust burden downstream of North Africa is very high.

3.7 Discussion

Our results provide insight into effects of transported dust on warm phase low cloud growth and help further elucidate the complex relationships between dust emission, regional meteorology, and aerosol-cloud interactions over the subtropical North Atlantic, downstream of continental high source regions. Transported North African dust and lower tropospheric North Atlantic cloud variations from the 150 year CESM simulation are obtained using a model with a realistic seasonal cycle of dust and African easterly jet formation and improved parameterization of cloud microphysics (*Gettelman et al.*, 2008; *Gent et al.*, 2011; *Neale et al.*, 2013). The analyses from the simulation strongly suggest that African dust and low cloud cover over the eastern North Atlantic are dynamically linked, and that transported African dust is enhancing lower tropospheric cloud cover over the open ocean via a semi-direct mechanism (*Koch and Del Genio*, 2010) that is likely overestimated due to the assume dust refractive index, which accentuates the sensitivity of such a modeling study to the absorptive properties of dust in the model used. The summertime transport of dust in the lower troposphere over the open ocean in CESM is consistent with observational studies that have investigated the mechanisms controlling the vertical structure of dust near the Saharan Planetary Boundary Layer (*Cuesta et al.*, 2009; *Knippertz and Todd*, 2012). Specifically, Figure 3.9 shows that during summer, there is a large relative increase in dust concentration above the boundary layer downstream of high source regions associated with the transport of dust by the lower tropospheric easterlies in the Saharan Air Layer. Our results also provide valuable insight on the long-term behavior of North African dust transport and its impact on lower tropospheric cloud growth, which is important due to the multi-year variability of North African boreal summer dust transport in CESM (not shown). In spite of the strong evidence for a semi-direct mechanism presented in this work, other factors are likely to contribute to the increase in EIS over the subtropical North Atlantic during boreal summer, including warm air advection of the Saharan Air Layer in the mid troposphere and ocean upwelling associated with the Canary Current, and should be explored further in future studies.

In complement to additional field measurements, further investigation of

these relationships could prove useful using different global climate model simulations with realistic atmospheric models to represent the behavior of dust and low clouds in this region. One caveat in using global climate models to investigate aerosol-cloud interactions is that each model parameterizes both clouds and mineral dust emission and optical properties differently and often does so at coarse vertical resolution. It is for this reason that we encourage examination of these interactions using a variety of climate models with different representations of stratiform clouds and different dust emission models. A particularly useful extension of our work is to analyze daily variables in order to diagnose the dust-cloud interactions over the spring and summer in this region, which will be explored in future studies.

3.8 Acknowledgements

This study forms a portion of the Ph.D. dissertation of MJD. Funding was provided by NSF (AGS-1048995) and by the U.S. Department of Energy, Office of Science, Decadal and Regional Climate Prediction using Earth System Models (EaSM program). The Pacific Northwest National Laboratory is operated for the DOE by Battelle Memorial Institute under contract DE-AC06-76RLO 1830. We are grateful for the contribution made by Joseph M. Prospero (RSMAS, U. Miami), who provided us with the Barbados dust record. Many detailed and insightful comments and suggestions made by the anonymous reviewers have led to significant improvements in this paper. Thanks to Joel Norris and Timothy Myers (SIO) for clarifications and ideas regarding lower tropospheric warm phase clouds, Amato Evan (SIO) for literature references and useful discussions regarding seasonal variability of Saharan dust, Li Xu (SIO) and Dave Erickson (ORNL) for assistance in calculating aerosol size distribution, and Didier Tanre and Joseph M. Prospero for their efforts in establishing and maintaining the Cape Verde and Barbados AERONET sites, respectively, used in this investigation. The CAM5 data used in this study can be accessed via an email inquiry (mdeflori@ucsd.edu).

Chapter 3 is published in its entirety in:

- **DeFlorio, M.J.**, S. J. Ghan, B. Singh, A. J. Miller, D. R. Cayan, L. M. Russell, and R. C. J. Somerville (2014), "Semi-direct dynamical and radiative effect of North African dust transport on lower tropospheric clouds over the subtropical North Atlantic in CESM 1.0", *J. Geophys. Res. Atmos.*, **119**, 8284-8303, doi:10.1002/2013JD020997.

Chapter 4

Interannual modulation of subtropical Atlantic boreal summer dust variability by ENSO

Dust variability in the climate system has been studied for several decades, yet there remains an incomplete understanding of the dynamical mechanisms controlling interannual and decadal variations in dust transport. The sparseness of multi-year observational datasets has limited our understanding of the relationship between climate variations and atmospheric dust. We use available in situ and satellite observations of dust and a century-length fully coupled Community Earth System Model (CESM) simulation to show that the El Nino-Southern Oscillation (ENSO) exerts a control on North African dust transport during boreal summer. In CESM, this relationship is stronger over the dusty tropical North Atlantic than near Barbados, one of the few sites having a multi-decadal observed record. During strong La Nina summers in CESM, a statistically significant increase in lower tropospheric easterly wind is associated with an increase in North African dust transport over the Atlantic. Barbados dust and Pacific SST variability are only weakly correlated in both observations and CESM, suggesting that other processes are controlling the cross-basin variability of dust. We also use our CESM simulation to show that the relationship between downstream North African dust transport and ENSO fluctuates on multidecadal timescales and is

associated with a phase shift in the North Atlantic Oscillation (NAO). Our findings indicate that existing observations of dust over the tropical North Atlantic are not extensive enough to completely describe the variability of dust and dust transport, and demonstrate the importance of global models to supplement and interpret observational records.

4.1 Introduction

The effects of aerosols on clouds, radiation, and atmospheric circulation operate locally on the order of days and weeks, yet can exert a global effect on climate over larger and longer spatiotemporal scales. In particular, mineral dust advected off the North African coast has been shown to modify stratocumulus cloud properties, fertilize minerals over the open ocean, and discourage the formation of North Atlantic tropical cyclones (*DeFlorio et al.*, 2014; *Doherty and Evan*, 2014; *Mahowald et al.*, 2010; *Evan et al.*, 2006a). Changes in local surface convergence impacting dust emission, wet and dry deposition removal rates and subsequent impacts on biogeochemistry, and Sahel desert precipitation are known to influence the variability of mineral dust in the atmosphere, both over the continent and the open ocean (*Marticorena and Bergametti*, 1995; *Doherty et al.*, 2014; *Erickson et al.*, 2003; *Prospero*, 1999; *Prospero and Nees*, 1977).

Recently, uncertainties in the parameters controlling dust emission have been reduced due to increased frequency of ground and aircraft based measurements, improved detection and retrieval of atmospheric dust particles through satellite measurements, and novel theoretical techniques resolving emitted dust size distributions (*Washington et al.*, 2006; *Heintzenberg*, 2009; *Koffi et al.*, 2012; *Evan et al.*, 2006a,c; *Kok*, 2011). However, our understanding of large-scale controls on dust transport and variability remains incomplete. Previous studies examining the variability of North African dust on interannual and decadal timescales have been hindered by limited record length of observations, but have nevertheless yielded important insights. *Mahowald and Kiehl* (2003) combined in-situ and satellite observations with an implementation of the DEAD dust module (*Zender*

et al., 2003) inside a chemical transport model to examine the global variation of column dust burden associated with two indices of large-scale climate fluctuations: the Nino 3.4 index (sea surface temperature anomalies averaged over 120W to 170W, 5S to 5N) and the Pacific Decadal Oscillation (PDO) index (the leading principal component of sea surface temperature anomalies in the region 110E to 100W, 20N to 65N; *Mantua et al.* (1997)). They found only tenuous relationships between dust and these coupled climate modes, possibly because of the limited record length. Specific to North African dust, *Evan et al.* (2006b) correlated wintertime North African dust to various climate indices using the Advanced Very High Resolution Radiometer (AVHRR) satellite dust climatology. They showed that wintertime dust fraction over the tropical Atlantic between -30W and -10W was moderately correlated with the Nino 3.4 index, and that lag correlations between Nino 3.4 and dust fraction (ENSO leading dust events) were not as strong as the winter-to-winter correlation of these two variables. These results were generally consistent with the conclusions drawn from *Prospero and Lamb* (2003), who analyzed interannual variability of the Barbados dust dataset.

Other studies have suggested links between North African dust transport and other coupled climate modes, including the North Atlantic Oscillation (NAO) (*Moulin et al.*, 1997; *Ginoux et al.*, 2004) and the Atlantic Multidecadal Oscillation (AMO) (*Evan et al.*, 2011). *Chiapello et al.* (2005) used the TOMS/Nimbus-7 and TOMS/Earth Probe satellite datasets to show that the influence of the NAO dominates winter export of dust to the eastern subtropical Atlantic. *Riemer et al.* (2006) implemented a "Centers Of Action" approach to show that fluctuations in the strength of the Azores High, and not the NAO, explained the highest percentage of wintertime variance in tropical and subtropical North Atlantic atmospheric dust concentration. *Doherty et al.* (2008) found that the relationship between the NAO and mineral dust observed in winter is non-existent during the summer. *Wang et al.* (2012) used a proxy-derived dataset of dust aerosol optical depth over the tropical North Atlantic to suggest a feedback between the AMO and tropical North Atlantic dust that operates through variations in Sahel rainfall. *Doherty et al.* (2014) focused on boreal summer variations in North African dust concen-

tration and showed that variations in the West African Convergence Zone (WACZ) partially control dust emission and transport westward towards the Caribbean.

Our work builds on these previous studies by characterizing variability of North African dust transport on interannual and decadal timescales using a fully-coupled GCM simulation with realistic ENSO variability (*Deser et al.*, 2012) and a reasonable seasonal cycle of North African dust burden (*DeFlorio et al.*, 2014). As noted in *Wang et al.* (2012), the CESM study was not possible using the previous generation of coupled climate models included in the Coupled Model Intercomparison Project 3 (CMIP3) because aerosol concentrations and emissions were prescribed (*Ghan and Schwartz*, 2007). However, the new generation of CMIP5 models enables dynamical processes to influence dust concentrations and emissions. This greatly enhances the value of using such models to study aerosol-climate interactions, provided the relevant physical processes are represented realistically (and interactively) in the model of choice; *Evan et al.* (2014) showed that historical simulations of CMIP5 models (including CESM) tend to underestimate dust production over North Africa. However, *DeFlorio et al.* (2014) showed that CESM represented quite well the Atlantic dust seasonal cycle and its relative natural variability on monthly to interannual time scales. Improving our fundamental understanding of the physical relationships between climate modes and dust in coupled climate models should improve our interpretations of climate projections, and can also be used to inform seasonal predictions of tropical cyclones over the tropical North Atlantic, which are influenced by North African dust outbreaks (*Evan et al.*, 2006a).

Instead of choosing a mode of climate variability a priori to relate to dust transport and variability, we first examine the relationship between dust anomalies over the tropical North Atlantic and global SST anomalies during boreal summer. We are interested in boreal summer because it is the season with the largest dust outbreaks over the tropical North Atlantic. These outbreaks have the greatest potential to affect regional radiation budgets, and it has been shown that they can subsequently discourage the formation of tropical cyclones (*Evan et al.*, 2006a).

4.2 Data

4.2.1 Model and observational datasets

Our primary dataset in this study is a 150-year pre-industrial control global coupled climate model simulation. We ran this simulation using CESM 1.0.3 with interactive dust emission and transport, which allows dust as well as other components of the aerosol to affect radiative budgets and cloud properties at each timestep (*Hurrell et al.*, 2013). The treatment of aerosol size distribution is trimodal, as described in *Liu et al.* (2012). The simulation was run at a horizontal resolution of 2.5° (longitude (lon)) x 1.9° (latitude (lat)). The Dust Entrainment and Deposition Model (*Zender et al.*, 2003) emits dust in both accumulation (0.1-1μm) and coarse (1-10 μm) modes. Dust is assumed to be internally mixed with the other components in each mode (see Table 1 of *DeFlorio et al.* (2014) for a list of all aerosol species included in this CESM simulation, partitioned by mode). *DeFlorio et al.* (2014) explored natural variability of dust-climate interactions and evaluated the CESM simulation's representation of aerosol optical depth and size distribution near Cape Verde and aerosol optical depth and concentration near Barbados. They found realistic representations of the seasonal cycles and coherent fluctuations of these variables that were associated with regional monthly circulation anomalies extending from Africa into the subtropical North Atlantic.

One drawback of our CESM simulation is that dust emission parameterization is empirically tuned to reproduce observations (*Ginoux et al.*, 2001; *Zender et al.*, 2003). Dust emissions in our simulation do depend on wind speed and soil moisture, which provide mechanisms for feedbacks with meteorology. However, *Kok et al.* (2014b) showed that models that use this type of emission parameterization tend to underestimate the sensitivity of vertical dust flux to the soil's threshold friction velocity, and therefore underestimate the global dust cycle sensitivity. In their companion paper (*Kok et al.*, 2014a), they implemented a new physically-based emission parameterization scheme which shifted emissions towards the world's most erodible regions and improved CESM's overall representation of dust emission. Consequently, dust emissions in our model simulation are

not as realistic as those produced by a model with the newer physically-based dust emission parameterization.

We also use 44 years of monthly mean dust concentration recorded at Barbados from 1965 to 2008 (*Prospero and Lamb*, 2003). This is the world's longest continuous record of in-situ dust concentration.

To evaluate the model's simulation of dust over the tropical North Atlantic, we use a dataset derived from the Advanced Very High Resolution Radiometer (AVHRR) instrument, which provides estimates of dust Aerosol Optical Depth (dust AOD). This dataset is available over the tropical North Atlantic Ocean (-65W to -10W, 0N to 30N) from January 1982 to May 2010 at 1° horizontal resolution. *Evan et al.* (2006b) calibrated this dataset to distinguish between optically thick dust and optically thick cloud over ocean surfaces. One limitation of using this dataset to examine interannual variability of dust is that it only spans 28 years, and therefore only contains approximately 7-8 ENSO events. The CESM model simulation has the advantage of spanning 150 years.

4.2.2 Dust variables used in this study

Three different dust variables are analyzed in this study: a) atmospheric surface concentration ($\mu g/m^3$), b) dust aerosol optical depth (dust AOD), and c) total atmospheric dust burden (kg/m^2). Concentrations are used for model comparison to the Barbados dust dataset, since those observations measure dust concentration in the surface atmospheric layer. Dust AOD is used for model comparison to the tropical North Atlantic AVHRR dataset. Dust burden is defined as vertically integrated dust concentration and is used to examine the response of changes in atmospheric dust to changes in circulation associated with ENSO.

4.3 Observed dust concentration at Barbados

The time series of monthly mean dust concentration at Barbados (Figure 4.1; adapted from *Prospero and Lamb* (2003)) is perhaps the most widely used observational dataset of dust, and for good reason. It is one of only two in-

situ dust datasets extending more than 40 years (the other is located at Miami, and is also maintained by the University of Miami's Rosenstiel School of Marine and Atmospheric Science), and a high percentage of the record is continuous. There are very few other available observations that adequately record interannual and decadal changes in atmospheric dust (e.g. *Evan and Mukhopadhyay* (2010)). Consequently, it is important to understand how the low frequency variability seen in the remote Barbados dataset relates to variability in dust transport originating upstream over North Africa.

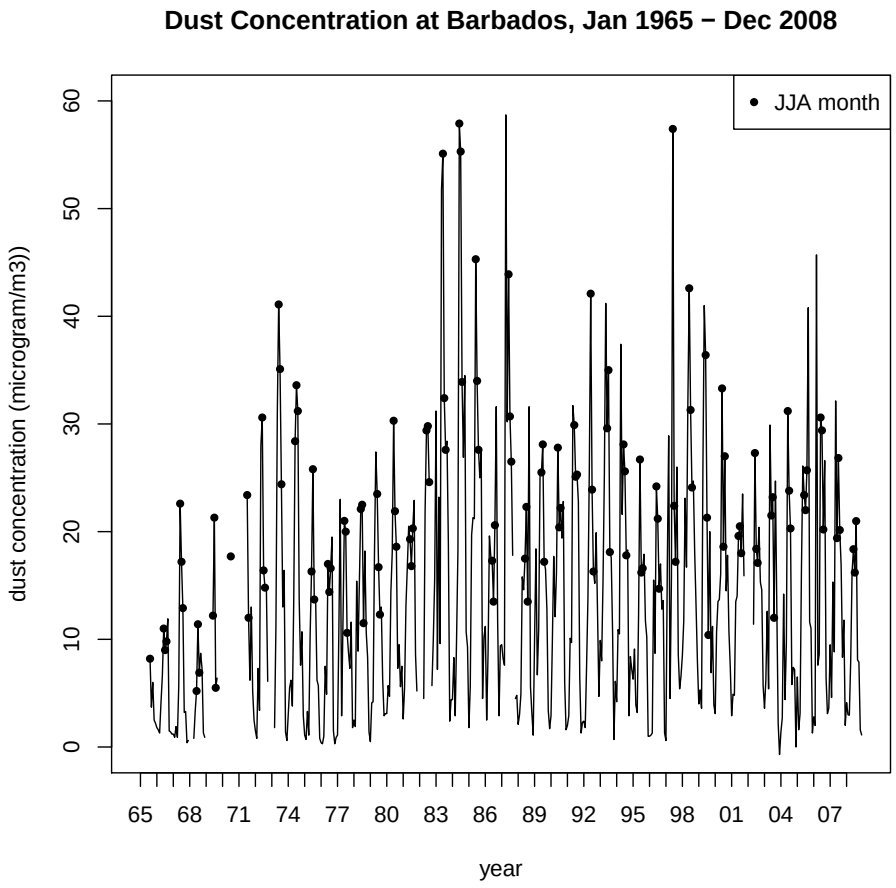

Figure 4.1: Observed monthly dust concentration ($\mu g/m^3$) at Barbados, January 1965 - December 2008. Filled dots denote June-July-August (JJA) months. Adapted from *Prospero and Lamb* (2003).

There is strong year-to-year variability in boreal summer (JJA) dust con-

centration anomalies ($\mu g/m^3$; long term monthly mean subtracted, then seasonally averaged) at the Barbados site (Figure 4.2). Maximum negative values occurred in the late 1960's, and maximum positive values occurred in the early 1980's.

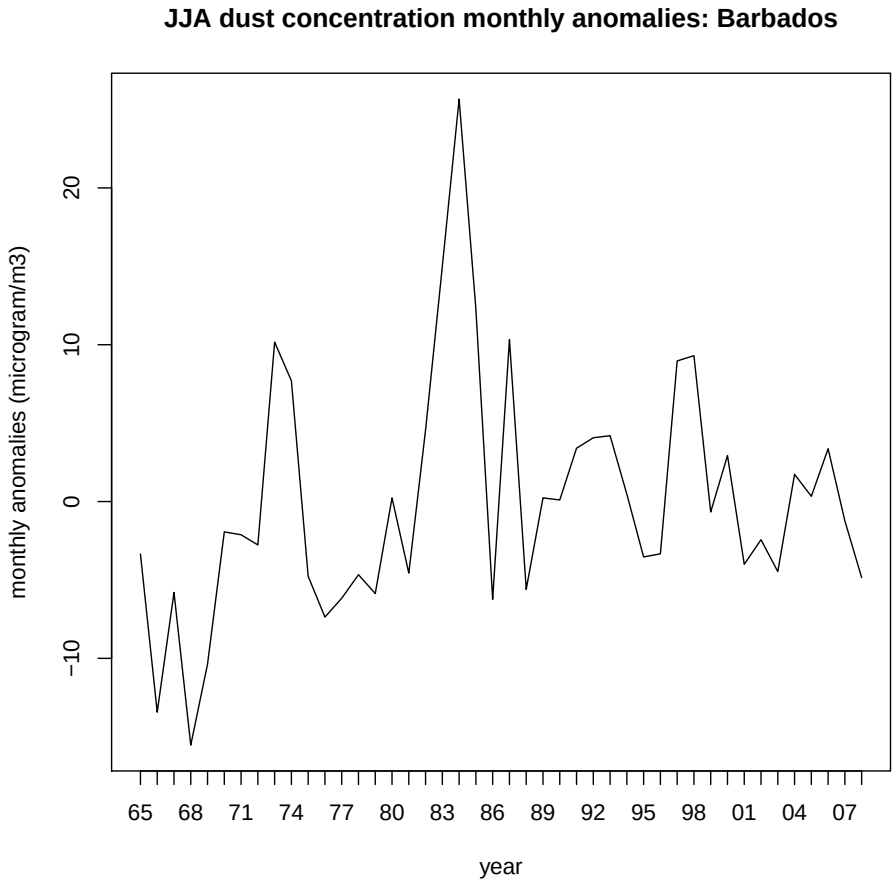

Figure 4.2: Observed JJA dust concentration anomalies ($\mu g/m^3$) at Barbados, January 1965 - December 2008.

Prospero and Lamb (2003) qualitatively suggested that many of the large dust outbreaks seen in the Barbados dataset might be related to the same-season or previous-season ENSO phase. Figure 4.3 explores this suggestion by regressing the JJA Multivariate ENSO Index (MEI) onto JJA dust concentration anomalies at Barbados. The MEI is defined as the leading principal component of the combined fields of sea level pressure, horizontal surface wind, sea surface temperature, surface air temperature, and cloud fraction. Positive MEI values are

associated with El Nino-like conditions in the eastern tropical Pacific (weakened westerly winds, increased sea surface temperature, and increased cloud fraction) and negative MEI values are associated with La Nina-like conditions in this region (strengthened westerly winds, decreased sea surface temperature, and decreased cloud fraction) (*Wolter and Timlin*, 1998).

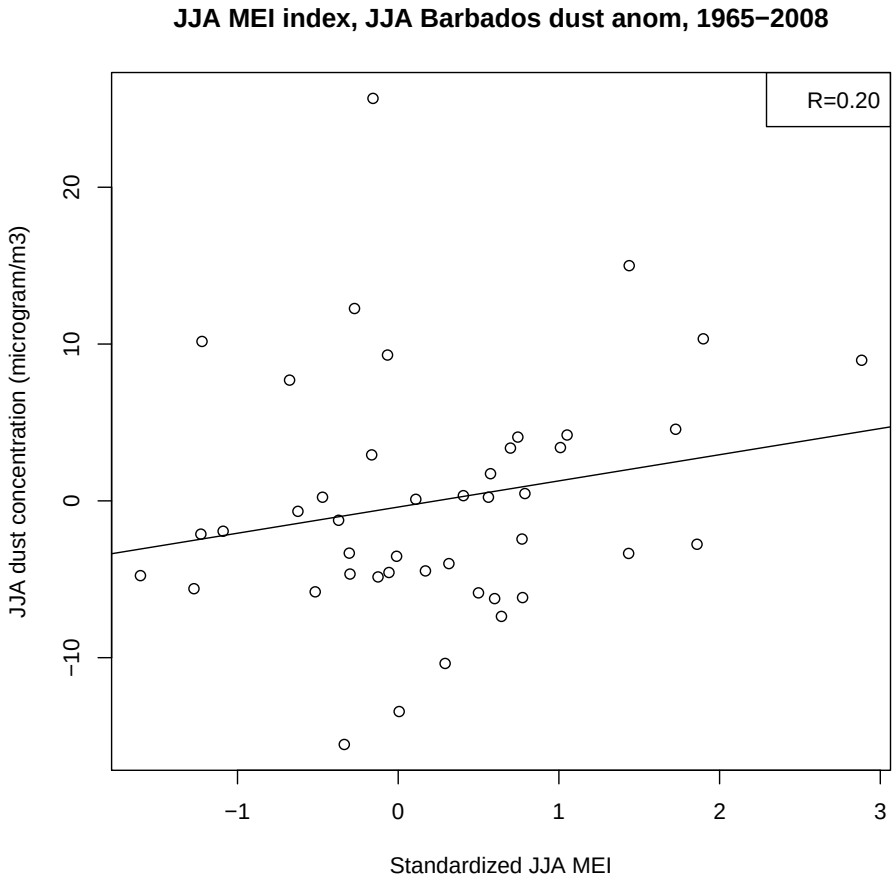

Figure 4.3: Scatterplot of JJA standardized multivariate ENSO Index and JJA Barbados dust concentration anomalies, January 1965 - December 2008.

The correlation between the two time series is 0.20, and no physically meaningful relationship is evident in this plot. A similarly weak correlation is seen in various lag-correlations of the two time series, and in the regression of the PDO index (*Mantua et al.*, 1997) onto JJA Barbados dust burden anomalies (not shown). *Doherty et al.* (2014) found similarly weak correlations ranging from -0.02 to 0.24

between Barbados dust concentration and various indices of ENSO.

4.4 Relating boreal summer tropical SST variability to North African dust

4.4.1 Interannual variability of atmospheric dust at Barbados

Figure 4.3 suggests that observed boreal summer dust concentration anomalies at Barbados are only weakly related to anomalous tropical Pacific SST variability. However, long-term observations of dust are essentially limited to this point-station dataset. Using our CESM simulation, which contains realistic ENSO variability (*Deser et al.*, 2012) and a correctly timed seasonal cycle of atmospheric dust at Barbados (*DeFlorio et al.*, 2014), what can we learn about the relationship of atmospheric dust anomalies to the major coupled-ocean atmosphere modes that drive interannual to decadal climate variability of many atmospheric variables?

The leading principal component of JJA tropical Pacific SST anomalies ("leading ENSO PC") is uncorrelated to JJA Barbados surface dust concentration anomalies ($\mu g/m^3$) in CESM (Figure 4.4; R = -0.04). The weak relationship found here is consistent with section 3 in *Doherty et al.* (2014) (Table 3), finding that the correlation of observed Barbados dust with ENSO can vary from weakly positive ($R_{max} = 0.24$) to weakly negative ($R_{min} = -0.02$) depending on the ENSO index used. In Figure 4.5 we examine the spatial structure of the relationship between CESM dust burden anomalies near Barbados and SST anomalies around the globe, which shows the point-by-point correlation of global JJA SST anomalies (3-dimensional) with JJA Barbados surface dust concentration anomalies over the entire 150-year simulation. There are only weakly negative correlation values over the central and eastern tropical Pacific, reinforcing other analyses indicating that tropical Pacific SST variability is not related to fluctuations in atmospheric dust at Barbados (see Figures 4.3-4.4). Moderate negative correlations are found with SST anomalies upstream of Barbados over the central tropical North Atlantic.

This is likely due to a combined effect of cooling of SSTs associated with large dust outbreaks (radiative effect) and increased ocean-to-atmosphere latent and sensible heat fluxes associated with increased trade winds in the southern easterly branch of the Azores High, which is prevalent during boreal summer over this region (*Doherty et al.*, 2012).

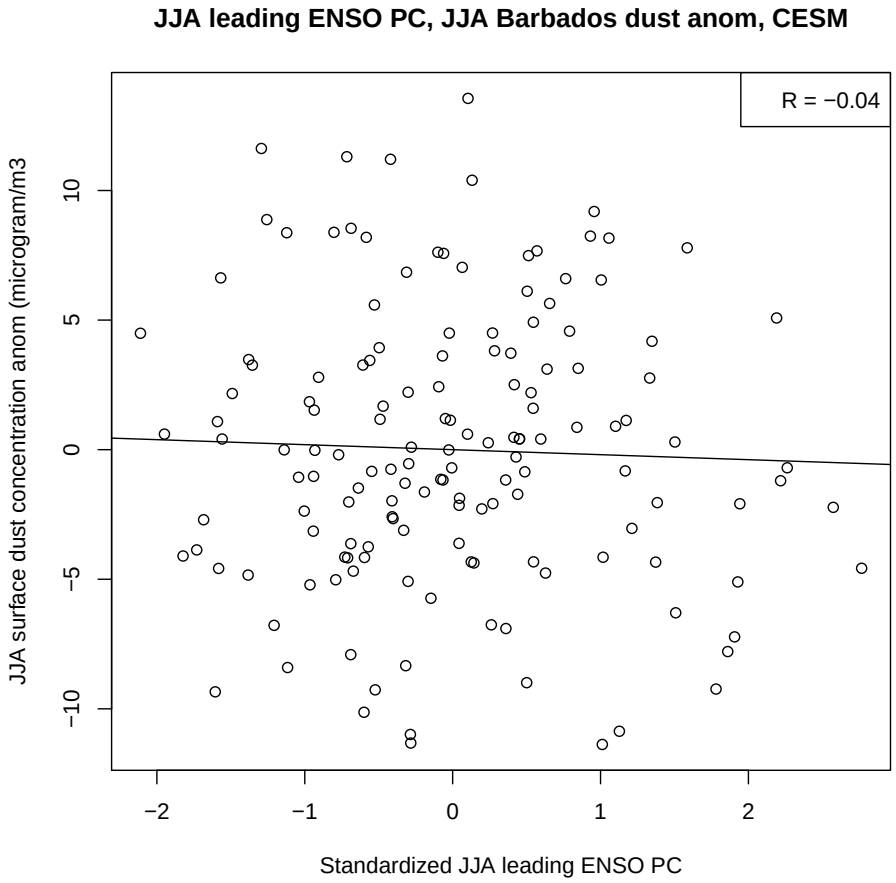

Figure 4.4: Scatterplot of JJA standardized leading principal components of tropical Pacific SST variability and JJA Barbados dust concentration anomalies in 150-year CESM simulation.

Dust plumes that originate over North Africa must travel across the entire tropical Atlantic basin before reaching Barbados. Consequently, atmospheric processes such as wet and dry deposition, vertical ascent into the upper troposphere, and cloud seeding can change the signature of dust as it travels westward across

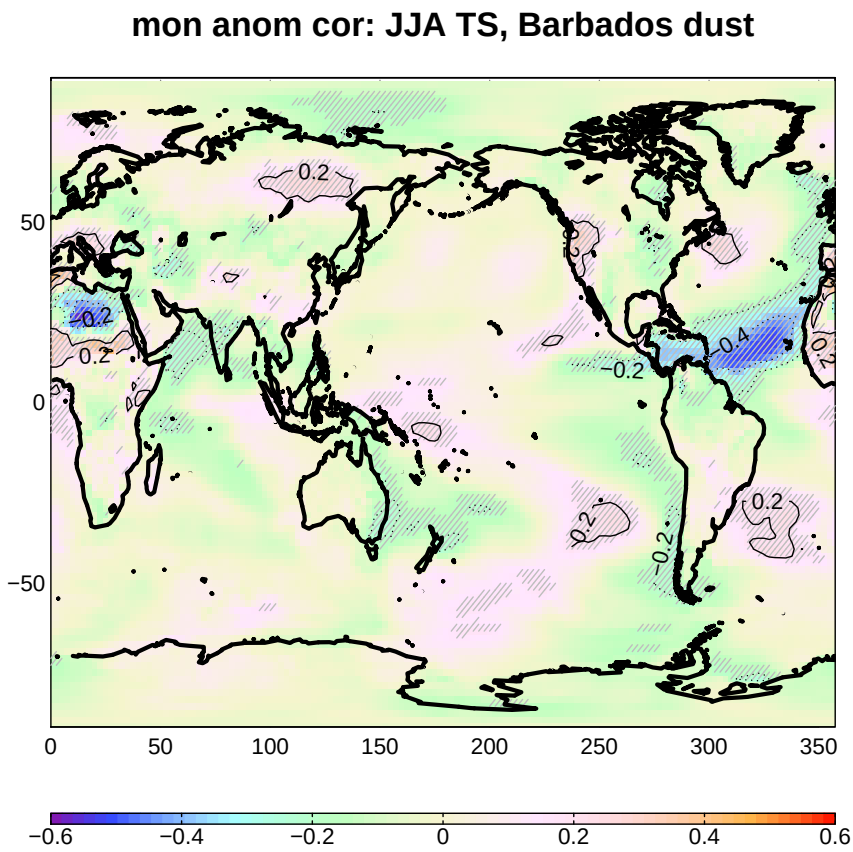

Figure 4.5: Pearson correlation of JJA Barbados dust concentration anomalies and global surface temperature anomalies in 150-year CESM simulation. Gray hatches indicate regions where there is 95% confidence that the true correlation is not equal to zero, using a two-sample t test.

the ocean, away from its continental source in the Sahara-Sahel desert region. Different atmospheric circulation patterns far from emission sources can also change the spatial structure of dust anomalies. Because of these processes, concentrations measured at Barbados are not always indicative of source region characteristics (*Prospero and Mayol-Bracero*, 2013; *Engelstaedter et al.*, 2009). Given this and our goal of understanding low frequency variability of North African dust in the climate system, it is useful to characterize the low frequency variability of atmospheric dust anomalies closer to the source of emission. To do so, we will use AVHRR satellite-derived observations in conjunction with the model simulation

to try to learn more about the relationship of interannual and decadal variability of North African dust anomalies to the major modes of global climate.

4.4.2 Interannual variability of atmospheric dust close to North African source regions

The raw and detrended time series of JJA dust AOD monthly anomalies from AVHRR downstream of North Africa (-40W to -20W, 15N to 25N) are shown in Figure 4.6. Interannual variations of dust AOD are present over this region, and a downward trend of dust AOD anomalies has been observed since 1982. Figure 4.7 shows the regression of the JJA MEI onto detrended JJA dust AOD anomalies over downstream North Africa. The correlation between the two time series is -0.23, suggesting a weak association between anomalously dusty summers and cool tropical Pacific SST anomalies over this region.

We now compare the observed interannual variability of dust anomalies over the tropical North Atlantic to our CESM simulation. Several interesting features exist in the 150-year model time series of area-averaged JJA downstream North Africa dust AOD anomalies, which is shown in Figure 4.8. Most importantly, strong interannual variations in dust AOD anomalies in this region exist. Discernable interannual variability can also be seen in observed dust concentration anomalies at Barbados (Figure 4.2), but Figure 4.3 and previous work both show that those summertime fluctuations are not strongly correlated to ENSO. In addition, the magnitude of boreal summer dust AOD anomalies in CESM is similar to observations (Figure 4.6). The correlation between the JJA leading ENSO principal component and JJA dust AOD anomalies over downstream North Africa is -0.63 (Figure 4.9), which is considerably higher than observed. However, the CESM simulation (150 years) is over five times as long as the AVHRR dataset (28 years).

The correlation between JJA downstream North Africa dust burden anomalies and simultaneous global SST anomalies shows a robust signature of tropical Pacific influences (Figure 4.10). Similar to the results obtained for Barbados dust in Figure 4.5, the correlation map for dust anomalies west of Africa is strongly neg-

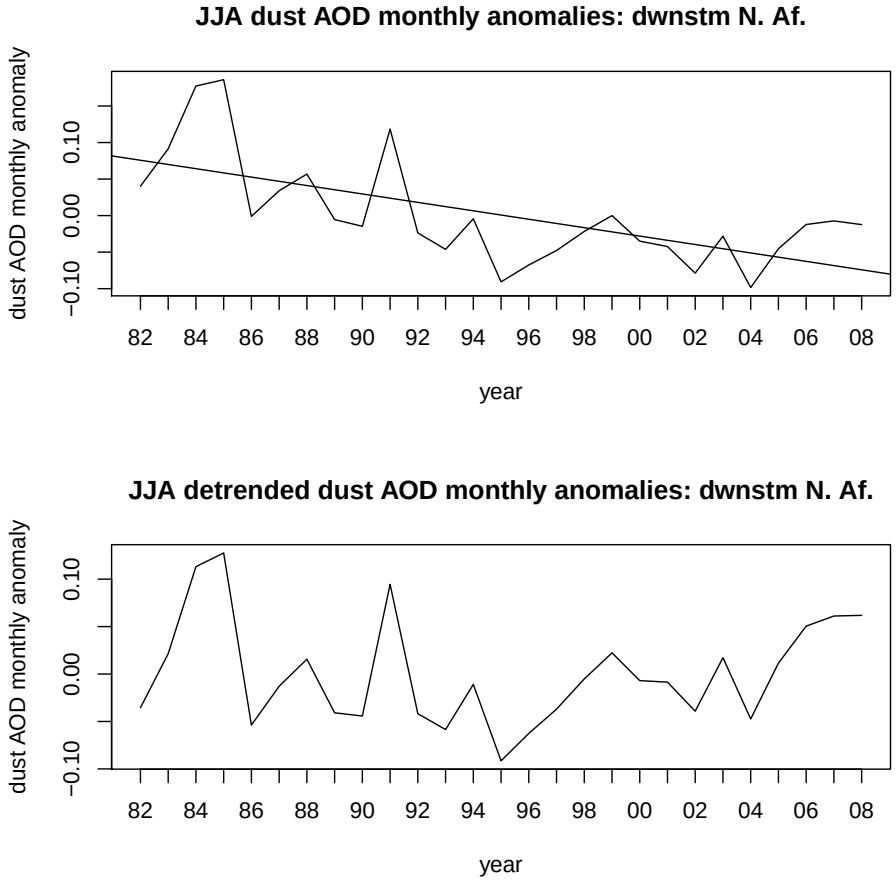

Figure 4.6: JJA downstream North Africa (-40W to -20W, 15N to 25N) dust aerosol optical depth (AOD) anomalies (top) and detrended dust AOD anomalies (bottom), January 1982 - December 2008. Data were derived from satellite estimates described in *Evan et al.* (2006c).

ative over the tropical North Atlantic, meaning that surface temperature anomalies are negative when dust concentrations are higher, indicating that under these conditions, more dust is blown off the African continent. However, a much different spatial structure from the Barbados map is found over the Pacific basin. For the anomalies west of Africa, large negative values are present in the central and tropical Pacific, very similar to the anomalous SST structure associated with strong ENSO events. Negative values in this region in Figure 4.10 indicate that anomalously strong JJA dust outbreaks downstream of North Africa over the tropical North Atlantic occur during anomalously cool SST summers over the central and

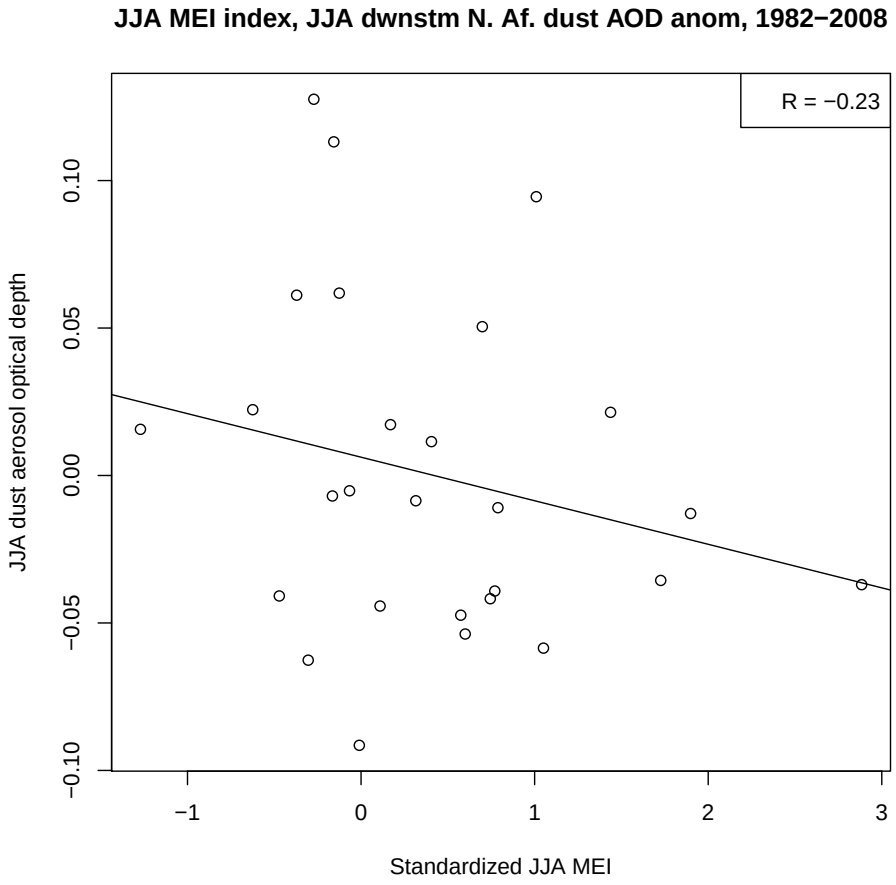

Figure 4.7: Scatterplot of JJA standardized multivariate ENSO Index and JJA detrended downstream North Africa dust AOD anomalies, January 1982 - December 2008.

eastern tropical Pacific. There is also structure of the correlation map over the North Pacific basin that is reminiscent of the Pacific Decadal Oscillation. These results suggest a relationship in CESM between anomalous Pacific SST variability and North African dust transport during boreal summer that is stronger than observed, particularly at Barbados, over the late 20th century.

It is important to more precisely quantify the associated timescale of variability of North African dust anomalies over the tropical North Atlantic. This is a region of great interest for seasonal forecasting, as it is the genesis region of many Atlantic hurricanes that form as a result of easterly waves propagating from con-

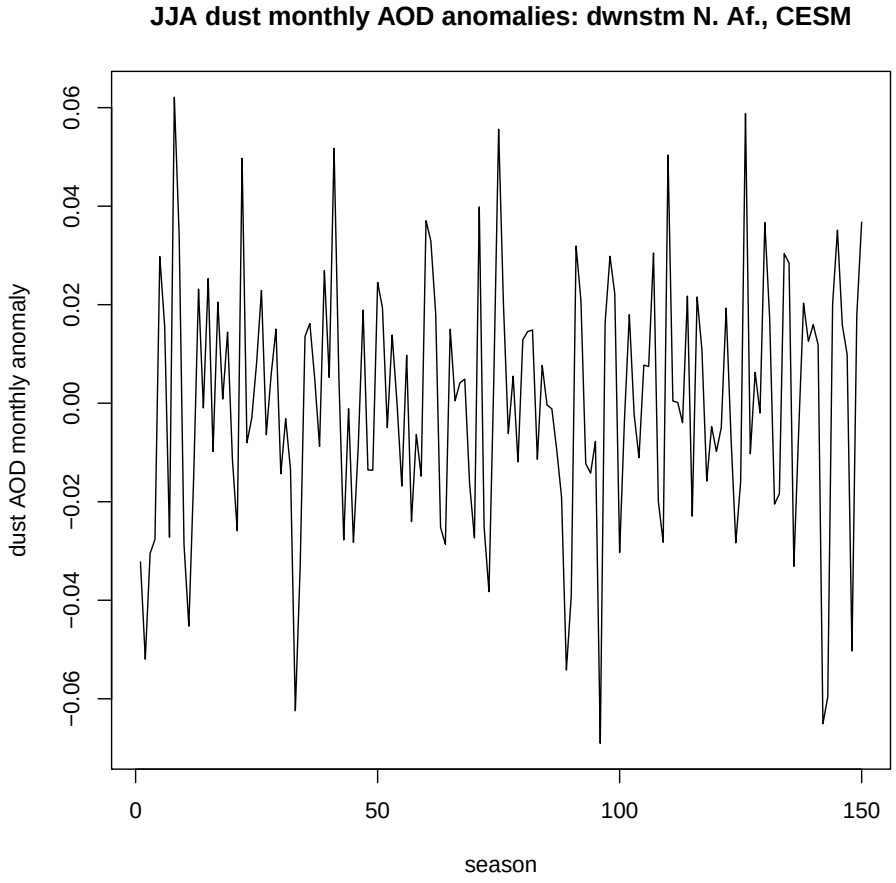

Figure 4.8: JJA downstream North Africa dust AOD anomalies, normalized by the downstream mean value of raw dust burden over this area.

tinental Africa. Because dust outbreaks discourage tropical cyclone formation due to cooling of underlying SST (*Evan et al.*, 2006a), associating anomalously dusty seasons with a more predictable component of the climate system (e.g. ENSO) has the potential to increase predictability of these related phenomena on shorter timescales.

We compute a time-evolving metric that encompasses the relationship between the downstream dust burden anomalies and global surface temperature anomalies by calculating the pseudo-principal component of boreal summer dust-surface temperature variability. Here, we define the pseudo-principal component of boreal summer dust-surface temperature variability as

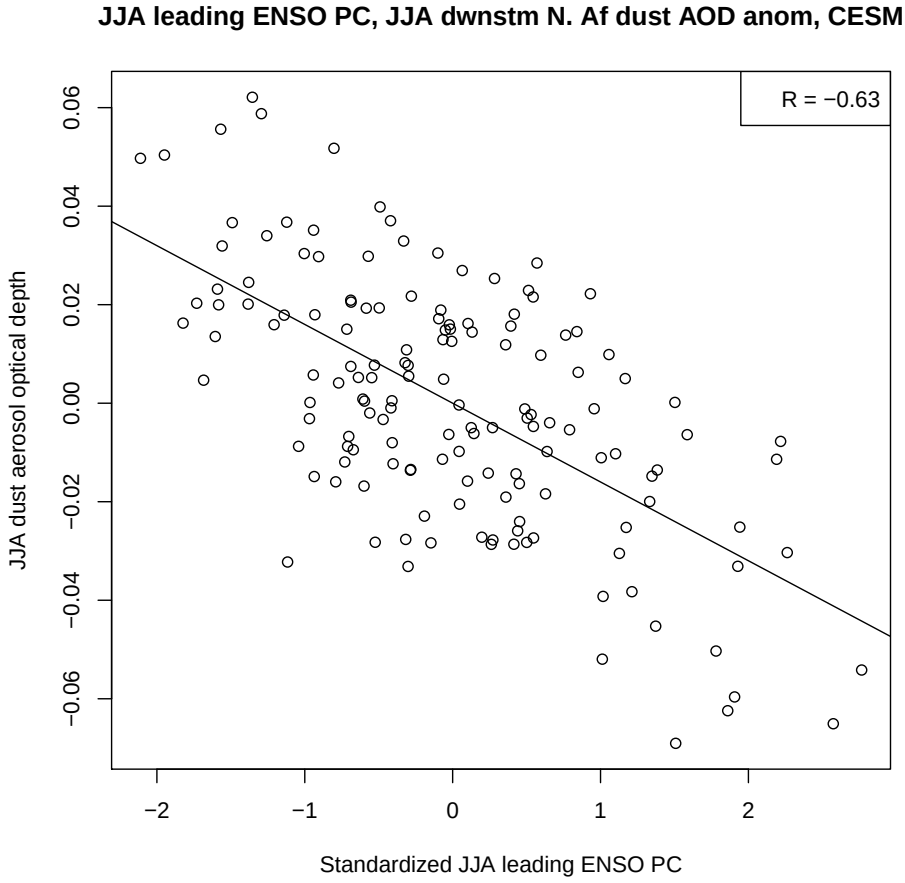

Figure 4.9: Scatterplot of JJA standardized leading principal components of tropical Pacific SST variability and JJA downstream North Africa dust AOD anomalies in 150-year CESM simulation.

$$Pseudo\ PC = \frac{1}{n} \sum_{i=1,j=1}^{n} \sum_{k=1}^{K} Cor_{i,j} \bullet TS_{i,j,k} \tag{4.1}$$

where n = total number of grid cells, K = number of model years, Cor = spatial pattern of correlations of boreal summer global surface temperature anomalies and downstream North African dust burden anomalies (e.g., Fig. 4.10), and TS = anomaly field of global surface temperature anomalies for each summer, k. The pseudo-PC shows how strongly global surface temperature anomalies project onto the pattern in Fig. 4.10 over time.

Figure 11 shows the boreal summer pseudo principal component time series

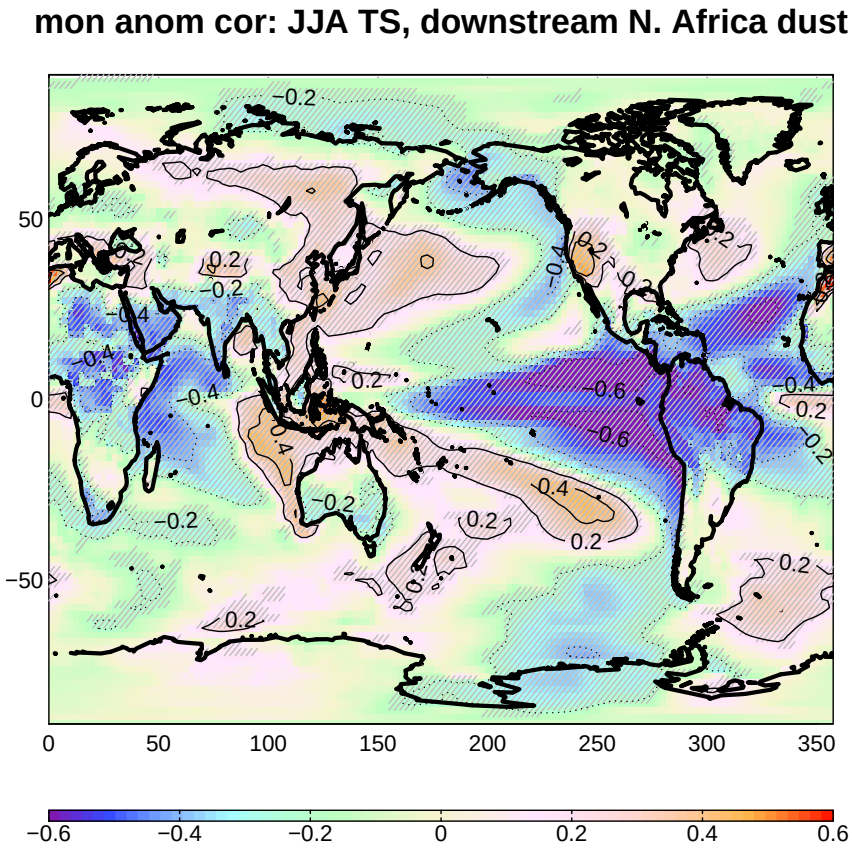

Figure 4.10: Pearson correlation of JJA downstream North Africa (320E-340E, 15N-25N) dust burden anomalies and global surface temperature anomalies in 150-year CESM simulation. Gray hatches indicate regions where there is 95% confidence that the true correlation is not equal to zero, using a two-sample t test.

(top panel) and its associated power spectrum (bottom panel) with 95% confidence bounds. The power spectrum was computed using a Thomson multitaper power spectral estimate (Percival and Walden 1993). There is a peak in the pseudo principal component spectrum around 5 years, with appreciable power in the decadal and multidecadal bands. This spectral estimate shows that the pseudo-PC, which mathematically encompasses the relationship between JJA downstream North African dust burden anomalies and global surface temperature anomalies, is varying most strongly on interannual timescales. This result is not surprising given the spatial structure of the correlations over the Pacific basin (Figure 10), but is

interesting in that it is consistent with the hypothesis that surface temperature variability in the Pacific basin could be remotely driving changes in dust burden anomalies over North Africa on interannual timescales.

Figure 4.11: Pseudo principal component of JJA global surface temperature and downstream North African dust anomalies in CESM (top) and associated power spectrum (bottom, blue) computed using a Thomson multitaper power spectral estimate. The spectrum is bounded by 95% confidence limits (red).

4.4.3 Composites of mineral dust and circulation on strong ENSO seasons

Composites of raw values of dust burden, surface zonal wind, and 700hPa zonal wind, averaged on the top 10% La Nina seasons (top panels) and the top 10% El Nino seasons (middle panels) are shown in Figures 4.12-4.14. The percentiles were defined using the leading principal component time series of tropical Pacific SST anomalies (Supplementary Figures 4.20-4.21). The bottom panel is the top

panel minus the middle panel. *DeFlorio et al.* (2014) showed that maximum boreal summer dust concentration over the open ocean is simulated around 700hPa in CESM, which is why we calculate zonal wind at the 700hPa level here. These three figures show that on strong La Nina seasons, downstream North African dust burden values in CESM increase due to statistically significant increases in lower tropospheric easterly wind. A similar qualitative picture emerges for decadal variability of dust transport, but the magnitude of the effect is smaller than for interannual variability (Supplementary Figures 4.24-4.26).

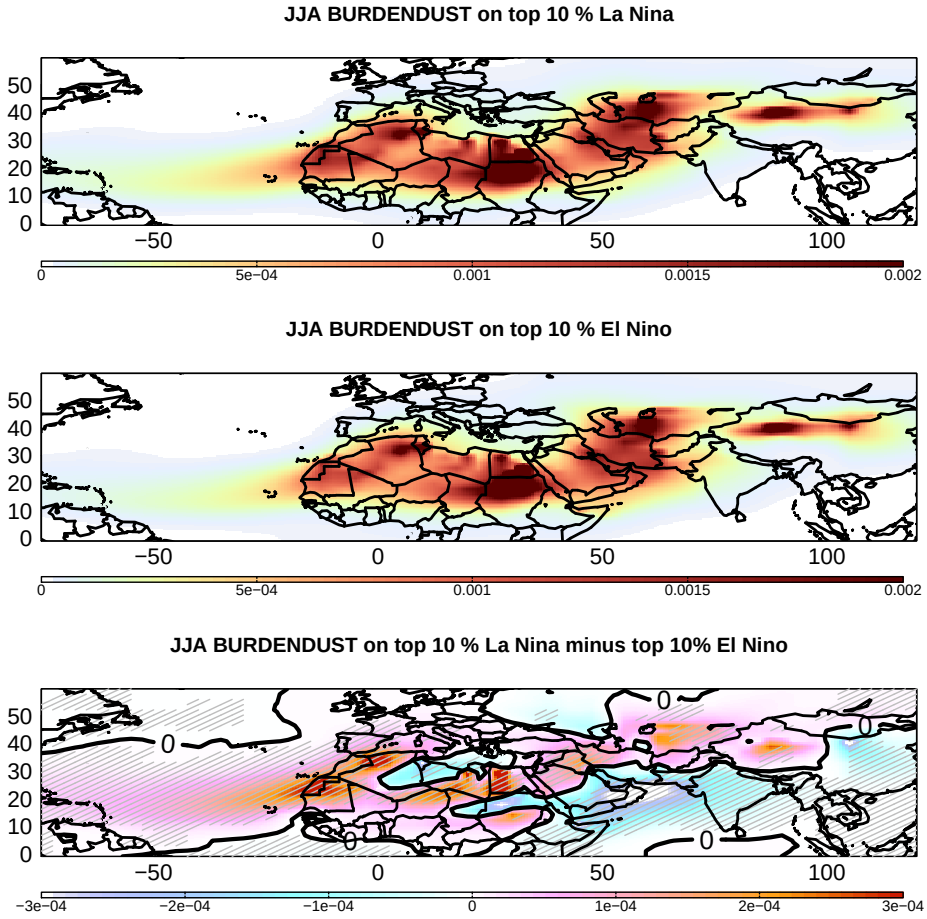

Figure 4.12: Composite of JJA dust burden (kg/m^2) on top 10% La Nina seasons (top) and top 10% El Nino seasons (middle) in CESM. The bottom panel is the top panel minus the middle panel. Gray hatches indicate regions where there is 95% confidence that the true correlation is not equal to zero, using a two-sample t test.

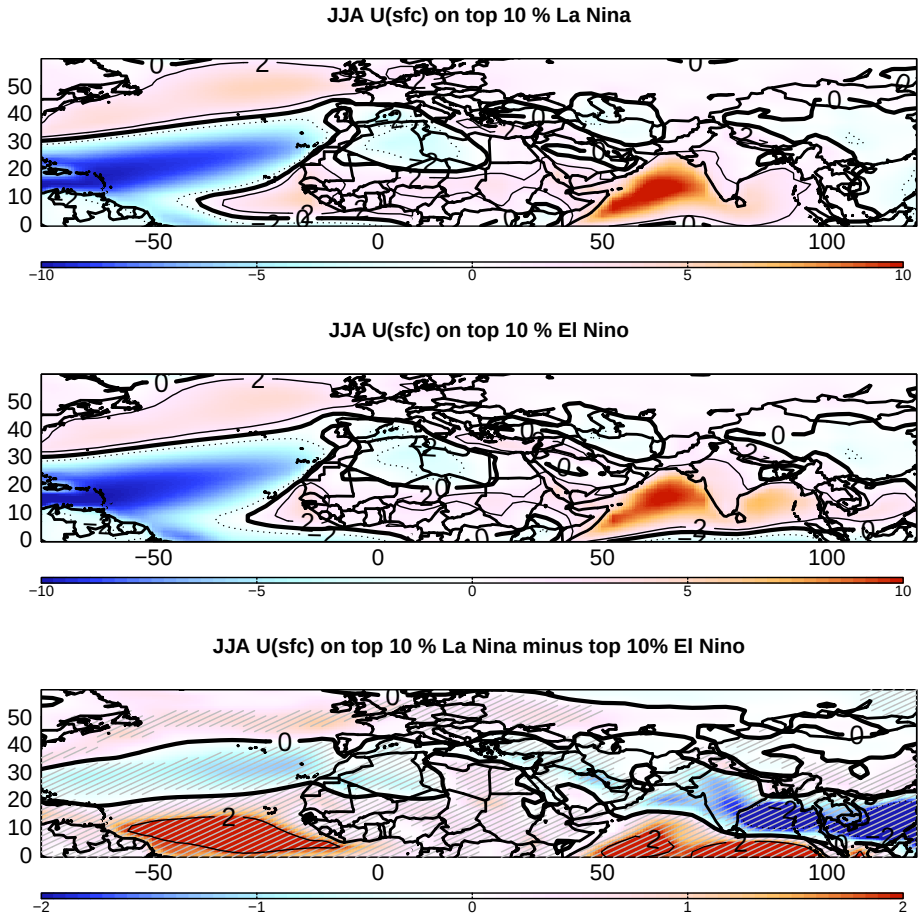

Figure 4.13: As in Fig. 4.12, but for surface zonal wind.

4.5 Modulation of ENSO-North African dust relationship on decadal timescales

The importance of the differing record lengths for observations and CESM is explored in Figure 4.15, which shows a 28-year sliding correlation of the JJA leading ENSO principal component and JJA dust AOD anomalies over downstream North Africa. The window length is chosen to be 28 years in order to match the length of the AVHRR dataset. The correlation coefficients range from -0.34 to -0.77, which demonstrates the sensitivity of the ENSO-dust regression to record length. This figure suggests that existing observations over the tropical North

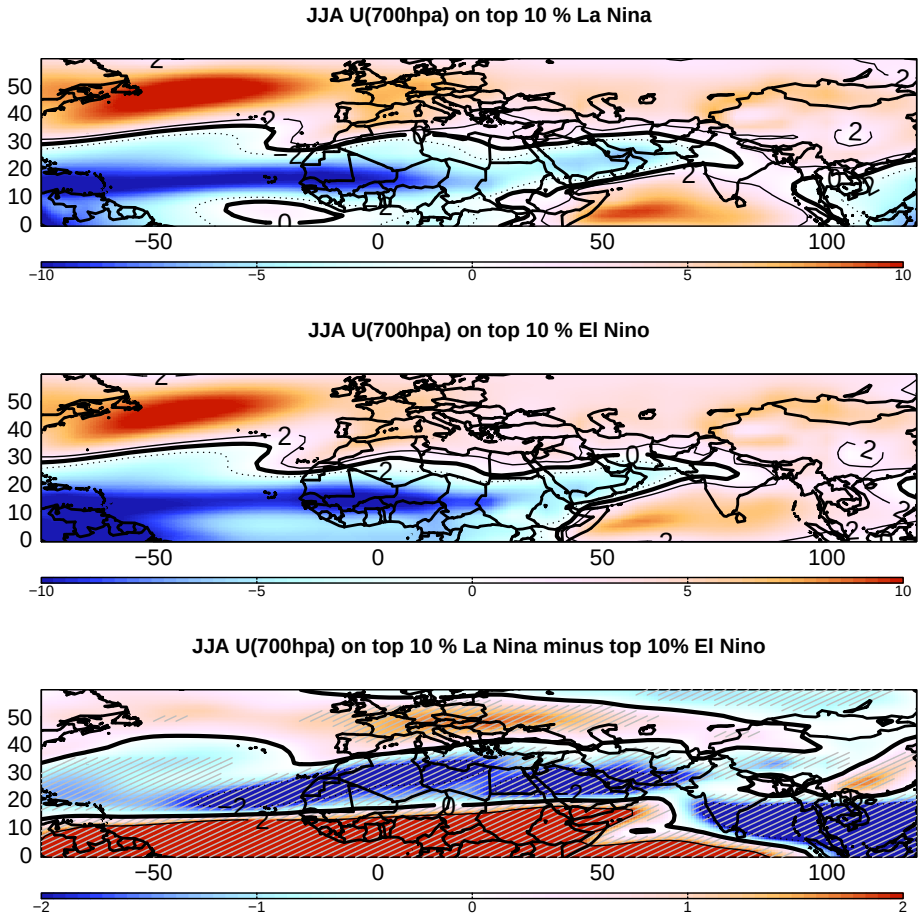

Figure 4.14: As in Fig. 4.13, but for 700hPa zonal wind.

Atlantic are not extensive enough to characterize the varying relationship between tropical Pacific SST variability and North African dust.

Sea level pressure (SLP) and 700 hPa zonal wind composites on the most and least negative ENSO-dust sliding correlation periods are shown in Figure 4.16. The composites are calculated as an average of top 10% most negative and top 10% least negative sliding correlation periods from Figure 4.15 (<-0.730 and >-0.435, respectively). The spatial structure of both SLP and lower tropospheric zonal wind anomalies are distinctly reminiscent of variability associated with the North Atlantic Oscillation (NAO). In addition, the 28-year sliding correlation of ENSO and downstream North African dust appears to be roughly out of phase with the 28-year running mean of the NAO index in CESM (Figure 4.17; R $\sim$ 0.54). Previous

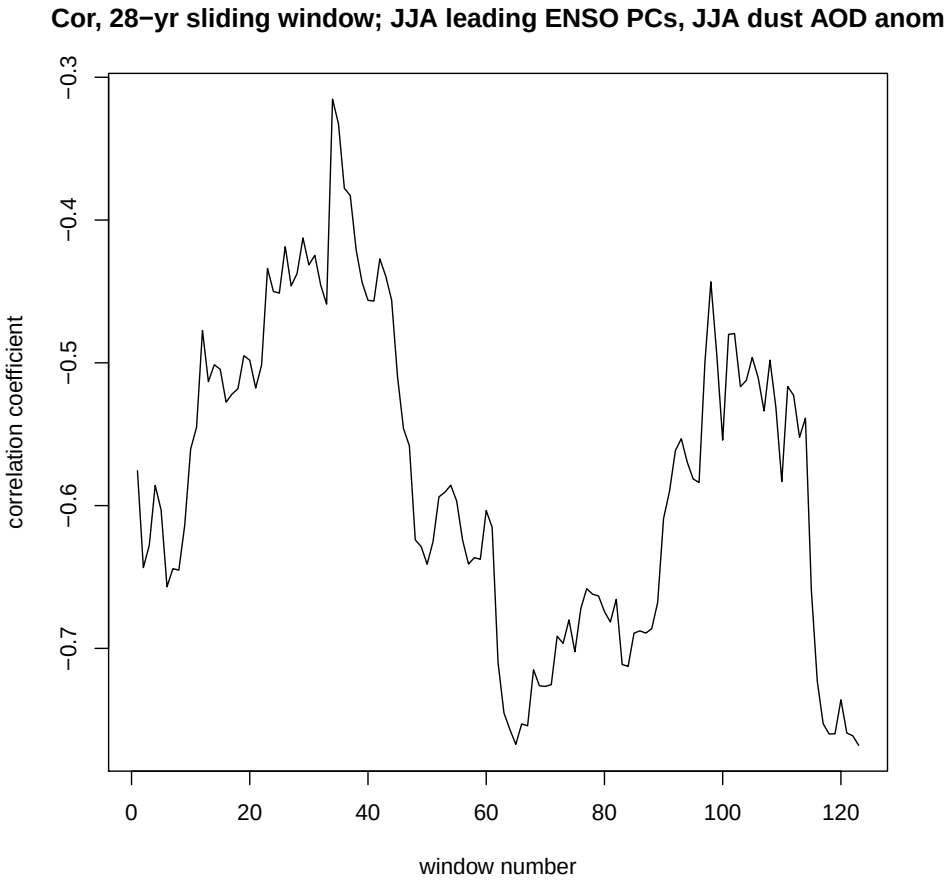

Figure 4.15: 28-year sliding correlation of JJA standardized leading principal components of tropical Pacific SST variability and JJA downstream North Africa dust AOD anomalies in CESM.

studies (e.g. *Riemer et al.* (2006)) have found no relationship between the NAO and North African dust variability during boreal summer, and the relationship between the JJA NAO index (which we define as the difference between monthly anomaly SLP values near Azores and Iceland) and downstream North Africa dust anomalies is weak in CESM (R $\sim$ 0.16). However, Figures 4.16 and 4.17 provide evidence in our model simulation that the NAO may be destructing the Pacific SST-North African dust relationship on decadal timescales.

The boreal summer NAO index is more strongly correlated to downstream North Africa dust AOD anomalies during the least negative ENSO-dust sliding cor-

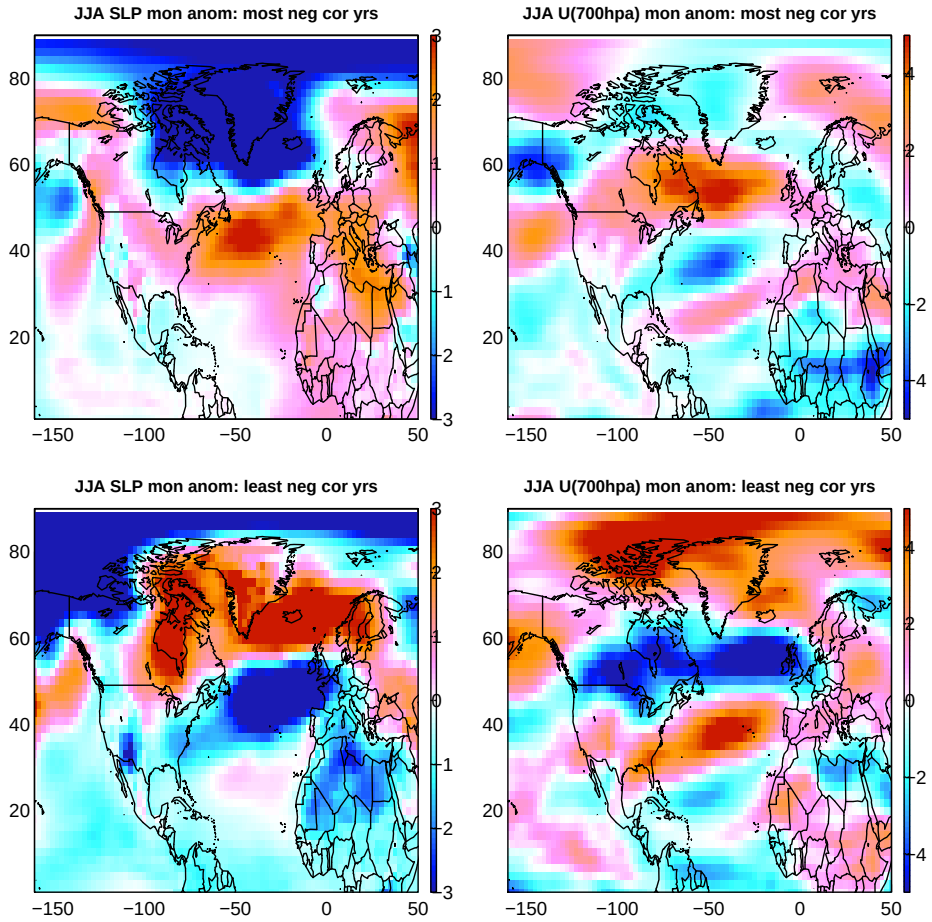

Figure 4.16: Composite of JJA sea level pressure monthly anomalies (left column) and 700hPa zonal wind anomalies (right column) on the most negative (top row) and least negative (bottom row) sliding correlation periods in CESM, determined from Fig. 4.15.

relation periods (Figure 4.18, top panel), but the relationship between the NAO index and lower tropospheric zonal wind during these periods is quite weak (Figure 4.18, bottom panel). We conclude that the NAO modulation of North African dust variability manifests itself via other atmospheric processes in the North African region. In addition, ENSO variability is larger during the most negative sliding correlation periods (Figure 4.19), suggesting that fluctuations in the strength of ENSO on decadal timescales may also be modulating the relationship between Pacific SST variability and North African dust. However, the regression shown in the top right panel of Figure 4.19 is very similar even after removing the anomalously

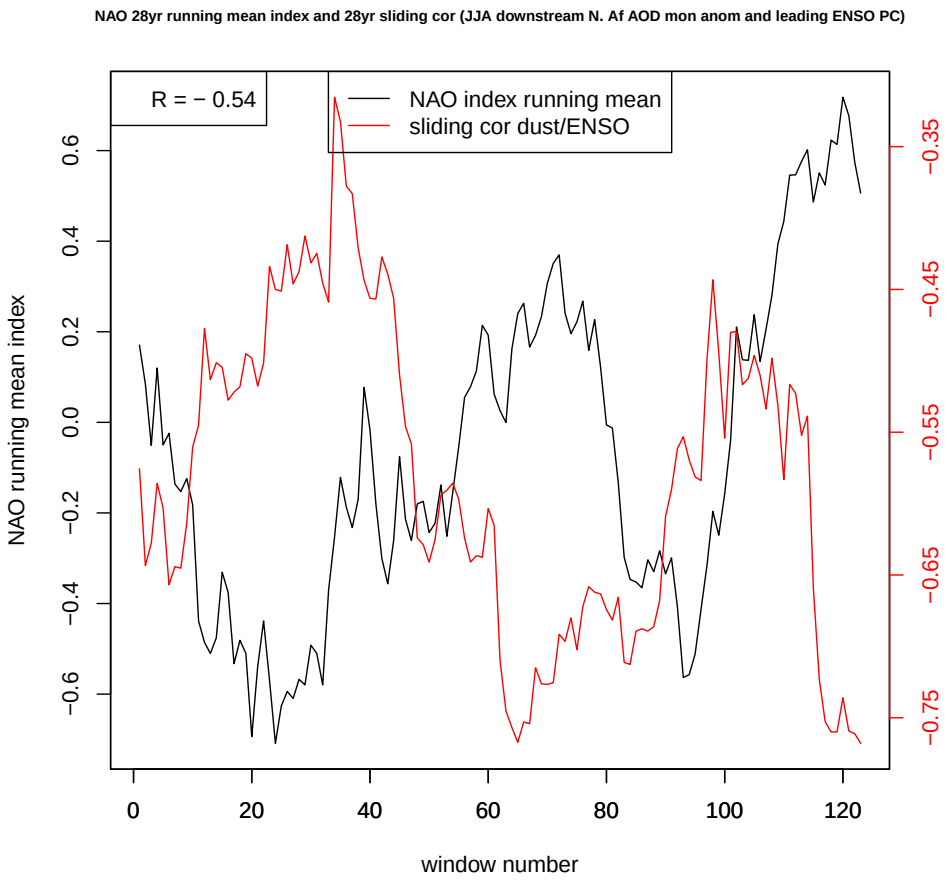

Figure 4.17: As in Fig. 4.15, but with JJA NAO index 28-year running mean (black line).

strong ENSO events (not shown), which weakens this hypothesis.

4.6 Conclusions and Discussion

In this study, we used a 150-year preindustrial control CESM 1.0 simulation, which complements existing observations of mineral dust at Barbados and over the tropical North Atlantic, to show that boreal summer dust variability over the eastern tropical North Atlantic may be strongly influenced by tropical and North Pacific SST variability. This influence manifests itself through changes in lower tropospheric atmospheric circulation patterns over the North African conti-

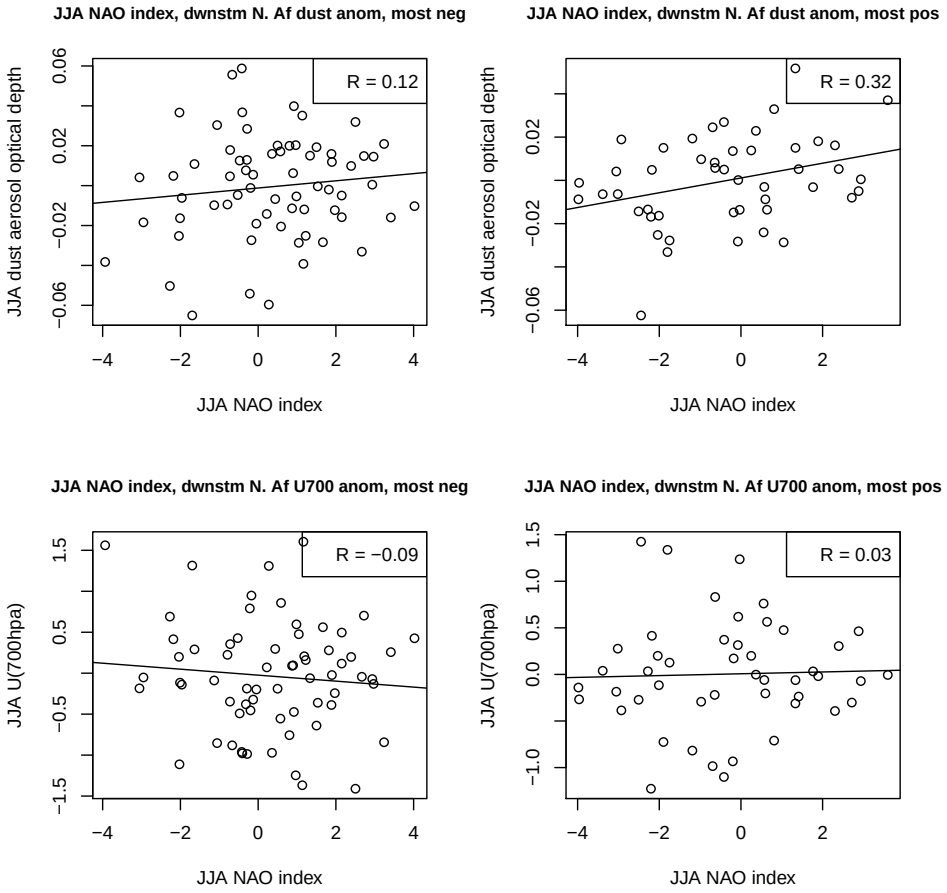

Figure 4.18: Scatterplot of JJA NAO index and JJA downstream North Africa dust AOD anomalies (top row) and 700hPa zonal wind anomalies (bottom row) on the most negative (left column) and least negative (right column) sliding correlation periods in CESM.

nent (Figures 4.12-4.14) that are reminiscent of a Walker Cell teleconnection. The relationship between Pacific SST variability and North African dust fluctuates on decadal to multidecadal timescales in CESM, and we show that this fluctuation is strongly associated with North Atlantic SST variability. We also show that observations of dust at Barbados are weakly correlated with observations of Pacific basin SST variability, and that the correlation is of opposite sign as observed dust AOD anomalies and Pacific basin SST variability over the tropical North Atlantic, downstream of North Africa. This suggests that other atmospheric processes and/or coupled-ocean atmosphere interactions are dominant in characterizing the

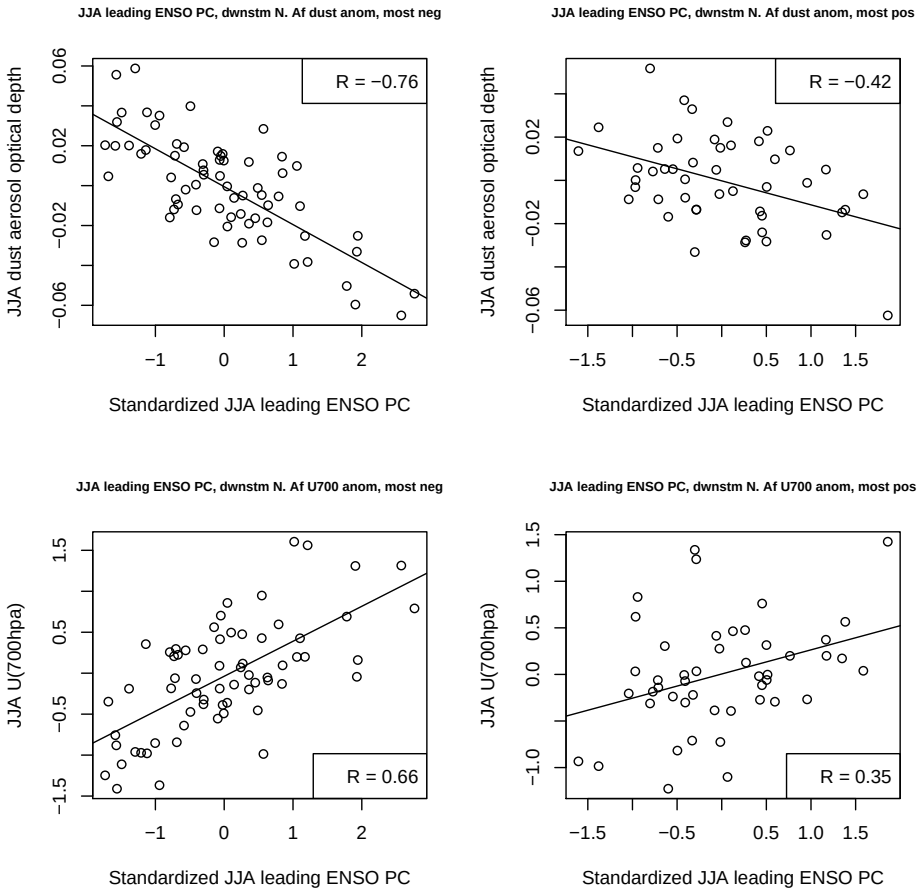

Figure 4.19: Scatterplot of JJA standardized leading principal components of tropical Pacific SST variability and JJA downstream North Africa dust AOD anomalies (top row) and 700hPa zonal wind anomalies (bottom row) on the most negative (left column) and least negative (right column) sliding correlation periods in CESM.

cross-basin variability of dust.

This work adds to previous studies that have demonstrated the complex response of atmospheric dust to perturbations in the climate system. It is important for future studies to better understand the relationship of the results here to recently published work which shows that a statistically significant portion of variability in dust concentrations at Barbados can be explained by fluctuations in the West African Convergence Zone (*Doherty et al.*, 2014).

One caveat of our work is that we use a CESM preindustrial control simu-

lation, but observations of dust at Barbados and over the tropical North Atlantic could reflect anthropogenic contributions to dust variability such as agricultural practices. *Ginoux et al.* (2012) estimate that up to 8% of North African dust emissions are anthropogenic, mostly due to land use changes in the Sahel region. In addition, late 20th century historical CMIP5 simulations have elucidated errors in the representation of dust emissions and interannual variability (*Evan et al.*, 2014).

Future studies are needed to explore the implications for seasonal predictability implied by the relationships found here between North African dust transport and tropical Pacific SST variability. ENSO is the dominant coupled-ocean atmosphere energetic component of the climate system, and because statistical and dynamical models have demonstrated some skill in predicting tropical Pacific SST interannual variability some months ahead (e.g. *Barnston et al.* (2012)), there may be potential to improve predictability of North African dust transport on similar timescales. This could subsequently lead to more skillful forecasts of the initiation of tropical cyclones over the eastern tropical Atlantic on seasonal timescales. Our work also suggests that we may learn more about the interaction of climate modes and North African dust variability in the coming decades, when our existing network of observations from both in situ measurements and satellite products becomes more extensive.

North African dust varies on timescales of seconds to millennia, and the characteristics of this variability depend critically on season, local conditions, and remote ocean-atmosphere teleconnection patterns. Because of sparsely available observations, the hybrid observational-modeling approach employed in this study is a useful and necessary tool for increasing our understanding of dust variability on long timescales.

4.7 Acknowledgements

This study forms a portion of the Ph.D. dissertation of M.J.D. Funding was provided by NSF (AGS-1048995), and by the U.S. Department of Energy, Office of Science, Decadal and Regional Climate Prediction using Earth System Mod-

els (EaSM program). Battelle Memorial Institute operates the Pacific Northwest National Laboratory for the DOE under contract DE-AC06-76RLO 1830. We are grateful for the contribution made by Joseph M. Prospero (RSMAS, U. Miami), who provided us with the Barbados dust record. We also acknowledge Cynthia Twohy (NorthWest Research Associates and SIO) and Diego Melgar (UC-Berkeley) for improving the manuscript, and for assistance with the pseudo-principal component spectral analysis used in this study. Our CESM simulation can be accessed via an email inquiry (mdeflori@ucsd.edu).

Chapter 4 is published in its entirety in:

- **DeFlorio, M.J.**, I. D. Goodwin, D. R. Cayan, A. J. Miller, S. J. Ghan, D. W. Pierce, L. M. Russell, and B. Singh (2015), "Interannual modulation of subtropical Atlantic boreal summer dust variability by ENSO", *Clim. Dyn., in press*, doi: 10.1007/s00382-015-2600-7.

4.8 Supplementary Figures

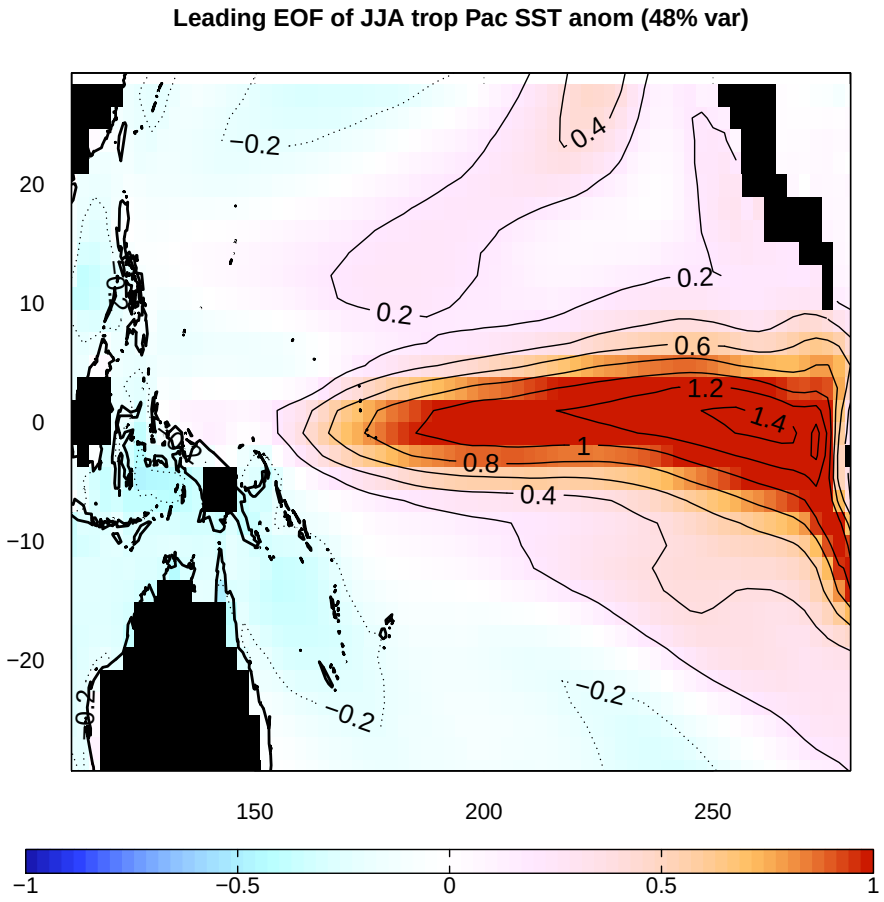

Figure 4.20: Leading EOF of JJA tropical Pacific (110E to 280E, 30S to 30N) SST anomalies in CESM. The values are normalized such that the EOF is in degrees C per standard deviation of the associated principal component shown in Figure 4.21.

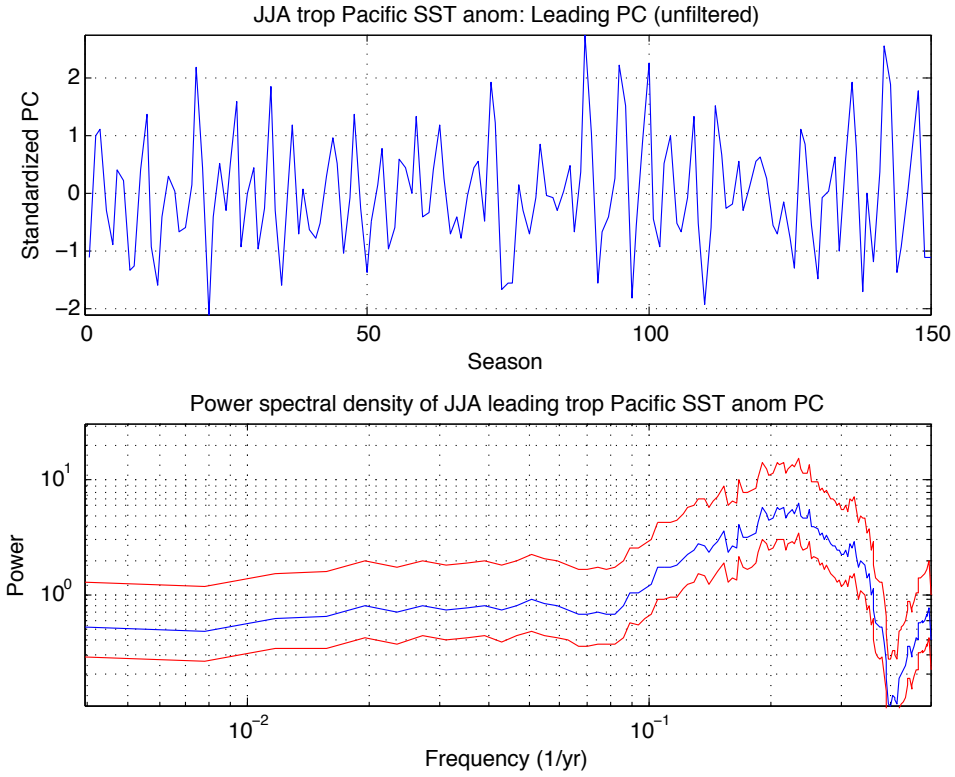

Figure 4.21: Leading standardized principal component of JJA tropical Pacific SST anomalies in CESM (top) and associated power spectrum (bottom, blue), computed using a Thomson multitaper power spectral estimate. The spectrum is bounded by 95% confidence limits (red).

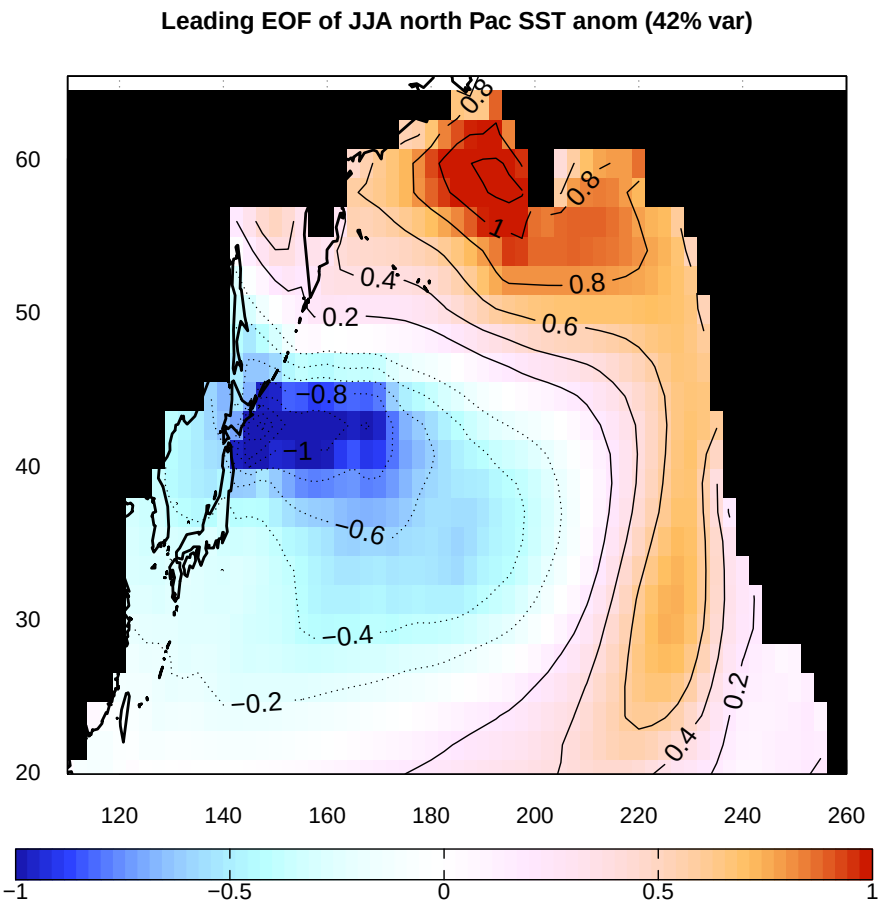

Figure 4.22: Leading EOF of JJA North Pacific (110E to 260E, 20N to 65N) SST anomalies in CESM. The values are normalized such that the EOF is in degrees C per standard deviation of the associated principal component shown in Figure 4.23.

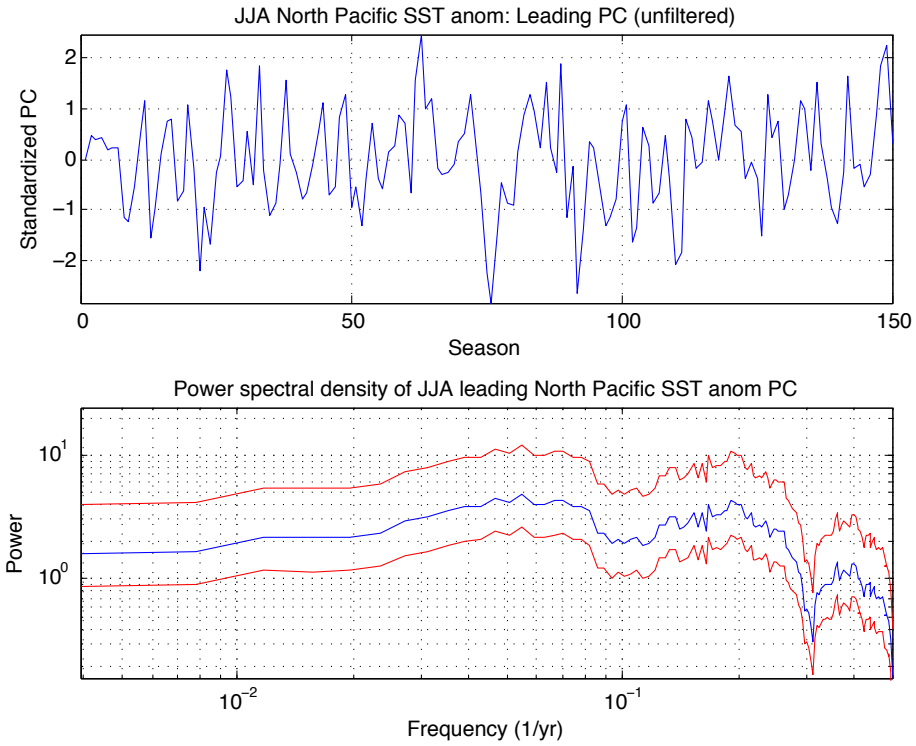

Figure 4.23: Leading standardized principal component of JJA North Pacific SST anomalies in CESM (top) and associated power spectrum (bottom, blue).

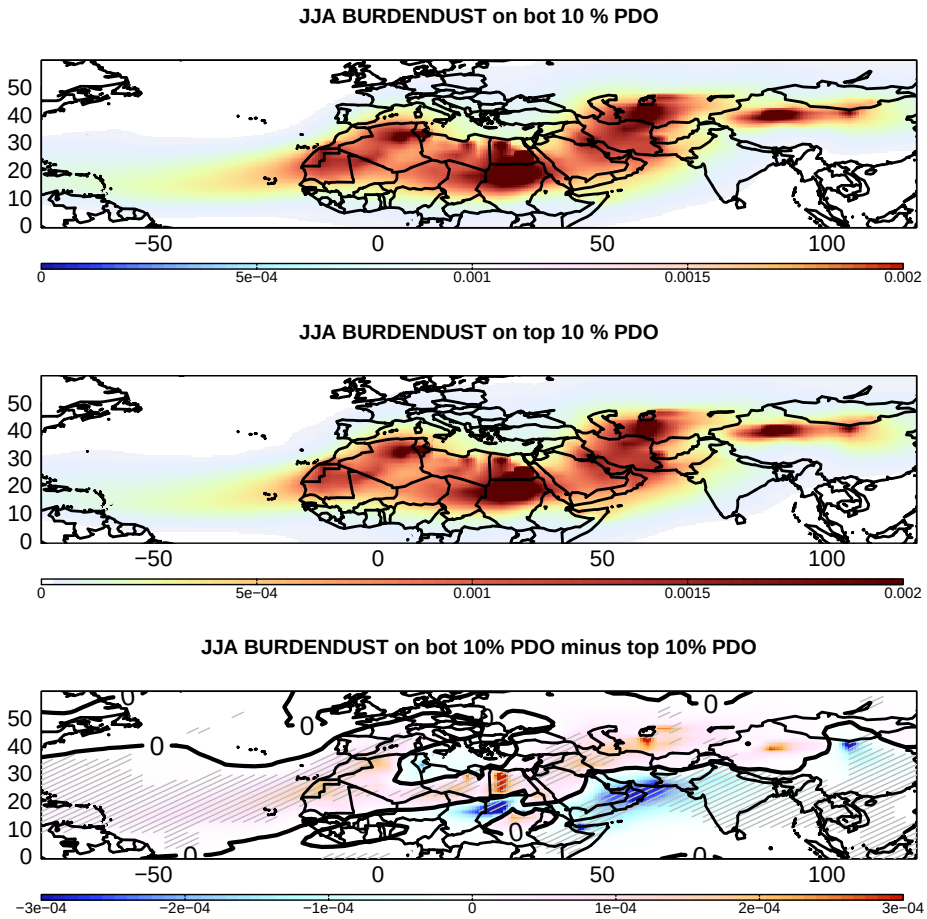

Figure 4.24: Composite of JJA dust burden (kg/m^2) on bottom 10% PDO seasons (top) and top 10% PDO seasons (middle) in CESM. The bottom panel is the top panel minus the middle panel. Grey hatches in the bottom panel indicate regions where there is 95% confidence that the true difference between the two samples is not zero, using a two-sample t test.

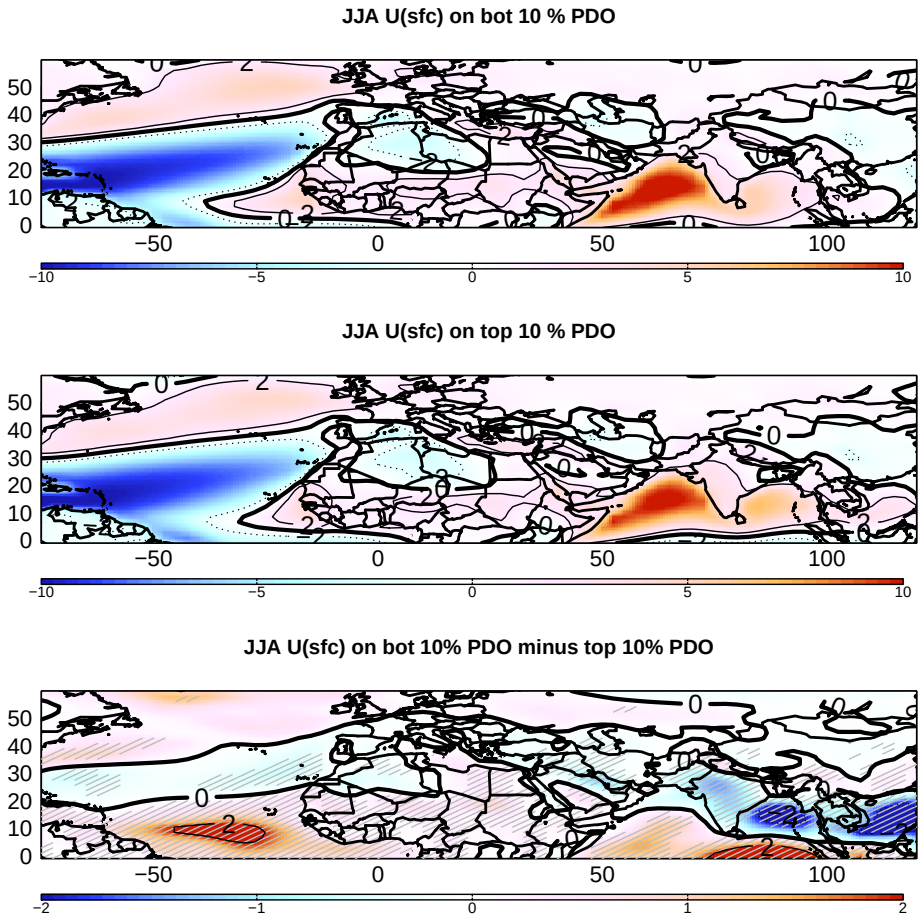

Figure 4.25: As in Fig. 4.24, but for surface zonal wind.

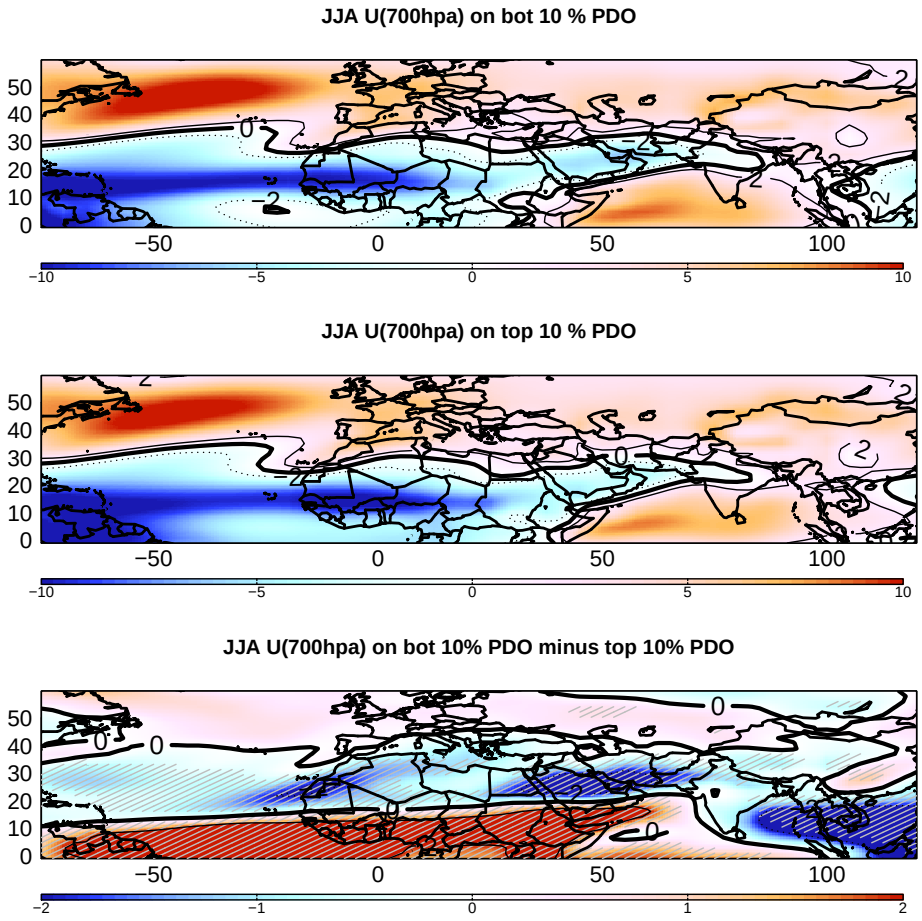

Figure 4.26: As in Fig. 4.24, but for 700hPa zonal wind.

Chapter 5

Role of North African Dust Outbreaks in Modulating Tropical Atlantic SST Variability on Interannual Timescales

Many oceanographic studies have identified latent heat flux to the atmosphere as the dominant source of month-to-month sea surface temperature (SST) cooling in the subtropics (*Cayan*, 1992; *Pickard and Emery*, 1990). However, recent work has suggested that massive North African dust storms that are advected westward over the subtropical North Atlantic can account for a large fraction of decadal changes in SST anomalies (*Evan et al.*, 2012). We examine the response of monthly SST anomalies to dust outbreaks on interannual and decadal timescales by comparing two 150-year Community Earth System Model (CESM) simulations: one containing aerosols that can interact with modeled meteorology (free to vary interannually), and one containing a prescribed seasonal cycle of aerosol concentration (no interannual variability). These comparisons show a substantial reduction in SST variance in the prescribed aerosol run that is co-located with climatologically high dust loading. This suggests that interannual variability of North African dust outbreaks can drive substantial changes in subtropical Atlantic SST

variability over climatologically dusty locations. In addition, we find that CESM is generally deficient in simulating the Atlantic Meridional Mode (AMM), which is consistent with previous findings using other CMIP5 models. Comparisons between the simulated AMM in the interactive and prescribed aerosol runs show only small differences in spatial structure and magnitude, which suggests that interannual variability of North African dust in this region is not a significant external forcing term for exciting the Atlantic Meridional Mode.

5.1 Background

The variability of Atlantic basin sea surface temperature (SST) has substantial impacts on regional and global climate change, and therefore on human life. Long term fluctuations in North Atlantic SST can perturb the near-surface atmosphere and alter storm tracks and associated surface air temperature and precipitation patterns across Europe and the Mediterranean (*Buchan et al.*, 2014; *Cattiaux et al.*, 2011; *Sutton and Hodson*, 2005; *Trigo et al.*, 2002; *Rogers*, 1997; *Hurrell*, 1995). These SST-related changes in regional climate have spawned deadly heat waves (*Cassou et al.*, 2005) and cold winters (*Buchan et al.*, 2014) across Europe. Increases in tropical North Atlantic SST, along with reductions in vertical wind shear, are directly tied to increases in tropical cyclone frequency (e.g. *Goldenberg et al.* (2001)) and Sahel rainfall (e.g. *Folland et al.* (1986)), especially on multidecadal timescales (*Booth et al.*, 2012; *Mohino et al.*, 2011; *Wang et al.*, 2012; *Zhang and Delworth*, 2006; *Giannini et al.*, 2003). Both local and remote economic conditions are greatly affected by the relationship between Atlantic SST variability and these resulting climate patterns.

Observed Atlantic SST variability on decadal and multidecadal timescales has long been attributed to natural variability of both ocean dynamics and near-surface layer atmospheric circulation (*Enfield et al.*, 2001; *Kushnir*, 1994; *Schlesinger and Ramankutty*, 1994; *Cayan*, 1992), while external forcings have been shown not to project onto the observed SST anomaly patterns (*Ting et al.*, 2009). However, many of the models used to identify physical mechanisms associated with

the observed Atlantic SST variability did not include external forcings such as atmospheric aerosols, which a plethora of studies have identified are important modulators of atmospheric circulation and mixed layer ocean characteristics (*Allen et al.*, 2012; *Evan et al.*, 2009; *Zhu et al.*, 2007). Indeed, studies that have sought to explain Atlantic SST variability using climate models with a greater number of relevant physical processes (e.g. interactive aerosol variability with meteorology and microphysics) have suggested that aerosols can explain up to 76% of simulated decadal and multidecadal Atlantic SST variability (e.g. *Booth et al.* (2012)).

One region within the Atlantic basin where aerosols are omnipresent is in the tropical and subtropical North Atlantic basin, where large quantities of mineral dust are advected from the North African continent year-round (*Prospero et al.* (1970), and many others). Because of its effectiveness as both a scatterer and absorber of solar radiation, dust has been shown to impact both sea surface temperature and cloud fraction due to direct and semi-direct radiative effects (*DeFlorio et al.*, 2014; *Doherty and Evan*, 2014; *Evan et al.*, 2009). *Booth et al.* (2012) showed that aerosol-cloud microphysical interactions, which were omitted from previous modeling studies, dominated the spatial pattern of aerosol forcing on North Atlantic SST variability during the 20th century.

In addition to the Atlantic Multidecadal Oscillation (AMO) (*Schlesinger and Ramankutty*, 1994), the Atlantic Meridional Mode (AMM) is a tropical Atlantic cross-hemispheric variation of SST that varies on interannual and decadal timescales (though the AMM can intermittently destruct on monthly timescales), and is the dominant source of coupled ocean-atmosphere variability in this region (*Vimont and Kossin*, 2007; *Chiang and Vimont*, 2004). It has been suggested that dust-forced variability of SST in this region is of comparable magnitude to observed variability (*Evan et al.*, 2012), and that decadal-scale dust outbreaks can modulate AMM activity (*A. Evan, private communication*, 2015).

The Community Earth System Model (CESM), which is included in the Coupled Model Intercomparison Project Phase 5 (CMIP5), contains state-of-the-art parameterizations for aerosols which allow species such as dust to interact with modeled meteorology and cloud microphysics. This is one of the models used in

studies such as *Booth et al.* (2012). Aerosol-cloud microphysics interactions were absent in CMIP3 models, and in many of the model studies used previously to analyze Atlantic basin SST variability on decadal timescales. The inclusion of these interactions, along with better aerosol parameterizations relevant to aerosol-radiation interactions, allows for utilization of CESM (and other CMIP5 models that include these aerosol processes) to investigate the relationship between North African dust outbreaks and low frequency variability of tropical Atlantic SSTs.

We seek to clarify the role of North African dust outbreaks in exciting the Atlantic Meridional Mode on interannual to decadal timescales. Understanding the trigger mechanism associated with fluctuations in cross-hemispheric tropical Atlantic SST is important because of the AMM's influence on northeast Brazilian rainfall and tropical cyclone development (*Foltz et al.*, 2012; *Vimont and Kossin*, 2007). Our method focuses on a comparison between two CESM simulations: one with interactive aerosols which are free to interact with modeled meteorology and vary on interannual and decadal timescales, and one with a prescribed seasonal cycle of aerosol concentration and no interannual and decadal variability.

5.2 Model description and data used

Two model simulations are compared in this study. Both are CESM 1.0.3 150-year pre-industrial control simulations run at a horizontal resolution of 2.5° longitude (lon) x 1.9° latitude (lat). The only difference in the configuration of the two simulations is that one contains fully interactive dust emission and transport, while the other prescribes the seasonal cycle of dust concentration using the climatology of the interactive run, such that there is no interannual variability of dust in the model. For more information regarding these specific simulations, see *DeFlorio et al.* (2014), *Hurrell et al.* (2013), *Liu et al.* (2012), and *Zender et al.* (2003).

For model evaluation, we use monthly mean SST and 10 meter horizontal winds from the National Centers for Environmental Prediction-National Center for Atmospheric Research (NCEP-NCAR) reanalysis (*Kalnay et al.*, 1996) from

January 1948 to December 2001. Though this particular reanalysis product may not be optimal in a physically realistic sense, it has been used in previous studies on this topic (e.g. *Chiang and Vimont* (2004)) and thus enables a direct comparison of those studies to our results. All fields have been detrended and we apply a 3-month running mean to the data. We also linearly regress out the influence of ENSO, since we are not interested in tropical Pacific SST influence on tropical Atlantic SST variability. We follow *Chiang and Vimont* (2004) and define ENSO using the cold tongue index (CTI) over the domain 6°S to 6°N, 180°W to 90°W.

5.3 Interannual variability of subtropical North Atlantic SST anomalies

The time evolution of dust burden over West Africa (central Mauritania; −10°W, 20°N) for both the interactive and prescribed CESM simulations is shown in Figure 5.1. There is clearly interannual and lower frequency variability in the interactive simulation, while there is no interannual or lower frequency variability in the prescribed simulation (by construction).

Dust burden is relatively high year-round between 5°N and 20°N over the North Atlantic in CESM (see Figure 6 of *DeFlorio et al.* (2014)). The variability of monthly SST anomalies in observations and both CESM simulations is shown in Figure 5.2. Standard deviation levels in observations and the interactive CESM simulation are higher over the climatologically high dust burden regions than in the prescribed CESM simulation. This suggests that interannual variability of North African dust outbreaks can drive substantial changes in subtropical Atlantic SST variability.

Figure 5.2 shows that there is strong monthly variability of tropical Atlantic SST anomalies. The leading and second modes of tropical Atlantic SST anomalies and their associated temporal evolution is shown in Figures 5.3 and 5.4. The leading mode is not recognizable as a previously identified climate mode of variability, but could be associated with hemispheric-wide low frequency fluctuations in SST anomalies associated with the AMO, or a teleconnected response to ENSO. We

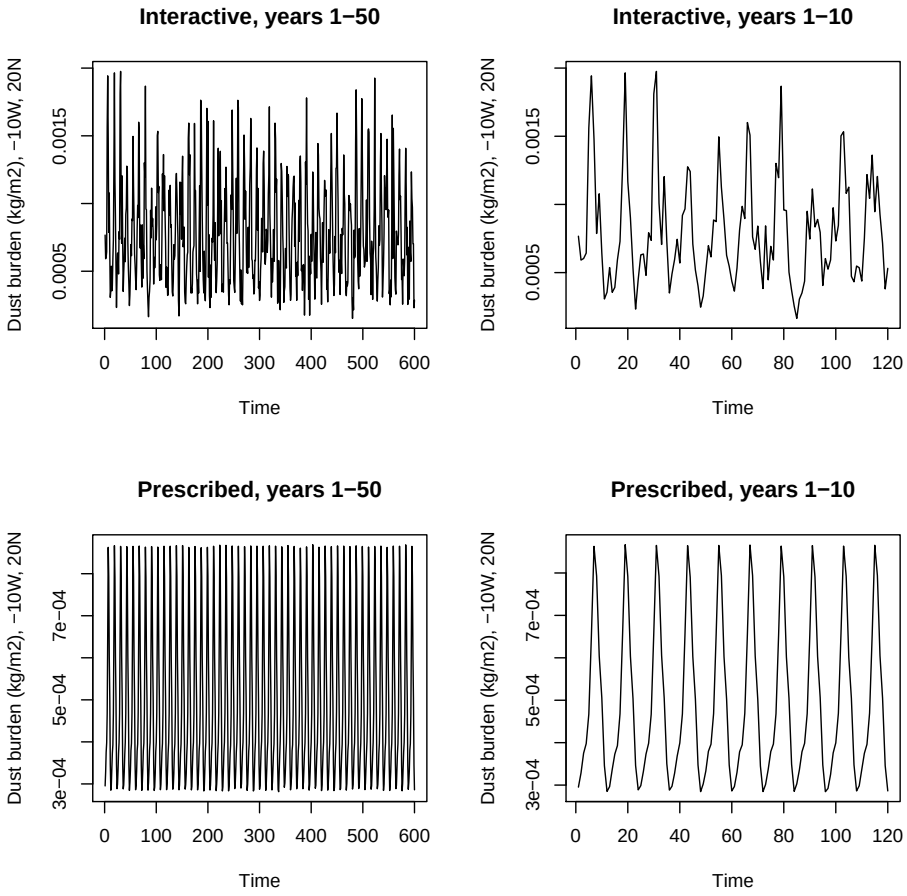

Figure 5.1: Dust burden (kg/m^2) over central Mauritania (West Africa) in CESM interactive aerosol (top) and prescribed aerosol (bottom) simulation for 50 (left) and 10 (right) year subsets of the 150-year simulation.

are most interested in the second mode of tropical Atlantic SST anomalies (Figure 5.4), which displays a spatial structure and interannual variation over time that is distinctly reminiscent of the AMM. Consistent with other CMIP5 models summarized in *Flato et al.* (2013), the AMM is too weak in magnitude in both interactive and prescribed CESM (middle, bottom), though the spatial structure agrees reasonably well with observations (top).

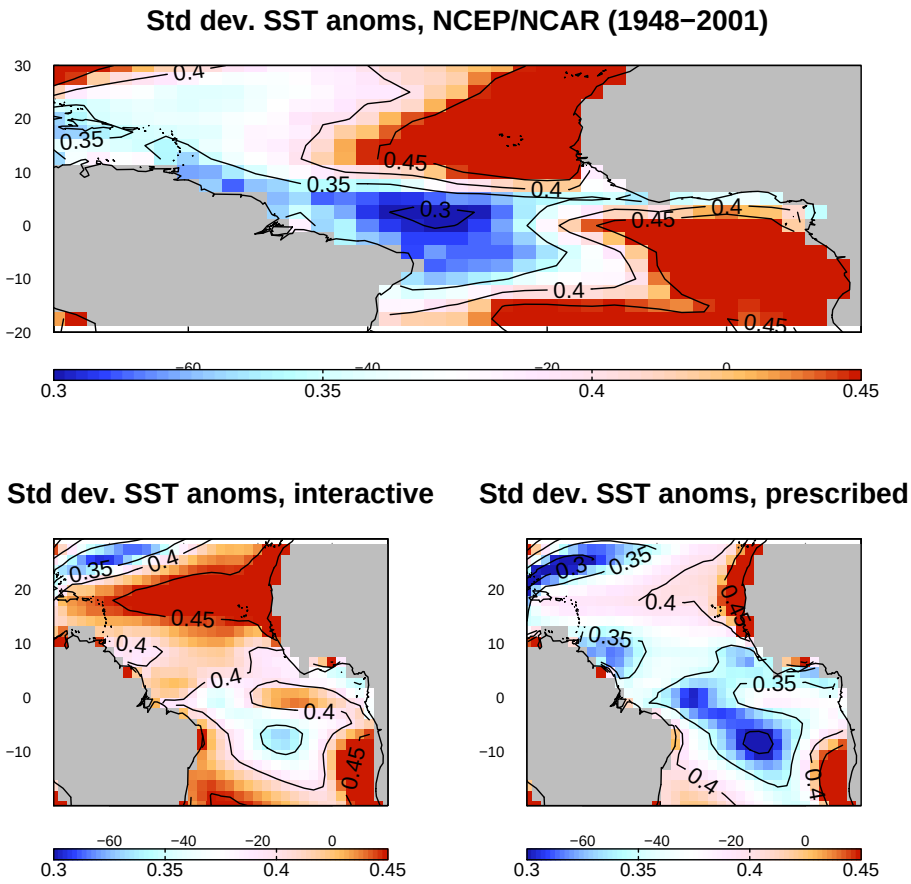

Figure 5.2: Standard deviation of detrended and smoothed monthly tropical Atlantic SST anomalies in NCAR/NCEP (top), interactive CESM (bottom left) and prescribed CESM (bottom right).

5.4 Coupled variability of horizontal winds and SST

Though the cross-equatorial dipole pattern associated with the AMM can be seen as the second mode of tropical Atlantic SST anomalies, an alternative approach is to define the AMM as the leading mode of coupled variability between horizontal surface winds and SST anomalies (*Chiang and Vimont*, 2004). This definition accounts for the cross-equatorial wind flow associated with shifts in the position of the Intertropical Convergence Zone (ITCZ) that are thought to

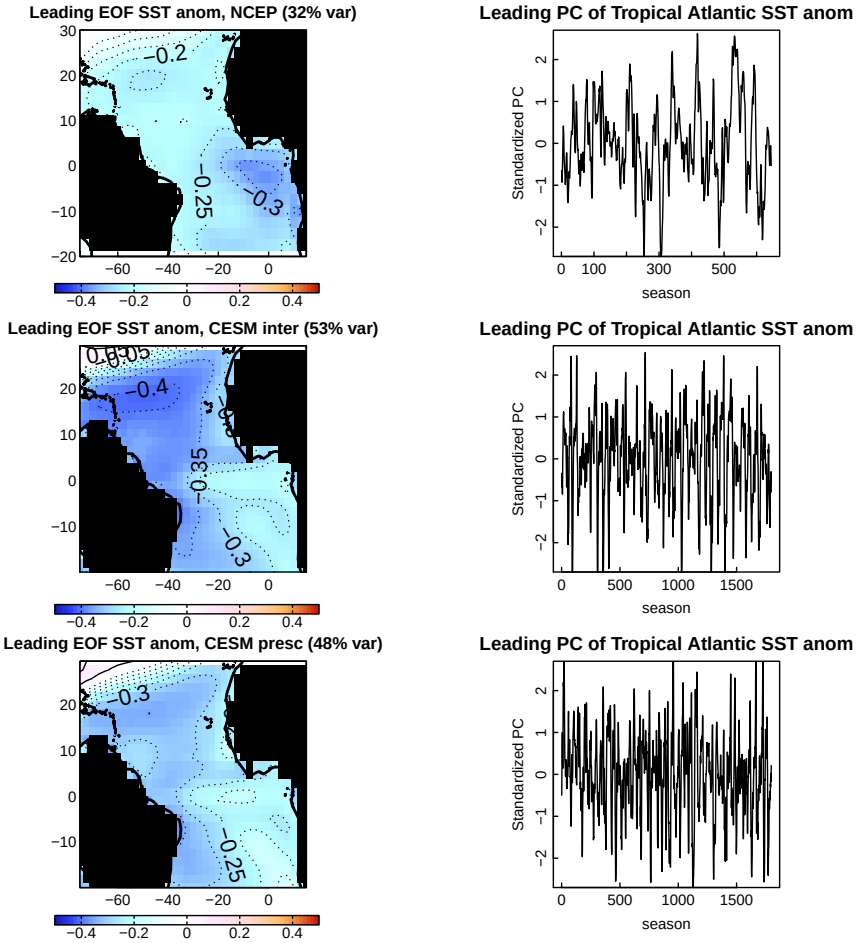

Figure 5.3: Leading EOF and associated PC of tropical Atlantic SST monthly anomalies for NCEP (top), interactive CESM (middle) and prescribed CESM (bottom).

externally force the SST anomalies associated with the AMM pattern (*Nobre and Shukla* (1996) and others).

The first four spatial modes of the singular value decomposition of the cross covariance matrix of horizontal surface wind and SST anomalies are shown in Figures 5.5, 5.6, and 5.7 for observations, interactive CESM, and prescribed CESM, respectively. Their associated principal components are shown in Figure 5.8. NCEP Mode 1 closely matches Figures 1b and 2d of *Chiang and Vimont* (2004) and is defined as the AMM. It accounts for 53% of the total variance of the signal. However, the AMM emerges as Mode 3 in both interactive and prescribed

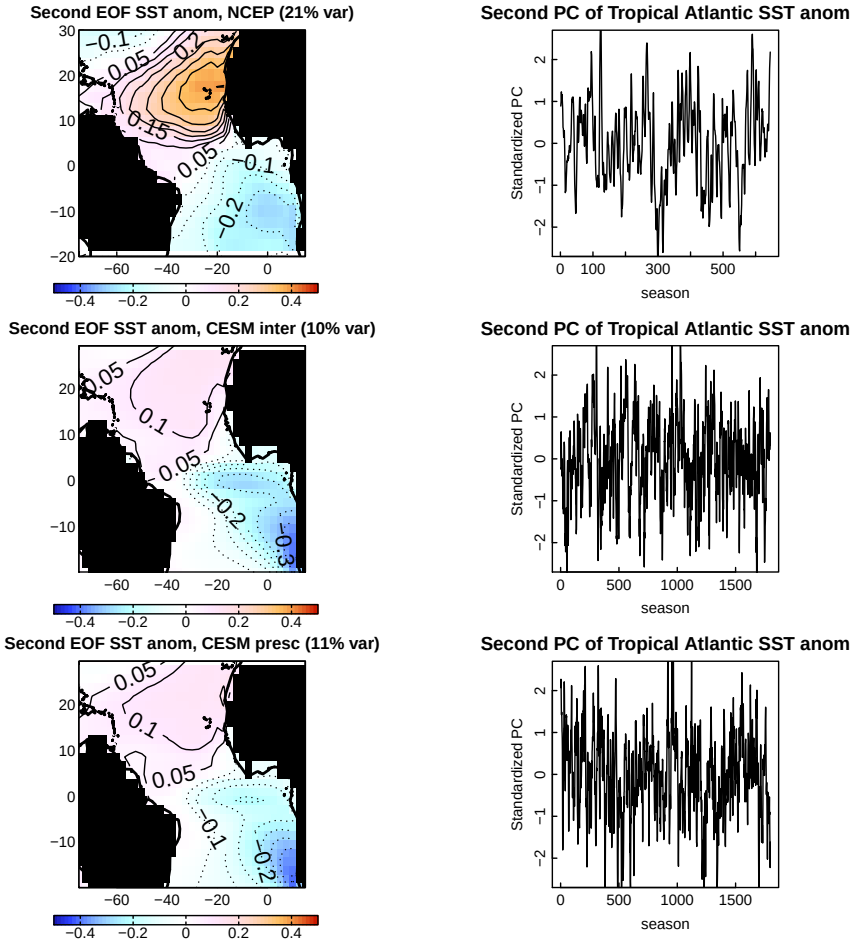

Figure 5.4: Second EOF and associated PC of tropical Atlantic SST monthly anomalies for NCEP (top), interactive CESM (middle) and prescribed CESM (bottom).

CESM, which only accounts for 2% and 15%, respectively, of the total variance of the signal. The variance of the interactive CESM "AMM" principal component time series (Figure 5.8, middle) is only slightly greater than that of the prescribed CESM time series (Figure 5.8, bottom) (3.10°C and 2.89°C, respectively). This suggests that interannual variability of North African dust in this region is not a significant external forcing term for exciting the Atlantic Meridional Mode.

5.5 Summary and preliminary conclusions

Our findings in this work are still in development, and are somewhat counterintuitive. On one hand, we show in Figure 5.2 that month-to-month variability in tropical Atlantic SST is reduced when prescribing the seasonal cycle of mineral dust in our model simulations, which suggests that interannual variability of dust can be an important driver of subtropical Atlantic SST variability over climatologically dusty regions. However, on the other hand, we find little difference in the spatial structure and temporal evolution of the coupled variability of horizontal surface winds and SST (i.e. the Atlantic Meridional Mode) in each model simulation, which suggests that interannual variability of dust is not an important external forcing parameter for exciting and sustaining the Atlantic Meridional Mode. Notably, CESM more realistically simulates the observed AMM in both the interactive and prescribed simulations when the singular value decomposition is performed on only SST (Figure 5.4) rather than the covarying SST and horizontal surface wind fields (Figures 5.5, 5.6, and 5.7).

An important next step will be to examine annually and decadally filtered time series of SST and winds in this framework, since previous studies have suggested that such low frequency variations in North African dust outbreaks could be important in influencing AMM development and persistence.

Compared to *Chiang and Vimont* (2004), the magnitude of the temporal component of the cross-covariance SVD is larger in this analysis by a factor of 5. This is a discrepancy that must be rectified before publication of this work. However, our re-creation of the AMM calculation used in *Chiang and Vimont* (2004) indicates that the *relative* (but not *absolute*) spatial and temporal components of the Mode 1 NCEP AMM and Mode 3 CESM AMM are simulated with some degree of realism.

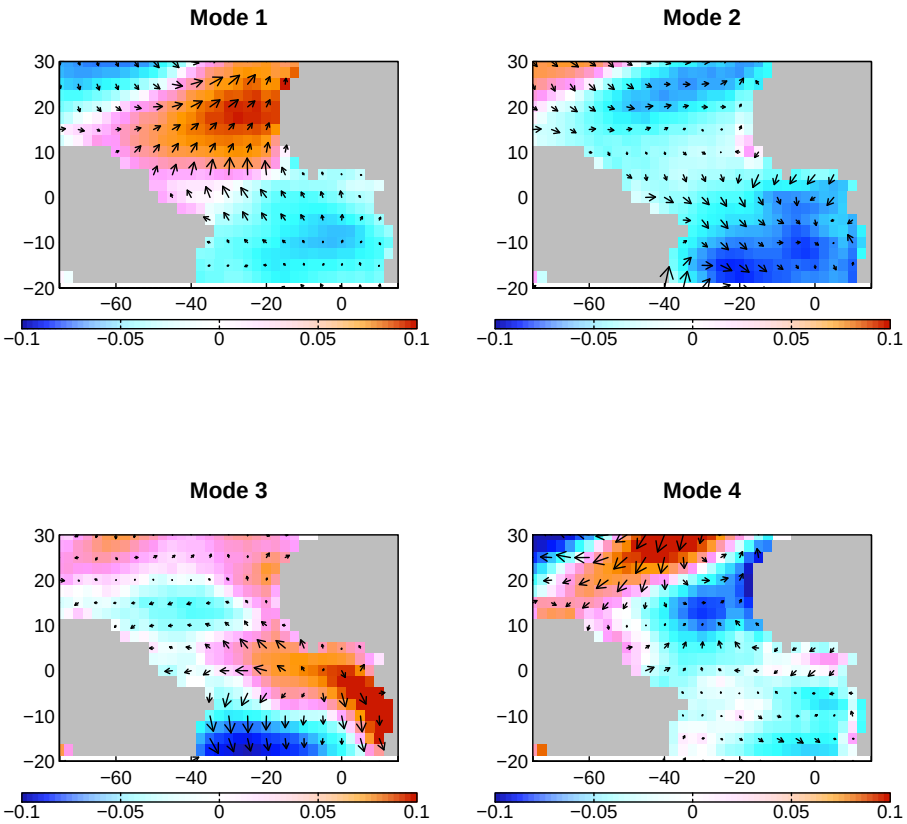

Figure 5.5: First four spatial modes of singular value decomposition of cross covariance matrix of horiztonal surface wind and SST anomalies, NCEP.

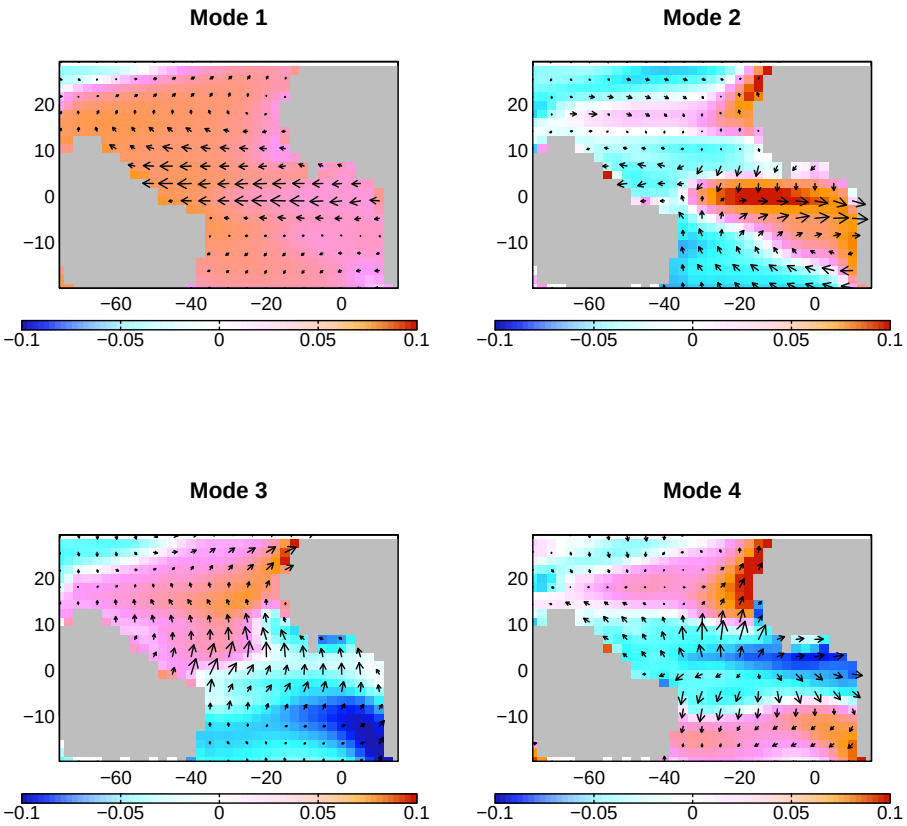

Figure 5.6: First four spatial modes of singular value decomposition of cross covariance matrix of horiztonal surface wind and SST anomalies, interactive CESM.

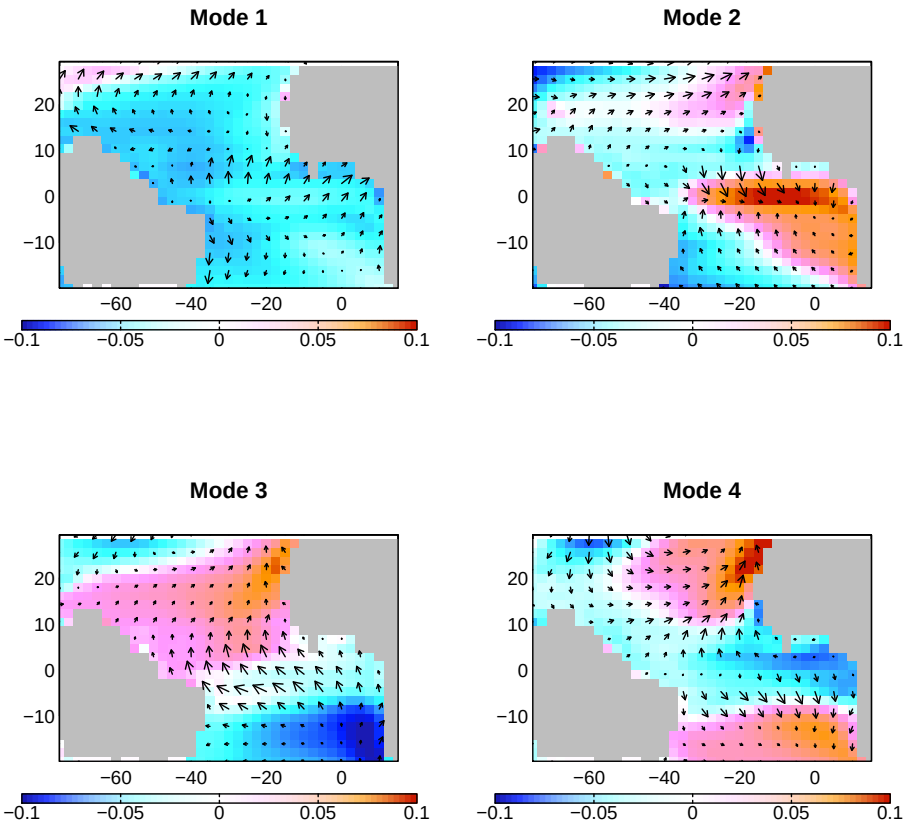

Figure 5.7: First four spatial modes of singular value decomposition of cross covariance matrix of horiztonal surface wind and SST anomalies, prescribed CESM.

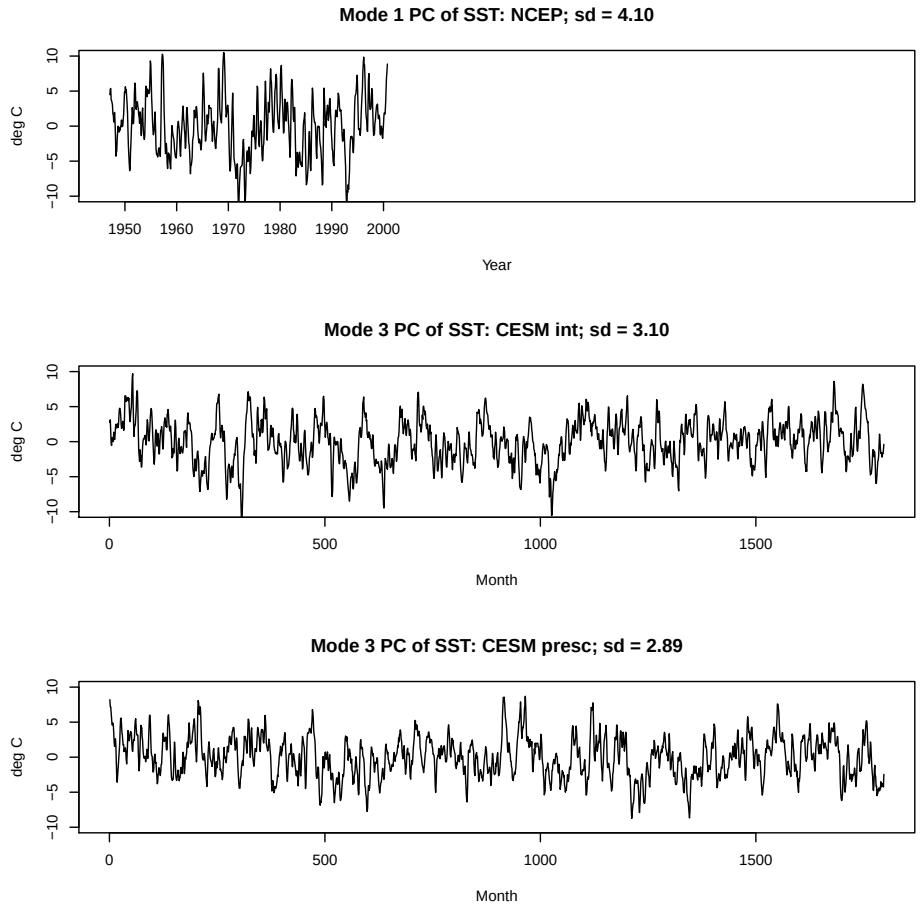

Figure 5.8: Principal component time series of Atlantic Meridional Mode in NCEP (top), interactive CESM (middle), and prescribed CESM (bottom). The associated percentage variances explained by the AMM mode for each dataset is 53%, 2%, and 15%, respectively.

Chapter 6

Conclusions and Comments

6.1 Unifying Theme and General Approach

The unifying theme of the work contained in this dissertation is the utilization of global coupled climate models to learn more about thermodynamical and dynamical processes within the climate system. Particular emphasis was placed on increasing understanding of aerosol-cloud-climate interactions and extreme precipitation events. This is prudent because of the large uncertainty associated with the historical global radiative forcing of climate due to aerosol-radiation and aerosol-cloud interactions (-0.4$\frac{W}{m^2}$ $\pm 0.5\frac{W}{m^2}$ and -0.6$\frac{W}{m^2}$ $\pm 0.6\frac{W}{m^2}$, respectvely), and because of the strong link between extreme precipitation and socioeconomic prosperity over the western United States.

As of the writing of this dissertation, it is common within the community to evaluate climate models using multimodel statistical moments (e.g. mean and variance) of temperature, precipitation, circulation, and other relevant variables. The calculation of these ensemble statistics is made using some or all of the CMIP5 suite of couple climate models, which is necessary for characterizing climate variables (both historical and projected) and their associated uncertainties in a robust manner. The approach implemented in this dissertation focuses on only one of these models (CESM). We evaluated this model using available observations, and designed experiments to increase our understanding of physical processes involving aerosols and other climate variables. Because we focus on only one model, our

results are not subject to potential obfuscation by the calculation of multi-model statistics. However, using an ensemble of models in the future may provide more insight to the results obtained herein.

6.2 Major Contributions

There are several major contributions to the scientific community contained within this dissertation:

1. We have shown that the representation of global teleconnection patterns associated with tropical Pacific modes of climate variability (ENSO, PDO) is substantially more realistic in the newest version of the Community Earth System Model, CESM. As an aside, it is remarkable that the CMIP3 models which simulated important Pacific circulation and precipitation teleconnection patterns so erroneously were used to make projections of temperature and precipitation over the western U.S., a region whose climate is quite sensitive to Pacific modes of climate variability.

2. We have exploited the improved representation of aerosol-cloud processes in CMIP5 models by using CESM in conjunction with satellite and in situ observations to discover a new aerosol semi-direct effect over the subtropical North Atlantic, whereby mineral dust heats the lower troposphere above the boreal summer stratocumulus cloud deck in the eastern subtropical Atlantic, which increases atmospheric stability and enhances lower tropospheric inversion strength. Although there are known errors in aerosol surface emissions and atmospheric burdens in historical simulations of climate (*Evan et al.*, 2014), we show that the seasonal cycle and interannual variability of dust over the subtropical North Atlantic are realistically represented in CESM.

3. We have used an extensive CESM simulation to present evidence that ENSO exerts a control on North African dust variability on interannual timescales. There is strong multidecadal variability in the strength of the dust-ENSO correlation, which may explain why limited observations of mineral dust near the North African continent are more weakly correlated to ENSO than in our extensive CESM

simulation.

4. We have investigated the role of North African dust in affecting tropical Atlantic SST variability on interannual timescales. Using simulations of CESM with and without interannually varying aerosols, we show that tropical Atlantic SST variance is higher when the effects of varying aerosols are included. We have also evaluated CESM's representation of the Atlantic Meridional Mode (AMM), which recent studies have suggested can be forced on interannual to decadal timescales by North African dust outbreaks. The AMM is too weak in CESM, and there are only small differences between the spatial structure and magnitude of the interactive and prescribed simulations, which suggests that North African dust outbreaks are not important in exciting or sustaining the AMM.

6.3 Future Outlook

There are many questions related to the work in this dissertation that can be addressed in future studies. Obtaining satisfactory answers will require the passage of time, which will yield more observations, and consequently more robust model evaluation.

Specifically, a companion CESM simulation with interactive and prescribed aerosol emissions (rather than concentrations) could help identify the importance of emissions in climate feedbacks over the tropical Atlantic region, as suggested by *Wang et al.* (2012); *Evan et al.* (2012) and others. Dust-precipitation interactions will also need to be examined more in future studies (e.g. changes in dust emissions and radiative forcing following extreme rainfall events, and the role of Asian dust in nucleating ice particles and enhancing orographic precipitation over the western U.S.).

Chapter 7

Bibliography

AchutaRao, K. and Sperber, K. R. (2006). ENSO simulation in coupled ocean-atmosphere models: are the current models better? *Climate Dynamics*, 27(1):1–15.

Ackerman, S. A. and Chung, H. (1992). Radiative effects of airborne dust on regional energy budgets at the top of the atmosphere. *Journal of Applied Meteorology*, 31(2):223–233.

Albani, S., Mahowald, N., Perry, A., Scanza, R., Zender, C., Heavens, N., Maggi, V., Kok, J., and Otto-Bliesner, B. (2014). Improved dust representation in the Community Atmosphere Model. *Journal of Advances in Modeling Earth Systems*, 6(3):541–570.

Albrecht, B. A. (1989). Aerosols, cloud microphysics, and fractional cloudiness. *Science*, 245(4923):1227–1230.

Allen, R. J., Sherwood, S. C., Norris, J. R., and Zender, C. S. (2012). Recent Northern Hemisphere tropical expansion primarily driven by black carbon and tropospheric ozone. *Nature*, 485(7398):350–354.

Ashpole, I. and Washington, R. (2013). A new high-resolution central and western Saharan summertime dust source map from automated satellite dust plume tracking. *Journal of Geophysical Research: Atmospheres*, 118(13):6981–6995.

Ault, A. P., Williams, C. R., White, A. B., Neiman, P. J., Creamean, J. M., Gaston, C. J., Ralph, F. M., and Prather, K. A. (2011). Detection of Asian dust in California orographic precipitation. *Journal of Geophysical Research: Atmospheres (1984–2012)*, 116(D16).

Barnston, A. G., Tippett, M. K., L'Heureux, M. L., Li, S., and DeWitt, D. G. (2012). Skill of Real-Time Seasonal ENSO Model Predictions during 2002-11: Is Our Capability Increasing? *Bulletin of the American Meteorological Society*, 93(5):631–651.

Bjerknes, J. (1969). Atmospheric teleconnections from the equatorial Pacific. *Monthly Weather Review*, 97(3):163–172.

Boer, G., Flato, G., and Ramsden, D. (2000). A transient climate change simulation with greenhouse gas and aerosol forcing: projected climate to the twenty-first century. *Climate Dynamics*, 16(6):427–450.

Bony, S. and Dufresne, J.-L. (2005). Marine boundary layer clouds at the heart of tropical cloud feedback uncertainties in climate models. *Geophysical Research Letters*, 32(20).

Booth, B. B., Dunstone, N. J., Halloran, P. R., Andrews, T., and Bellouin, N. (2012). Aerosols implicated as a prime driver of twentieth-century North Atlantic climate variability. *Nature*, 484(7393):228–232.

Bradley, R., Diaz, H., Kiladis, G., and Eischeid, J. (1987). ENSO signal in continental temperature and precipitation records. *Nature*, 327(6122):497–501.

Bretherton, C. S. and Park, S. (2009). A new moist turbulence parameterization in the Community Atmosphere Model. *Journal of Climate*, 22(12):3422–3448.

Bryson, R. A. and Baerreis, D. A. (1967). Possibilities of major climatic modification and their implications: Northwest India, a case for study. *Bulletin of the American Meteorological Socoiety*.

Buchan, J., Hirschi, J. J.-M., Blaker, A. T., and Sinha, B. (2014). North Atlantic SST anomalies and the cold north European weather events of winter 2009/10 and December 2010. *Monthly Weather Review*, 142(2):922–932.

Carslaw, K., Boucher, O., Spracklen, D., Mann, G., Rae, J., Woodward, S., and Kulmala, M. (2010). A review of natural aerosol interactions and feedbacks within the Earth system. *Atmospheric Chemistry and Physics*, 10(4):1701–1737.

Cassou, C., Terray, L., and Phillips, A. S. (2005). Tropical Atlantic influence on European heat waves. *Journal of climate*, 18(15):2805–2811.

Cattiaux, J., Vautard, R., and Yiou, P. (2011). North-Atlantic SST amplified recent wintertime European land temperature extremes and trends. *Climate dynamics*, 36(11-12):2113–2128.

Cayan, D. R. (1992). Latent and sensible heat flux anomalies over the northern oceans: Driving the sea surface temperature. *Journal of Physical Oceanography*, 22(8):859–881.

Cayan, D. R., Das, T., Pierce, D. W., Barnett, T. P., Tyree, M., and Gershunov, A. (2010). Future dryness in the southwest US and the hydrology of the early 21st century drought. *Proceedings of the National Academy of Sciences*, 107(50):21271–21276.

Chen, C.-T. and Knutson, T. (2008). On the verification and comparison of extreme rainfall indices from climate models. *Journal of Climate*, 21(7):1605–1621.

Chiang, J. C. and Vimont, D. J. (2004). Analogous Pacific and Atlantic Meridional Modes of Tropical Atmosphere-Ocean Variability. *Journal of Climate*, 17(21):4143–4158.

Chiapello, I., Moulin, C., and Prospero, J. M. (2005). Understanding the long-term variability of African dust transport across the Atlantic as recorded in both Barbados surface concentrations and large-scale Total Ozone Mapping Spectrometer (TOMS) optical thickness. *Journal of Geophysical Research: Atmospheres (1984–2012)*, 110(D18).

Collins, W. D., Rasch, P. J., Boville, B. A., Hack, J. J., McCaa, J. R., Williamson, D. L., Briegleb, B. P., Bitz, C. M., Lin, S.-J., and Zhang, M. (2006). The formulation and atmospheric simulation of the Community Atmosphere Model version 3 (CAM3). *Journal of Climate*, 19(11):2144–2161.

Cuesta, J., Marsham, J. H., Parker, D. J., and Flamant, C. (2009). Dynamical mechanisms controlling the vertical redistribution of dust and the thermodynamic structure of the West Saharan atmospheric boundary layer during summer. *Atmospheric Science Letters*, 10(1):34–42.

Da Silva, A., Young, C., and Levitus, S. (1994). Atlas of Surface Marine Data 1994, Volume 1: Algorithms and Procedures. NOAA Atlas Series.

Dai, A. (2006). Precipitation characteristics in eighteen coupled climate models. *Journal of Climate*, 19(18):4605–4630.

Daly, C., Gibson, W. P., Taylor, G. H., Johnson, G. L., and Pasteris, P. (2002). A knowledge-based approach to the statistical mapping of climate. *Climate research*, 22(2):99–113.

Daly, C., Neilson, R. P., and Phillips, D. L. (1994). A statistical-topographic model for mapping climatological precipitation over mountainous terrain. *Journal of applied meteorology*, 33(2):140–158.

Darwin, C. and Bettany, G. T. (1890). *Journal of researches into the natural history and geology of the countries visited during the voyage of HMS "Beagle" round the world: under the command of Capt. Fitz Roy, RN*. Ward, Lock.

DeFlorio, M. J., Ghan, S. J., Singh, B., Miller, A. J., Cayan, D. R., Russell, L. M., and Somerville, R. C. (2014). Semidirect dynamical and radiative effect of North African dust transport on lower tropospheric clouds over the subtropical North Atlantic in CESM 1.0. *Journal of Geophysical Research: Atmospheres*, 119(13):8284–8303.

DeMott, P., Cziczo, D., Prenni, A., Murphy, D., Kreidenweis, S., Thomson, D., Borys, R., and Rogers, D. (2003). Measurements of the concentration and composition of nuclei for cirrus formation. *Proceedings of the National Academy of Sciences*, 100(25):14655–14660.

Deser, C., Capotondi, A., Saravanan, R., and Phillips, A. S. (2006). Tropical Pacific and Atlantic climate variability in CCSM3. *Journal of Climate*, 19(11):2451–2481.

Deser, C., Phillips, A. S., Tomas, R. A., Okumura, Y. M., Alexander, M. A., Capotondi, A., Scott, J. D., Kwon, Y.-O., and Ohba, M. (2012). ENSO and Pacific decadal variability in the Community Climate System Model version 4. *Journal of Climate*, 25(8):2622–2651.

Dettinger, M., Redmond, K., and Cayan, D. (2004). Winter orographic precipitation ratios in the Sierra Nevada-Large-scale atmospheric circulations and hydrologic consequences. *Journal of Hydrometeorology*, 5(6):1102–1116.

Doherty, O., Riemer, N., and Hameed, S. (2008). Saharan mineral dust transport into the Caribbean: Observed atmospheric controls and trends. *Journal of Geophysical Research: Atmospheres (1984–2012)*, 113(D7).

Doherty, O., Riemer, N., and Hameed, S. (2012). Control of Saharan mineral dust transport to Barbados in winter by the Intertropical Convergence Zone over West Africa. *Journal of Geophysical Research: Atmospheres (1984–2012)*, 117(D19).

Doherty, O. M. and Evan, A. T. (2014). Identification of a new dust-stratocumulus indirect effect over the tropical North Atlantic. *Geophysical Research Letters*, 41(19):6935–6942.

Doherty, O. M., Riemer, N., and Hameed, S. (2014). Role of the convergence zone over West Africa in controlling Saharan mineral dust load and transport in the boreal summer. *Tellus B*, 66.

Dubovik, O. and King, M. D. (2000). A flexible inversion algorithm for retrieval of aerosol optical properties from Sun and sky radiance measurements. *Journal of Geophysical Research: Atmospheres (1984–2012)*, 105(D16):20673–20696.

Emanuel, K., Oouchi, K., Satoh, M., Tomita, H., and Yamada, Y. (2010). Comparison of Explicitly Simulated and Downscaled Tropical Cyclone Activity in a High-Resolution Global Climate Model. *Journal of Advances in Modeling Earth Systems*, 2(4).

Enfield, D. B., Mestas-Nuñez, A. M., and Trimble, P. J. (2001). The Atlantic multidecadal oscillation and its relation to rainfall and river flows in the continental US. *Geophysical Research Letters*, 28(10):2077–2080.

Engelstaedter, S., Tegen, I., and Washington, R. (2006). North African dust emissions and transport. *Earth-Science Reviews*, 79(1):73–100.

Engelstaedter, S., Washington, R., and Mahowald, N. (2009). Impact of changes in atmospheric conditions in modulating summer dust concentration at Barbados: A back-trajectory analysis. *Journal of Geophysical Research: Atmospheres (1984–2012)*, 114(D17).

Erickson, D. J., Hernandez, J. L., Ginoux, P., Gregg, W., McClain, C., and Christian, J. (2003). Atmospheric iron delivery and surface ocean biological activity in the Southern Ocean and Patagonian region. *Geophysical Research Letters*, 30(12).

Evan, A. T., Dunion, J., Foley, J. A., Heidinger, A. K., and Velden, C. S. (2006a). New evidence for a relationship between Atlantic tropical cyclone activity and African dust outbreaks. *Geophysical Research Letters*, 33(19).

Evan, A. T., Flamant, C., Fiedler, S., and Doherty, O. (2014). An analysis of aeolian dust in climate models. *Geophysical Research Letters*, 41(16):5996–6001.

Evan, A. T., Foltz, G. R., and Zhang, D. (2012). Physical response of the tropical-subtropical North Atlantic Ocean to decadal-multidecadal forcing by African dust. *Journal of Climate*, 25(17):5817–5829.

Evan, A. T., Foltz, G. R., Zhang, D., and Vimont, D. J. (2011). Influence of African dust on ocean-atmosphere variability in the tropical Atlantic. *Nature Geoscience*, 4(11):762–765.

Evan, A. T., Heidinger, A. K., and Knippertz, P. (2006b). Analysis of winter dust activity off the coast of West Africa using a new 24-year over-water advanced very high resolution radiometer satellite dust climatology. *Journal of Geophysical Research: Atmospheres (1984–2012)*, 111(D12).

Evan, A. T., Heidinger, A. K., and Pavolonis, M. J. (2006c). Development of a new over-water Advanced Very High Resolution Radiometer dust detection algorithm. *International Journal of Remote Sensing*, 27(18):3903–3924.

Evan, A. T. and Mukhopadhyay, S. (2010). African dust over the northern tropical Atlantic: 1955-2008. *Journal of Applied Meteorology and Climatology*, 49(11):2213–2229.

Evan, A. T., Vimont, D. J., Heidinger, A. K., Kossin, J. P., and Bennartz, R. (2009). The role of aerosols in the evolution of tropical North Atlantic Ocean temperature anomalies. *Science*, 324(5928):778–781.

Flato, G., Marotzke, J., Abiodun, B., Braconnot, P., Chou, S. C., Collins, W., Cox, P., Driouech, F., Emori, S., Eyring, V., et al. (2013). Evaluation of climate models. In *Climate Change 2013: The Physical Science Basis. Contribution of Working Group I to the Fifth Assessment Report of the Intergovernmental Panel on Climate Change*, pages 741–866. Cambridge University Press.

Folland, C., Palmer, T., and Parker, D. (1986). Sahel rainfall and worldwide sea temperatures, 1901-85. *Nature*, 320(6063):602–607.

Foltz, G. R., McPhaden, M. J., and Lumpkin, R. (2012). A Strong Atlantic Meridional Mode Event in 2009: The Role of Mixed Layer Dynamics. *Journal of Climate*, 25(1):363–380.

Garay, M. J., de Szoeke, S. P., and Moroney, C. M. (2008). Comparison of marine stratocumulus cloud top heights in the southeastern Pacific retrieved from satellites with coincident ship-based observations. *Journal of Geophysical Research: Atmospheres (1984–2012)*, 113(D18).

Gent, P. R., Danabasoglu, G., Donner, L. J., Holland, M. M., Hunke, E. C., Jayne, S. R., Lawrence, D. M., Neale, R. B., Rasch, P. J., Vertenstein, M., et al. (2011). The Community Climate System Model version 4. *Journal of Climate*, 24(19):4973–4991.

Gershunov, A. and Barnett, T. P. (1998). Interdecadal modulation of ENSO teleconnections. *Bulletin of the American Meteorological Society*, 79(12):2715–2725.

Gettelman, A., Morrison, H., and Ghan, S. J. (2008). A new two-moment bulk stratiform cloud microphysics scheme in the Community Atmosphere Model, version 3 (CAM3). Part ii: Single-column and global results. *Journal of Climate*, 21(15):3660–3679.

Ghan, S. J. and Schwartz, S. E. (2007). Aerosol properties and processes: A path from field and laboratory measurements to global climate models. *Bulletin of the American Meteorological Society*, 88(7):1059–1083.

Ghan, S. J. and Zaveri, R. A. (2007). Parameterization of optical properties for hydrated internally mixed aerosol. *Journal of Geophysical Research: Atmospheres (1984–2012)*, 112(D10).

Giannini, A., Saravanan, R., and Chang, P. (2003). Oceanic forcing of Sahel rainfall on interannual to interdecadal time scales. *Science*, 302(5647):1027–1030.

Ginoux, P., Chin, M., Tegen, I., Prospero, J. M., Holben, B., Dubovik, O., and Lin, S.-J. (2001). Sources and distributions of dust aerosols simulated with the GOCART model. *Journal of Geophysical Research: Atmospheres (1984–2012)*, 106(D17):20255–20273.

Ginoux, P., Prospero, J. M., Gill, T. E., Hsu, N. C., and Zhao, M. (2012). Global-scale attribution of anthropogenic and natural dust sources and their emission rates based on MODIS Deep Blue aerosol products. *Reviews of Geophysics*, 50(3).

Ginoux, P., Prospero, J. M., Torres, O., and Chin, M. (2004). Long-term simulation of global dust distribution with the GOCART model: correlation with North Atlantic Oscillation. *Environmental Modelling & Software*, 19(2):113–128.

Goldenberg, S. B., Landsea, C. W., Mestas-Nuñez, A. M., and Gray, W. M. (2001). The recent increase in Atlantic hurricane activity: Causes and implications. *Science*, 293(5529):474–479.

Haagen-Smit, A. (1952). Chemistry and physiology of Los Angeles smog. *Industrial & Engineering Chemistry*, 44(6):1342–1346.

Hamlet, A. F. and Lettenmaier, D. P. (1999). Columbia River streamflow forecasting based on ENSO and PDO climate signals. *Journal of Water Resources Planning and Management*, 125(6):333–341.

Hamlet, A. F. and Lettenmaier, D. P. (2005). Production of Temporally Consistent Gridded Precipitation and Temperature Fields for the Continental United States. *Journal of Hydrometeorology*, 6(3):330–336.

Hartmann, D. L. (1994). *Global physical climatology*, volume 56. Academic press.

Heintzenberg, J. (2009). The SAMUM-1 experiment over southern Morocco: Overview and introduction. *Tellus B*, 61(1):2–11.

Hess, M., Koepke, P., and Schult, I. (1998). Optical properties of aerosols and clouds: The software package OPAC. *Bulletin of the American meteorological society*, 79(5):831–844.

Hidalgo, H. G. and Dracup, J. A. (2003). Enso and PDO effects on hydroclimatic variations of the Upper Colorado River Basin. *Journal of Hydrometeorology*, 4(1):5–23.

Holton, J. R. (2013). *An introduction to dynamic meteorology*. Academic press.

Houghton, H. G. (1968). On precipitation mechanisms and their artificial modification. *Journal of Applied Meteorology*, 7(5):851–859.

Huneeus, N., Schulz, M., Balkanski, Y., Griesfeller, J., Prospero, J., Kinne, S., Bauer, S., Boucher, O., Chin, M., Dentener, F., et al. (2011). Global dust model intercomparison in AeroCom phase I. *Atmospheric Chemistry and Physics*, 11(15).

Hurrell, J. W. (1995). Decadal trends in the North Atlantic Oscillation: regional temperatures and precipitation. *Science*, 269(5224):676–679.

Hurrell, J. W., Holland, M. M., Gent, P. R., Ghan, S., Kay, J. E., Kushner, P., Lamarque, J.-F., Large, W. G., Lawrence, D., Lindsay, K., et al. (2013). The Community Earth System Model: A framework for collaborative research. *Bulletin of the American Meteorological Society*, 94(9):1339–1360.

Jones, A., Roberts, D., and Slingo, A. (1994). A climate model study of indirect radiative forcing. *Nature*, 370:450–453.

Kalnay, E., Kanamitsu, M., Kistler, R., Collins, W., Deaven, D., Gandin, L., Iredell, M., Saha, S., White, G., Woollen, J., et al. (1996). The NCEP/NCAR 40-year reanalysis project. *Bulletin of the American meteorological Society*, 77(3):437–471.

Kaufman, Y., Koren, I., Remer, L., Tanré, D., Ginoux, P., and Fan, S. (2005). Dust transport and deposition observed from the Terra-Moderate Resolution Imaging Spectroradiometer (MODIS) spacecraft over the Atlantic Ocean. *Journal of Geophysical Research: Atmospheres (1984–2012)*, 110(D10).

Kiehl, J. and Briegleb, B. (1993). The relative roles of sulfate aerosols and greenhouse gases in climate forcing. *Science*, 260(5106):311–314.

Klocke, D., Pincus, R., and Quaas, J. (2011). On constraining estimates of climate sensitivity with present-day observations through model weighting. *Journal of Climate*, 24(23):6092–6099.

Knippertz, P. and Todd, M. C. (2012). Mineral dust aerosols over the Sahara: Meteorological controls on emission and transport and implications for modeling. *Reviews of Geophysics*, 50(1).

Koch, D. and Del Genio, A. (2010). Black carbon semi-direct effects on cloud cover: review and synthesis. *Atmospheric Chemistry and Physics*, 10(16):7685–7696.

Koffi, B., Schulz, M., Bréon, F.-M., Griesfeller, J., Winker, D., Balkanski, Y., Bauer, S., Berntsen, T., Chin, M., Collins, W. D., et al. (2012). Application of the CALIOP layer product to evaluate the vertical distribution of aerosols estimated by global models: AeroCom phase I results. *Journal of Geophysical Research: Atmospheres (1984–2012)*, 117(D10).

Kok, J. F. (2011). A scaling theory for the size distribution of emitted dust aerosols suggests climate models underestimate the size of the global dust cycle. *Proceedings of the National Academy of Sciences*, 108(3):1016–1021.

Kok, J. F., Albani, S., Mahowald, N. M., and Ward, D. S. (2014a). An improved dust emission model Part 2: Evaluation in the Community Earth System Model, with implications for the use of dust source functions. *Atmospheric Chemistry and Physics*, 14(23):13043–13061.

Kok, J. F., Mahowald, N. M., Fratini, G., Gillies, J. A., Ishizuka, M., Leys, J. F., Mikami, M., Park, M.-S., Park, S.-U., Van Pelt, R. S., and Zobeck, T. M. (2014b). An improved dust emission model Part 1: Model description and comparison against measurements. *Atmospheric Chemistry and Physics*, 14(23):13023–13041.

Kushnir, Y. (1994). Interdecadal variations in North Atlantic sea surface temperature and associated atmospheric conditions. *Journal of Climate*, 7(1):141–157.

Leaitch, W., Isaac, G., Strapp, J., Banic, C., and Wiebe, H. (1992). The relationship between cloud droplet number concentrations and anthropogenic pollution: Observations and climatic implications. *Journal of Geophysical Research: Atmospheres (1984–2012)*, 97(D2):2463–2474.

Lee, J.-E., Pierrehumbert, R., Swann, A., and Lintner, B. R. (2009). Sensitivity of stable water isotopic values to convective parameterization schemes. *Geophysical Research Letters*, 36(23).

Liu, X., Easter, R. C., Ghan, S. J., Zaveri, R., Rasch, P., Shi, X., Lamarque, J.-F., Gettelman, A., Morrison, H., Vitt, F., et al. (2012). Toward a minimal representation of aerosols in climate models: Description and evaluation in the Community Atmosphere Model CAM5. *Geoscientific Model Development*, 5:709–739.

Lohmann, U. and Feichter, J. (2005). Global indirect aerosol effects: a review. *Atmospheric Chemistry and Physics*, 5(3):715–737.

Mace, G. G., Benson, S., Sonntag, K. L., Kato, S., Min, Q., Minnis, P., Twohy, C. H., Poellot, M., Dong, X., Long, C., et al. (2006). Cloud radiative forcing at the atmospheric radiation measurement program climate research facility: 1. Technique, validation, and comparison to satellite-derived diagnostic quantities. *Journal of Geophysical Research: Atmospheres (1984–2012)*, 111(D11).

Mahowald, N. M. and Kiehl, L. M. (2003). Mineral aerosol and cloud interactions. *Geophysical Research Letters*, 30(9).

Mahowald, N. M., Kloster, S., Engelstaedter, S., Moore, J. K., Mukhopadhyay, S., McConnell, J. R., Albani, S., Doney, S. C., Bhattacharya, A., Curran, M., et al. (2010). Observed 20th century desert dust variability: impact on climate and biogeochemistry. *Atmospheric Chemistry and Physics*, 10(22):10875–10893.

Mantua, N. J. and Hare, S. R. (2002). The pacific decadal oscillation. *Journal of Oceanography*, 58(1):35–44.

Mantua, N. J., Hare, S. R., Zhang, Y., Wallace, J. M., and Francis, R. C. (1997). A Pacific interdecadal climate oscillation with impacts on salmon production. *Bulletin of the american Meteorological Society*, 78(6):1069–1079.

Marticorena, B. and Bergametti, G. (1995). Modeling the atmospheric dust cycle: 1. Design of a soil-derived dust emission scheme. *Journal of Geophysical Research: Atmospheres (1984–2012)*, 100(D8):16415–16430.

Marticorena, B., Chatenet, B., Rajot, J.-L., Traoré, S., Coulibaly, M., Diallo, A., Koné, I., Maman, A., NDiaye, T., and Zakou, A. (2010). Temporal variability of mineral dust concentrations over West Africa: analyses of a pluriannual monitoring from the AMMA Sahelian Dust Transect. *Atmospheric Chemistry and Physics*, 10(18):8899–8915.

Martin, J. H. (1990). Glacial-interglacial CO2 change: The iron hypothesis. *Paleoceanography*, 5(1):1–13.

McCabe, G. J. and Dettinger, M. D. (1999). Decadal variations in the strength of ENSO teleconnections with precipitation in the western United States. *International Journal of Climatology*, 19(13):1399–1410.

Meehl, G. A., Covey, C., Taylor, K. E., Delworth, T., Stouffer, R. J., Latif, M., McAvaney, B., and Mitchell, J. F. (2007). The WCRP CMIP3 multimodel dataset: A new era in climate change research. *Bulletin of the American Meteorological Society*, 88(9):1383–1394.

Meehl, G. A., Washington, W. M., Wigley, T., Arblaster, J. M., and Dai, A. (2003). Solar and greenhouse gas forcing and climate response in the twentieth century. *Journal of Climate*, 16(3):426–444.

Mitchell, J., Johns, T., Gregory, J., and Tett, S. (1995). Climate response to increasing levels of greenhouse gases and sulphate aerosols. *Nature*, 376(6540):501–504.

Mitchell Jr, J. M. (1971). The effect of atmospheric aerosols on climate with special reference to temperature near the earth's surface. *Journal of Applied Meteorology*, 10(4):703–714.

Mohino, E., Janicot, S., and Bader, J. (2011). Sahel rainfall and decadal to multidecadal sea surface temperature variability. *Climate dynamics*, 37(3-4):419–440.

Moulin, C., Lambert, C. E., Dulac, F., and Dayan, U. (1997). Control of atmospheric export of dust from North Africa by the North Atlantic Oscillation. *Nature*, 387(6634):691–694.

Myers, T. A. and Norris, J. R. (2013). Observational evidence that enhanced subsidence reduces subtropical marine boundary layer cloudiness. *Journal of Climate*, 26(19):7507–7524.

Neale, R. B., Richter, J., Park, S., Lauritzen, P. H., Vavrus, S. J., Rasch, P. J., and Zhang, M. (2013). The mean climate of the Community Atmosphere Model (CAM4) in forced SST and fully coupled experiments. *Journal of Climate*, 26(14):5150–5168.

Neale, R. B., Richter, J. H., and Jochum, M. (2008). The impact of convection on ENSO: From a delayed oscillator to a series of events. *Journal of climate*, 21(22):5904–5924.

Newman, M., Compo, G. P., and Alexander, M. A. (2003). Enso-forced variability of the Pacific decadal oscillation. *Journal of Climate*, 16(23):3853–3857.

Nobre, P. and Shukla, J. (1996). Variations of sea surface temperature, wind stress, and rainfall over the tropical Atlantic and South America. *Journal of Climate*, 9(10):2464–2479.

Okin, G. S., Mahowald, N., Chadwick, O. A., and Artaxo, P. (2004). Impact of desert dust on the biogeochemistry of phosphorus in terrestrial ecosystems. *Global Biogeochemical Cycles*, 18(2).

Park, S. and Bretherton, C. S. (2009). The University of Washington shallow convection and moist turbulence schemes and their impact on climate simulations with the Community Atmosphere Model. *Journal of Climate*, 22(12):3449–3469.

Parker, K. (2010). Population, immigration, and the drying of the American Southwest. *Center for Immigration Studies Backgrounder*.

Penner, J. E., Andreae, M., Annegarn, H., Barrie, L., Feichter, J., Hegg, D., Jayaraman, A., Leaitch, R., Murphy, D., Nganga, J., et al. (2001). Aerosols, their direct and indirect effects. In *Climate Change 2001: The Scientific Basis. Contribution of Working Group I to the Third Assessment Report of the Intergovernmental Panel on Climate Change*, pages 289–348. Cambridge University Press.

Petters, M. and Kreidenweis, S. (2007). A single parameter representation of hygroscopic growth and cloud condensation nucleus activity. *Atmospheric Chemistry and Physics*, 7(8):1961–1971.

Pickard, G. L. and Emery, W. J. (1990). *Descriptive physical oceanography: an introduction*. Elsevier.

Pierce, D. (2012). Water Supply and Flooding. In *California Climate Extremes Workshop Report*.

Pierce, D. W. (2001). Distinguishing coupled ocean-atmosphere interactions from background noise in the North Pacific. *Progress in Oceanography*, 49(1):331–352.

Pierce, D. W. (2002). The role of sea surface temperatures in interactions between ENSO and the North Pacific Oscillation. *Journal of Climate*, 15(11):1295–1308.

Pierce, D. W., Barnett, T. P., and Latif, M. (2000). Connections between the Pacific Ocean tropics and midlatitudes on decadal timescales. *Journal of Climate*, 13(6):1173–1194.

Prospero, J. M. (1999). Long-range transport of mineral dust in the global atmosphere: Impact of African dust on the environment of the southeastern United States. *Proceedings of the National Academy of Sciences*, 96(7):3396–3403.

Prospero, J. M. and Bonatti, E. (1969). Continental dust in the atmosphere of the eastern equatorial Pacific. *Journal of geophysical research*, 74(13):3362–3371.

Prospero, J. M., Bonatti, E., Schubert, C., and Carlson, T. N. (1970). Dust in the Caribbean atmosphere traced to an African dust storm. *Earth and Planetary Science Letters*, 9(3):287–293.

Prospero, J. M. and Lamb, P. J. (2003). African droughts and dust transport to the Caribbean: Climate change implications. *Science*, 302(5647):1024–1027.

Prospero, J. M. and Mayol-Bracero, O. L. (2013). Understanding the transport and impact of African dust on the Caribbean basin. *Bulletin of the American Meteorological Society*, 94(9):1329–1337.

Prospero, J. M. and Nees, R. T. (1977). Dust concentration in the atmosphere of the equatorial North Atlantic: Possible relationship to the Sahelian drought. *Science*, 196(4295):1196–1198.

Prospero, J. M. and Nees, R. T. (1986). Impact of the North African drought and El Nino on mineral dust in the Barbados trade winds. *Nature*, 320:735–738.

Qu, X., Hall, A., Klein, S. A., and Caldwell, P. M. (2014). On the spread of changes in marine low cloud cover in climate model simulations of the 21st century. *Climate Dynamics*, 42(9-10):2603–2626.

Rasmusson, E. M. and Wallace, J. M. (1983). Meteorological aspects of the El Nino/Southern Oscillation. *Science*, 222(4629):1195–1202.

Reynolds, R. W., Rayner, N. A., Smith, T. M., Stokes, D. C., and Wang, W. (2002). An improved in situ and satellite SST analysis for climate. *Journal of climate*, 15(13):1609–1625.

Riemer, N., Doherty, O., and Hameed, S. (2006). On the variability of African dust transport across the Atlantic. *Geophysical research letters*, 33(13).

Rogers, J. C. (1997). North Atlantic storm track variability and its association to the North Atlantic Oscillation and climate variability of northern Europe. *Journal of Climate*, 10(7):1635–1647.

Ropelewski, C. F. and Halpert, M. S. (1986). North American precipitation and temperature patterns associated with the El Niño/Southern Oscillation (ENSO). *Monthly Weather Review*, 114(12):2352–2362.

Rosenfeld, D., Rudich, Y., and Lahav, R. (2001). Desert dust suppressing precipitation: A possible desertification feedback loop. *Proceedings of the National Academy of Sciences*, 98(11):5975–5980.

Rosenfeld, D., Woodley, W. L., Axisa, D., Freud, E., Hudson, J. G., and Givati, A. (2008). Aircraft measurements of the impacts of pollution aerosols on clouds and precipitation over the Sierra Nevada. *Journal of Geophysical Research: Atmospheres (1984–2012)*, 113(D15).

Rossow, W. B. and Schiffer, R. A. (1991). ISCCP cloud data products. *Bulletin of the American Meteorological Society*, 72(1):2–20.

Rozendaal, M. A., Leovy, C. B., and Klein, S. A. (1995). An observational study of diurnal variations of marine stratiform cloud. *Journal of climate*, 8(7):1795–1809.

Saha, S., Moorthi, S., Pan, H.-L., Wu, X., Wang, J., Nadiga, S., Tripp, P., Kistler, R., Woollen, J., Behringer, D., et al. (2010). The NCEP climate forecast system reanalysis. *Bulletin of the American Meteorological Society*, 91(8):1015–1057.

Saillant, C. (2010). Homeowners forced to buy flood insurance after FEMA redraws maps. *Los Angeles Times*.

Sassen, K., DeMott, P. J., Prospero, J. M., and Poellot, M. R. (2003). Saharan dust storms and indirect aerosol effects on clouds: CRYSTAL-FACE results. *Geophysical Research Letters*, 30(12).

Schlesinger, M. E. and Ramankutty, N. (1994). An oscillation in the global climate system of period 65-70 years. *Nature*, (367):723–726.

Schneider, N. and Cornuelle, B. D. (2005). The Forcing of the Pacific Decadal Oscillation. *Journal of Climate*, 18(21):4355–4373.

Seinfeld, J. H. and Pandis, S. N. (2012). *Atmospheric chemistry and physics: from air pollution to climate change*. John Wiley & Sons.

Sinyuk, A., Torres, O., and Dubovik, O. (2003). Combined use of satellite and surface observations to infer the imaginary part of refractive index of Saharan dust. *Geophysical Research Letters*, 30(2).

Smirnov, A., Holben, B., Eck, T., Dubovik, O., and Slutsker, I. (2000). Cloud-screening and quality control algorithms for the AERONET database. *Remote Sensing of Environment*, 73(3):337–349.

Smoydzin, L., Teller, A., Tost, H., Fnais, M., and Lelieveld, J. (2012). Impact of mineral dust on cloud formation in a Saharan outflow region. *Atmospheric Chemistry and Physics*, 12(23):11383–11393.

Sokolik, I., Winker, D., Bergametti, G., Gillette, D., Carmichael, G., Kaufman, Y., Gomes, L., Schuetz, L., and Penner, J. (2001). Introduction to special section: Outstanding problems in quantifying the radiative impacts of mineral dust. *Journal of Geophysical Research: Atmospheres (1984–2012)*, 106(D16):18015–18027.

Solomon, S. (2007). *Climate change 2007-the physical science basis: Working group I contribution to the fourth assessment report of the IPCC*, volume 4. Cambridge University Press.

Stevens, B. and Feingold, G. (2009). Untangling aerosol effects on clouds and precipitation in a buffered system. *Nature*, 461(7264):607–613.

Sutton, R. T. and Hodson, D. L. (2005). Atlantic Ocean forcing of North American and European summer climate. *Science*, 309(5731):115–118.

Tegen, I. (2003). Modeling the mineral dust aerosol cycle in the climate system. *Quaternary Science Reviews*, 22(18):1821–1834.

Tegen, I., Lacis, A. A., and Fung, I. (1996). The influence on climate forcing of mineral aerosols from disturbed soils. *Nature*, 380(6573):419–422.

Ting, M., Kushnir, Y., Seager, R., and Li, C. (2009). Forced and internal twentieth-century SST Trends in the North Atlantic. *Journal of Climate*, 22(6):1469–1481.

Trenberth, K. E. (1976). Spatial and temporal variations of the Southern Oscillation. *Quarterly Journal of the Royal Meteorological Society*, 102(433):639–653.

Trenberth, K. E. and Hurrell, J. W. (1994). Decadal atmosphere-ocean variations in the Pacific. *Climate Dynamics*, 9(6):303–319.

Trigo, R. M., Osborn, T. J., Corte-Real, J. M., et al. (2002). The North Atlantic Oscillation influence on Europe: climate impacts and associated physical mechanisms. *Climate Research*, 20(1):9–17.

Twomey, S. (1974). Pollution and the planetary albedo. *Atmospheric Environment (1967)*, 8(12):1251–1256.

Ulbrich, U., Pinto, J., Kupfer, H., Leckebusch, G., Spangehl, T., and Reyers, M. (2008). Changing Northern Hemisphere storm tracks in an ensemble of IPCC climate change simulations. *Journal of climate*, 21(8):1669–1679.

Vimont, D. J. and Kossin, J. P. (2007). The Atlantic meridional mode and hurricane activity. *Geophysical Research Letters*, 34(7).

Wang, C., Dong, S., Evan, A. T., Foltz, G. R., and Lee, S.-K. (2012). Multidecadal covariability of North Atlantic sea surface temperature, African dust, Sahel rainfall, and Atlantic hurricanes. *Journal of Climate*, 25(15):5404–5415.

Washington, R., Todd, M. C., Engelstaedter, S., Mbainayel, S., and Mitchell, F. (2006). Dust and the low-level circulation over the Bodélé Depression, Chad: Observations from BoDEx 2005. *Journal of Geophysical Research: Atmospheres (1984–2012)*, 111(D3).

Weart, S. R. (2008). *The discovery of global warming: revised and expanded edition*. Harvard University Press.

Wehner, M. F., Smith, R. L., Bala, G., and Duffy, P. (2010). The effect of horizontal resolution on simulation of very extreme US precipitation events in a global atmosphere model. *Climate dynamics*, 34(2-3):241–247.

Wolter, K. and Timlin, M. S. (1998). Measuring the strength of ENSO events: how does 1997/98 rank? *Weather*, 53(9):315–324.

Wood, R. (2012). Stratocumulus clouds. *Monthly Weather Review*, 140(8):2373–2423.

Wood, R. and Bretherton, C. S. (2006). On the relationship between stratiform low cloud cover and lower-tropospheric stability. *Journal of climate*, 19(24):6425–6432.

Yokohata, T., Webb, M. J., Collins, M., Williams, K. D., Yoshimori, M., Hargreaves, J. C., and Annan, J. D. (2010). Structural similarities and differences in climate responses to CO2 increase between two perturbed physics ensembles. *Journal of Climate*, 23(6):1392–1410.

Zender, C. S., Bian, H., and Newman, D. (2003). Mineral Dust Entrainment and Deposition (DEAD) model: Description and 1990s dust climatology. *Journal of Geophysical Research: Atmospheres (1984–2012)*, 108(D14).

Zhang, R. and Delworth, T. L. (2006). Impact of Atlantic multidecadal oscillations on India/Sahel rainfall and Atlantic hurricanes. *Geophysical Research Letters*, 33(17).

Zhu, A., Ramanathan, V., Li, F., and Kim, D. (2007). Dust plumes over the Pacific, Indian, and Atlantic oceans: Climatology and radiative impact. *Journal of Geophysical Research: Atmospheres (1984–2012)*, 112(D16).

Zhu, C., Pierce, D. W., Barnett, T. P., Wood, A. W., and Lettenmaier, D. P. (2004). Evaluation of hydrologically relevant PCM climate variables and large-scale variability over the continental US. *Climatic Change*, 62(1-3):45–74.